

Mechanisms of chromosome segregation errors in mammalian oocytes



Eirini Bellou

Göttingen, 2022

Mechanisms of chromosome segregation errors in mammalian oocytes

Dissertation

for the award of the degree

“Doctor rerum naturalium”

of the Georg-August-Universität Göttingen

within the doctoral program *Physics of Biological and Complex Systems*

of the Georg-August University School of Science (GAUSS)

submitted by

Eirini Bellou

from Ioannina, Greece

Göttingen, 2022

Thesis Committee

Dr. Melina Schuh

Department of Meiosis, Max Planck Institute for Multidisciplinary Sciences

Prof. Dr. Rüdiger Behr

Research Platform Degenerative Diseases, German Primate Center

Prof. Dr. Sarah Köster

Institute for X-Ray Physics, Georg-August-University Göttingen

Members of the Examination Board

Dr. Melina Schuh

Department of Meiosis, Max Planck Institute for Multidisciplinary Sciences

Prof. Dr. Timo Betz

Third Institute of Physics-Biophysics, Georg-August-University Göttingen

Further members of the Examination Board

Dr. Peter Lénárt

Cytoskeletal Dynamics in Oocytes, Max Planck Institute for Multidisciplinary Sciences

Dr. Ufuk Günesdogan

Department of Developmental Biology, Georg-August-University Göttingen

Date of oral examination: 12th April 2022

Mechanisms of chromosome segregation errors in mammalian oocytes

Eirini Bellou

Abstract

During fertilization, a human embryo needs to inherit precisely one copy of each chromosome from both parents. However, human eggs frequently carry an incorrect number of chromosomes, they are aneuploid. Aneuploidy is the leading cause of aberrant embryonic development, resulting in miscarriages and genetic disorders such as Down syndrome. Early cytogenetic studies have shown that aneuploidy rates during meiosis differ for individual chromosomes. The reasons for variable aneuploidy rates are unknown. In this thesis, I used live-cell and super-resolution microscopy to investigate the behaviour of chromosomes with high and low aneuploidy rates in both human and porcine oocytes. In particular, I tested three different hypotheses for the origin of variable aneuploidy rates. First, I studied whether the precise architecture of the chromosomes affects their segregation behaviour. Second, I investigated whether chromosomes differ in how they interact with the microtubule spindle, the machinery which segregates the chromosomes during both meiosis I and meiosis II. Third, I investigated whether differences in chromosome cohesion biases subsets of chromosomes towards aneuploidy. Together, my results identify several reasons for the high aneuploidy rates of subsets of chromosomes, and reveal a new factor that contributes to chromosome-specific aneuploidy in meiosis.

Acknowledgments

First and foremost, I would like to thank my supervisor, Dr. Melina Schuh, for her invaluable advice, continuous support and constant guidance throughout my PhD. I am very grateful to have had the chance to work in her lab and learn from her.

I am grateful to my thesis advisory committee members Prof. Dr. Rüdiger Behr and Prof. Dr. Sarah Köster for their support during our meetings. I would also like to thank Prof. Dr. Timo Betz, for reviewing my thesis and participating in my examination board and Dr. Peter Lenart, and Dr. Ufuk Günesdogan for kindly participating in my examination committee.

Furthermore, I would like to express my sincere gratitude to members of the Schuh lab. Special thanks to Chun So for helpful discussions and support with the project, for comments on the manuscript, and for being a great office mate. I would also like to thank Lena Wartosch for helping with the human oocytes and Martina Daniel for all the help with the porcine ovaries and the organizational things in the lab. I would also like to thank Agata Zielinska for initiating this study by finding the sequences of the TALEs and designing the acrocentric-TALE. Furthermore, I would like to thank Tommaso Cavazza for being a great teammate in the seminar series organization and together with Chun So, and Ina Harasimov for discussions about improvements in porcine oocyte culture. Also, Eike Mönnich for his help with analyses using Imaris and MATLAB. I am really grateful to Chloe Charalambous, Alexandre Webster, Ida Jentoft, and Debojit Saha for all their support and for a cherished time spent together inside and outside of the lab. Additionally a big thanks to all the Schuh lab members for their insightful comments, feedback, and fun times in the past four years.

I would also like to thank the live-cell imaging facility and Peter Lenart for helpful advice. Antonio Politi for helpful discussions and for taking part in the project. The embryology team at Fertility Center Berlin and all the patients donating the oocytes. Finally, I am deeply grateful to all my former supervisors, for their guidance and support.

Last but not least I would like to express my gratitude to my friends in Göttingen, for making life here so much fun, to my friends in Greece for being so close despite the physical distance, and to my parents for their constant support in all my steps. Their tremendous understanding and encouragement in the past years, made everything possible. I dedicate this thesis to my family and friends who supported me on this journey.

Table of Contents

Abstract.....	1
Acknowledgments.....	3
Table of Contents.....	5
1. Introduction.....	7
1.1 Sexual reproduction.....	7
1.2 Mammalian oogenesis.....	7
1.3 Homologous chromosome pairing.....	9
1.4 Meiosis.....	10
1.5 Roles of cohesin in meiosis I and II.....	12
1.5.1 Shugoshin 2 protects centromeric cohesin.....	12
1.6 Kinetochores drive chromosome segregation.....	13
1.6.1 Kinetochores structure.....	13
1.6.2 Types of kinetochores-microtubules interactions.....	15
1.6.3 Regulation of kinetochores-microtubule attachment.....	17
1.6.4 Spindle assembly checkpoint (SAC).....	17
1.7 The importance of doing it right.....	18
1.7.1 Oocytes from young females are error-prone.....	18
1.8 Types of errors in meiosis I.....	18
1.8.1 MI Non-disjunction (MI-NDJ).....	19
1.8.2 Premature separation of sister chromatids (PSSC).....	19
1.8.3 Reverse segregation (RS).....	19
1.9 Types of errors in meiosis II.....	21
1.10 Causes of aneuploidy in human eggs.....	22
1.10.1 Spindle instability.....	22
1.10.2 Spindle assembly checkpoint.....	23
1.10.3 Position of chiasmata.....	23
1.11 Causes of age-related aneuploidy in human eggs.....	24
1.11.1 Sister kinetochores separation.....	24
1.11.2 Bivalents split into univalents.....	25
1.12 Not all chromosomes are equally affected by aneuploidy.....	25
2. Objectives.....	28
3. Manuscript 1.....	30

4. Manuscript 2.....	77
5. Discussion.....	121
5.1 New factors contributing to human oocyte aneuploidy.....	121
5.2 Porcine oocytes are a suitable model for studying human meiosis.....	121
5.3 Bivalent morphology is associated with missegregation.....	122
5.4 Chromosome labelling with TALEs.....	123
5.5 Two different configurations of the small arm of acrocentric chromosomes.....	124
5.6 Kinetochores of acrocentric chromosomes.....	125
5.7 Spermatocytes and aneuploidy.....	125
5.8 Differences between meiosis and mitosis in missegregation.....	126
5.9 Other factors that have been suggested to affect chromosome aneuploidy.....	127
5.10 Aging and aneuploidy.....	128
5.11 Conclusion.....	129
6. References.....	130

1. Introduction

1.1 Sexual reproduction

Life starts with the fusion of an egg and a sperm into a single cell. This cell then undergoes multiple divisions and eventually gives rise to all the cells of the new organism (Clift & Schuh, 2013). The two gametes contribute an equal amount of genetic materials. Thus, they both must contain half the genetic materials compared to all the other cells. This makes gametes a unique type of cell that needs to undergo a specialized division that leads to the reduction of chromosomes. This division is called meiosis (Herbert et al., 2015).

1.2 Mammalian oogenesis

Meiosis generates haploid gametes from diploid precursor cells. In females, the precursor cells are called oocytes (Herbert et al., 2015). Oocytes are differentiated from primordial germ cells (PGCs). PGCs undergo multiple mitotic divisions to produce oogonia, which continue to divide multiple times without completing cytokinesis (Wang & Pepling, 2021). Thus, the cells remain connected through intracellular bridges, forming clusters (Syncytia) known as germ cell nests (Gershon & Dekel, 2020; Pepling & Spradling, 1998). Meiosis in mice starts at 13.5 days post coitum (dpc) (Bullejos & Koopman, 2004). Oogonia advance through prophase I to form the oocytes. During prophase I, the oocytes undergo the process of recombination and pairing of homologous chromosomes and subsequently arrest at the diplotene stage of prophase until puberty (Rojas et al., 2015). This prolonged resting phase is called dictyate arrest (Sanchez & Smitz, 2012). Homologous chromosomes remain physically paired during this period. Oocytes are surrounded by one layer of somatic cells at this stage, forming the primordial follicles. The majority of primordial follicles eventually undergo programmed cell death (Gershon & Dekel, 2020). The remaining follicles are generally thought to constitute the total number

of oocytes available to the female throughout the reproductive lifespan (Rojas et al., 2015; Sanchez & Smitz, 2012; Wang & Pepling, 2021).

Primordial follicles are activated in cohorts to initiate folliculogenesis and eventually develop into primary follicles. The surrounding somatic cells, called granulosa cells accompany this transition with morphological changes and become cuboidal (Gershon & Dekel, 2020). Primary follicles have a single layer of granulosa cells, grow in size, and eventually give rise to secondary follicles (Sanchez & Smitz, 2012). Each secondary follicle contains a growing oocyte and has at least two layers of granulosa cells, which exhibit an upregulated hormonal receptor expression (Rojas et al., 2015). Follicular development until the preantral stage is independent of hormonal stimulation and rather driven by intraovarian factors and bidirectional communication between the oocyte and the somatic cells (Gershon & Dekel, 2020; Rimon-Dahari et al., 2016; Rojas et al., 2015; Sanchez & Smitz, 2012). In preantral stages, granulosa cells proliferate at high rates and give rise to a multi-layer follicle, followed by an increase in the follicle size and the appearance of a cavity. The fluid-filled cavities that appear are finally united to form the antrum (Gershon & Dekel, 2020).

Antral development is initiated and characterized by the differentiation of the granulosa cells into cumulus and mural cell compartments (Sanchez & Smitz, 2012). The oocyte is now fully competent to resume meiosis. Progression of the cells through the antral stages is dependent on the pituitary-secreted gonadotropins, follicle-stimulating hormone (FSH) and luteinizing hormone (LH). FSH is crucial for the antral development and induces the expression of LH receptors, which will allow the follicles to respond to LH hormone. LH is important for initializing ovulation (Rimon-Dahari et al., 2016). Antral follicles expressing a high concentration of LH receptors react to hormonal signal and transform into the preovulatory/Graafian follicle (Gershon & Dekel, 2020; Rimon-Dahari et al., 2016; Rojas et al., 2015). Preovulatory follicles with fully grown oocytes can undergo ovulation and extrude the oocyte

after the hormonal stimulation (Gershon & Dekel, 2020; Sanchez & Smitz, 2012). The hormonal stimulation happens once every menstrual cycle and the oocytes turn into fertilizable eggs (Clift & Schuh, 2013). During the oogenesis period, oocytes synthesize and accumulate all the necessary RNAs and proteins that are crucial for their growth and the development of preimplantation embryos (Sanchez & Smitz, 2012).

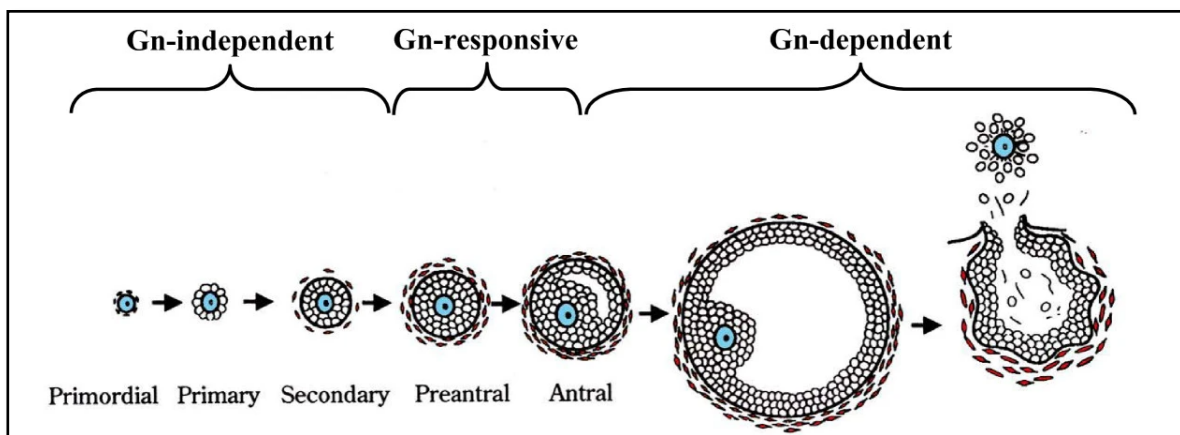


Figure 1: Mammalian oogenesis

Schematic representation of the development of the primordial follicles to fully grown oocytes. The image presents the relative size of the follicle and the Gonadotropin dependence. Adapted from (Orisaka et al., 2009)

1.3 Homologous chromosome pairing

To achieve a reductional division, the homologous chromosomes from the different parental origins have to pair with each other in gametes (Herbert et al., 2015). Pairing is a consequence of meiotic recombination which happens during prophase I. Meiotic recombination is initiated by the formation of double-strand breaks (DSB) and the recruitment of DNA repair proteins to the recombination foci. DSB repair can result in either the formation of crossovers or noncrossovers (Herbert et al., 2015). Noncrossovers result only in local gene exchange and do not connect the homologs. In contrast, crossovers result in the exchange of the chromatid arm region that is distal to the crossover site

between the two homologs (MacLennan et al., 2015). Crossovers serve two purposes: 1) they increase genetic diversity and 2) they form a physical linkage between the two parental homologs. The linked homologs form a structure named bivalent (MacLennan et al., 2015). Bivalents remain connected by the formation of chiasmata until the completion of meiosis I. They are stabilized by arm cohesion from the chromosome parts that have not undergone exchange (Herbert et al., 2015; MacLennan et al., 2015; Petronczki et al., 2003).

1.4 Meiosis

Meiosis begins with the replication of DNA; as a result, the oocyte contains four chromatids, two of maternal origin and two of paternal origin. The four chromatids must be distributed in four different cells in order to obtain a haploid gamete in the end. For that, meiosis is composed of two sequential divisions, without an intermediate DNA replication. Previously paired homologous chromosomes separate during the first meiosis (Meiosis I) (Petronczki et al., 2003). Arm cohesion that maintains the bivalents together is dissolved during anaphase I and half of the chromosomes are extruded as the first Polar Body. The second meiosis follows with equatorial segregation of sister chromatids, with half of them extruded in the second Polar Body (Meiosis II) (Clift & Schuh, 2013). Meiosis II is arrested at metaphase and resume only if fertilization occurs (Clift & Schuh, 2013).

For accurate segregation of chromosomes during meiosis I, it is important that the sister kinetochores of each homolog are oriented side by side, towards the same pole. Mono-orientation is unique to meiosis I and is essential for the reductional division. In contrast, in meiosis II, chromosomes have a “mitosis-like” configuration with the sister kinetochores biorienting and interacting with microtubules from different poles (Herbert et al., 2015; Petronczki et al., 2003).

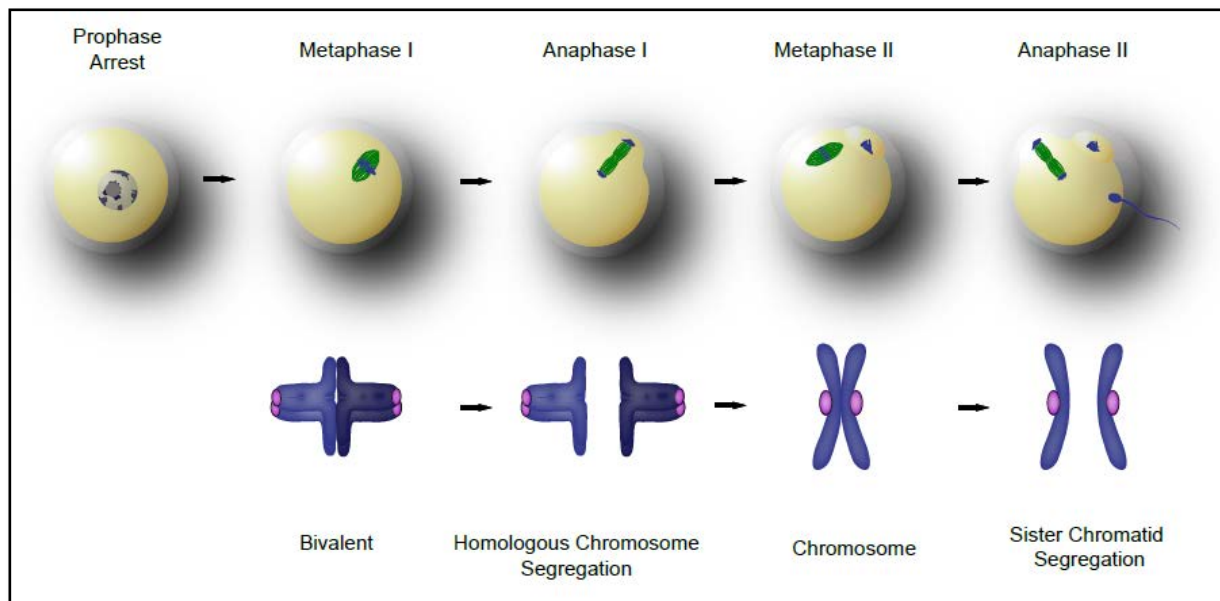


Figure 2: Meiosis in mammalian oocytes

Meiosis is composed of two sequential divisions. In meiosis I, homologous chromosomes pair together to create the bivalents. Sister chromatids orient towards the same spindle pole and the homologous chromosomes separate during anaphase. Half of the chromosomes are extruded in the first polar body. The cell subsequently arrests in meiosis II. Resumption of the second meiosis will happen only if fertilization occurs. In meiosis II, the sister chromatids orient towards the opposite poles and separate from each other during anaphase II. (Based on an illustration by Melina Schuh).

At the molecular level, oocytes are maintained in the dictyate arrest by high levels of cyclic AMP (cAMP). During this arrest, they possess an intact nucleus known as the germinal vesicle (GV) (Rojas et al., 2015). At the beginning of meiosis, LH induces the breakdown of intracellular junctions between the granulosa cells and the oocyte. As a consequence, there is a reduction in the levels of cAMP and the M-phase kinase, Cdk1, is activated. The resumption of meiosis is marked by nuclear envelope breakdown (Rojas et al., 2015; Sanchez & Smitz, 2012). The meiosis I spindle is assembled and migrates to the oocyte cortex by an actin-dependent mechanism (Schuh & Ellenberg, 2008). Upon the completion of meiosis I and polar body extrusion the oocyte immediately enters meiosis II. In meiosis II, maturation promoting factor (MPF) is maintained at stable level and the oocyte arrests at metaphase II. The arrest is maintained by Emi2, which inhibits the anaphase-promoting complex/cyclosome (APC/C) (Clift & Schuh, 2013). The inhibition prevents parthenogenetic activation and the creation of an embryo without contribution of paternal genome (Rojas et al., 2015). While the

oocyte matures the follicle ruptures and the egg is released into the oviduct (Clift & Schuh, 2013). In the oviduct, the oocyte resumes meiosis II only if it is fertilized by a sperm. Sperm entry induces an increase of free Ca^{2+} which activates the calcium-calmodulin Protein Kinase II (CaMKII) and release Emi2 from inhibition after Emi2 phosphorylation (Clift & Schuh, 2013; Rojas et al., 2015).

1.5 Roles of cohesin in meiosis I and II

In meiosis I, cohesin localizes to the centromeric region of sister chromatids as well as along the chromosome arms. Apart from mitotic cohesins, there are also meiosis-specific cohesins, like REC8 (Ishiguro, 2019). To complete meiosis I, REC8 has to be cleaved from the chromosome arms to allow the resolution of chiasmata and separation of homologs. However, it is necessary to be retained in between kinetochores, so that the sister chromatids remain connected (Ishiguro, 2019; Webster & Schuh, 2017). Cohesin is removed by separase-mediated cleavage in both meiosis and mitosis (Kudo et al., 2006). In meiosis phosphorylation of Rec8 makes it more susceptible to cleavage. In mice, this is mediated by Polo-like kinase (PLK1) (Ishiguro, 2019).

1.5.1 Shugoshin 2 protects centromeric cohesin

Centromeric REC8 has to be intact until meiosis II. To this end, it is protected from separase-mediated cleavage during anaphase I and eventually cleaved during anaphase II, in case of fertilization and resumption of meiosis II. The guardian of centromeric REC8 is the family of Shugoshin proteins (Ishiguro, 2019; Kitajima et al., 2004). More specifically, Shugoshin2 (SGO2) forms a complex with PP2A to protect centromeric REC8 cohesin from separase-mediated cleavage during meiotic anaphase I (Llano et al., 2008). Loss of SGO2 in mice results in premature release of REC8 from the centromeres and failure to keep sister chromatids together (Llano et al., 2008).

Apart from maintaining sister chromatids together, accumulating data suggest that REC8-mediated sister chromatid cohesion plays a crucial role in orienting the sister kinetochores towards the same pole in meiosis I. The geometric restriction of REC8 helps the sister kinetochores to take the side-by-side configuration (Ishiguro, 2019).

1.6 Kinetochores drive chromosome segregation

To ensure accurate chromosome segregation the cells need a machinery that fulfills the following criteria: 1) Recognizes each chromosome separately, 2) physically connects each chromosome to the segregation machinery 3) generates force to ensure the proper movement of the chromosome in the cellular space (Cheeseman, 2014). In eukaryotes, all the above functions are mediated through a macromolecular structure called the kinetochore. More than 100 proteins are part of the kinetochore structure (Nagpal & Fukagawa, 2016).

Each chromosome has a specific region, which is termed the centromere on which the kinetochore is assembled. Centromeres are defined by a Histone H3 variant that is called CENP-A. CENP-A remains associated with chromosomes throughout the cell cycle, even during DNA replication, and new CENP-A is only placed on sites that CENP-A already exists (Palmer et al., 1987).

1.6.1 Kinetochore structure

The kinetochore structure is composed of three different layers: 1) the inner kinetochore which connects to the DNA and forms the platform to build the other kinetochore layers 2) the outer kinetochore which interacts with microtubules and 3) the regulatory part, which is composed of proteins that monitor kinetochore activity and interactions with microtubules (Cheeseman, 2014). Many kinetochore proteins are evolutionary conserved and they have a similar assembly pathway in different species (Maiato et al., 2004). Furthermore, many studies show that kinetochores are not

formed in a linear pathway, but multiple pathways are involved to coordinate their assembly (Nagpal & Fukagawa, 2016).

The kinetochore is a highly dynamic structure that assembles and disassembles during the cell cycle (Cheeseman, 2014). In human cells, only a small number of the kinetochore proteins remain connected to the centromere throughout the cell cycle. This group of proteins are called constitutive centromere-associated network—CCAN (Cheeseman & Desai, 2008; Nagpal & Fukagawa, 2016). The rest of the proteins are recruited to the centromere only in late G2 or in prophase and remain there till anaphase. After anaphase onset, the majority of the proteins dissociate from the kinetochore (Cheeseman & Desai, 2008; Maiato et al., 2004). One of the important players of the inner kinetochore is the protein CENP-C, which is involved in the recruitment of a large number of proteins at the kinetochore (Cheeseman & Desai, 2008; Liu et al., 2006). CENP-C and also Aurora B pathways specify the size and dimension of the kinetochore plates. CENP-C depletion can lead to small-size kinetochores with an altered-size outer plate (Liu et al., 2006).

The outer plate of the kinetochore is responsible for the interactions of kinetochore with microtubules. The key player that directly interacts with microtubules is NDC80, which forms a tetramer and has a rod-shaped structure (Ciferri et al., 2008). Another important protein that directly interacts with microtubules is the kinesin CENP-E. CENP-E interacts with microtubules laterally and plays a role in chromosome congression (Cheeseman, 2014).

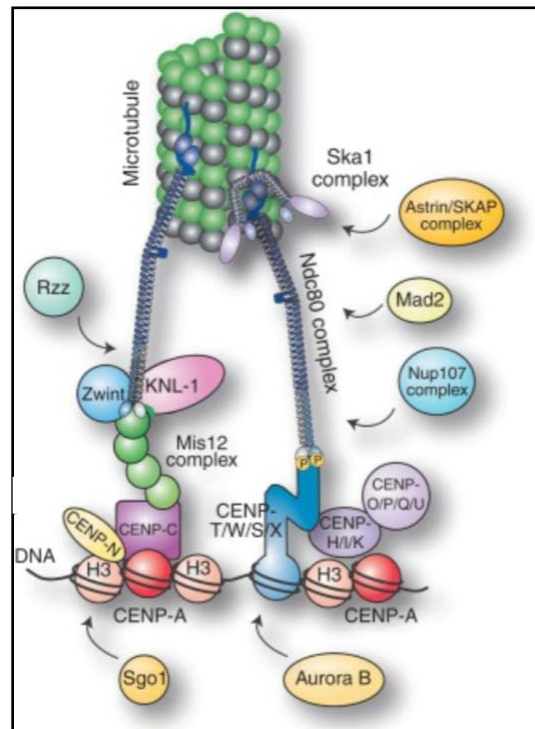


Figure 3: Kinetochore organization in mitosis

The structure of the different layers of the kinetochore is depicted in the image. The kinetochore is composed of a total of more than a hundred proteins but only some key components are shown in the image. Adapted from (Cheeseman, 2014).

1.6.2 Types of kinetochore-microtubules interactions

To ensure faithful segregation of chromosomes to the two daughter cells, it is important to establish stable kinetochore-microtubule attachments. A typical microtubule (composed of 13 protofilaments) interacts with the kinetochore and generates forces to direct chromosome movement. In a stable kinetochore-microtubule attachment, the microtubule plus-end is directly embedded in the kinetochore and the attachment is called “end-on” (Cheeseman, 2014; Cheeseman & Desai, 2008). Kinetochore can directly influence microtubule dynamics by controlling the polymerization status. Kinetochore proteins can directly promote or inhibit the polymerization of the microtubules (Cheeseman, 2014).

Initial interactions of microtubule and kinetochore are mediated by lateral attachments in the prometaphase rosette (Itoh et al., 2018). They are driven by microtubule motor-dependent forces,

mainly from CENP-E (Craske & Welburn, 2020). The main role of CENP-E is to bring unattached or mono-oriented chromosomes from the poles to the central region of the spindle (Kapoor et al., 2006). Thus, lateral attachments are an important intermediate step for chromosome bi-orientation and alignment (Itoh et al., 2018).

Apart from the aforementioned interactions, a number of incorrect attachments can occur. Kinetochores can fail in establishing an attachment and remain “unattached” from one or both sides. Also, kinetochores can interact with microtubules from both spindle poles at the same time and form a “merotelic attachment”. If unattached kinetochores or incorrect attachments persist during anaphase onset, this will lead to errors during chromosome segregation. For that, the cells need mechanisms to detect and correct them (Cheeseman, 2014).

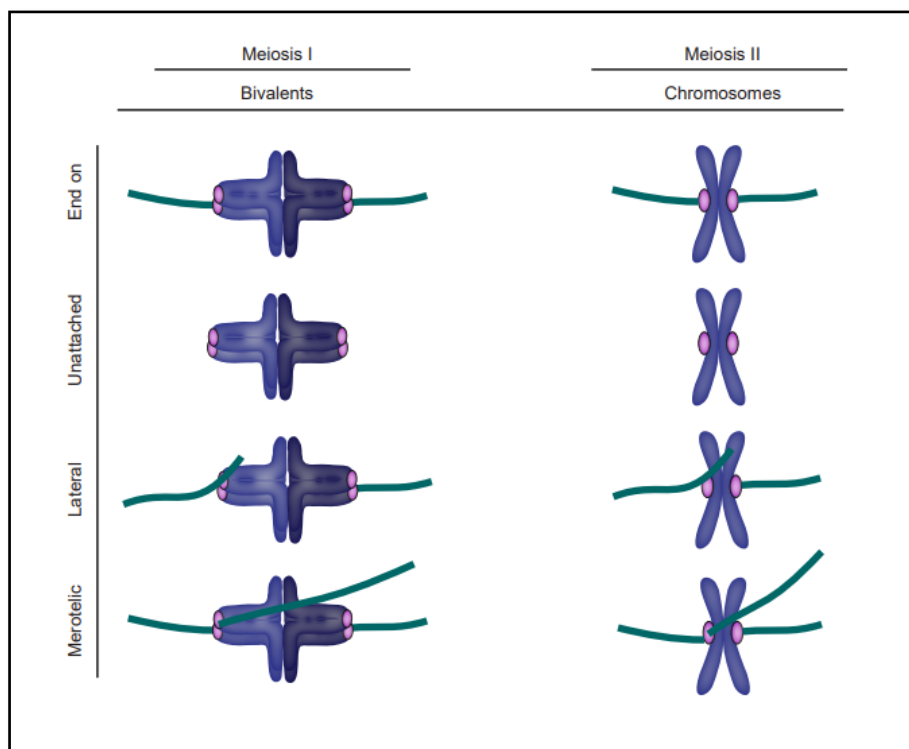


Figure 4: Types of kinetochore-microtubule attachments

In meiosis I, homologous chromosomes pair and sister kinetochores orient towards the same spindle pole. In meiosis II, chromosomes have a mitosis-like configuration and the sister kinetochores are facing the opposite poles. The illustration depicts the different ways that kinetochores interact with the microtubules. The desired attachment for correct chromosome segregation is the end-on attachment. Lateral and merotelic attachments as well as unattached chromosomes can lead to chromosome segregation errors.

1.6.3 Regulation of kinetochore-microtubule attachment

One of the key regulatory players of kinetochore-microtubule attachments is the kinase Aurora B. Aurora B localizes to the inner centromere and eliminates incorrect kinetochore-microtubule attachments by phosphorylation. This correction is tension-sensitive and is based on phosphorylations of the outer kinetochore substrates. Aurora B resets the kinetochore as unattached such that new attachments can form (Cheeseman, 2014; Touati & Wassmann, 2016). The tension-sensitive model suggests that the force that is created when the chromosome is bioriented separates Aurora B from the outer kinetochore substrates. This makes the outer parts of the kinetochore less accessible to Aurora B and decreases the chances of being phosphorylation (Cheeseman, 2014; Lampson & Cheeseman, 2011; Touati & Wassmann, 2016). The spatial separation explains how the kinase distinguishes between bioriented chromosomes and chromosomes attached to microtubules from the same pole (Lampson & Cheeseman, 2011).

1.6.4 Spindle assembly checkpoint (SAC)

Correct chromosome segregation depends on the establishment of correct attachments before anaphase onset. Thus, the cell needs a mechanism to delay the progression into anaphase until all the chromosomes are properly attached. This is achieved via a regulatory mechanism at the outer kinetochore, the Spindle Assembly Checkpoint complex (SAC) (Cheeseman, 2014; Musacchio & Salmon, 2007). The SAC complex detects incorrectly attached kinetochores and arrests the cell at metaphase. The SAC is active on kinetochores in prometaphase and becomes inactivated once all the chromosomes are correctly attached in mitosis (Musacchio & Salmon, 2007). Once SAC is deactivated separase is free to cleave cohesin and separate the homologous chromosomes (Musacchio & Salmon, 2007).

1.7 The importance of doing it right

As discussed above the cells have many different ways to regulate and monitor the process of division and correct chromosome segregation. Having the correct number of chromosomes is important for the health of every cell. Moreover, it is crucial to produce healthy gametes as errors that arise during meiotic division will be inherited by the whole new organism. Cells that do not contain the correct number of chromosomes are aneuploid (Webster & Schuh, 2017). Despite the necessity of doing it right, oocytes are surprisingly error-prone. Aneuploid oocytes will lead to miscarriages or embryos with severe congenital abnormalities (Hassold & Hunt, 2001). It is currently routine for fertility clinics to monitor the development of the embryos. From those data, we now know that roughly ~50% of the human embryos develop until the blastocyst stage, and only ~50% of those implant into the uterus (Thomas et al., 2021).

1.7.1 Oocytes from young females are error-prone

Oocytes are produced during fetal development and remain in dictyate arrest for many years before they resume meiosis. This can last from ~12 to ~45 years, meaning from the start of puberty until menopause. Numerous studies have reported that oocytes from women of older age are more often to be aneuploid (Nagaoka et al., 2012). However, we now know that even oocytes from younger women often contain errors. It is estimated that women in their 20s have 25% of eggs being aneuploid, and this increases to up to 50% with age (Gruhn et al., 2019; Wartosch et al., 2021).

1.8 Types of errors in meiosis I

The aim of meiosis I is to separate the two homologs from each other. The oocyte has 4 chromatids and after the completion of meiosis I, either the maternal or paternal copy of chromosomes should remain in the egg, while the other half will be extruded to the Polar Body (outcome 2:2). However, this

is not always happening correctly and 3 different types of errors can occur in meiosis I (Nagaoka et al., 2012; Wartosch et al., 2021).

1.8.1 MI Non-disjunction (MI-NDJ)

The first type of error happens when the bivalent fails to segregate into two parts after meiosis I. Thus, both homologs segregate to the same pole— either to the oocyte or to the polar body (outcome 4:0) (Wartosch et al., 2021). This can be an outcome of chromosome misalignment in the spindle. When the bivalent is not properly aligned in the equator before anaphase onset, spindle microtubules fail to separate it into two homologs. Another reason why the homologs may fail to separate is because of improper chiasmata position (Herbert et al., 2015).

1.8.2 Premature separation of sister chromatids (PSSC)

The second type of missegregation is PSSC, in which the two sister chromatids are prematurely separated during meiosis I, and the outcome of the segregation is 3:1. The major cause of PSSC is premature loss of centromeric cohesion in combination with merotelic attachments (Hassold & Hunt, 2001; Wartosch et al., 2021).

1.8.3 Reverse segregation (RS)

The third type of missegregation is the reverse segregation. This happens when one chromatid from the maternal homolog and one chromatid from the paternal homolog segregate to the same pole (Ottolini et al., 2015). The outcome of this error is that 2 chromatids of different parental origins remain in the same cell (outcome 2:2), which phenotypically maintains the correct number of chromosomes.

However, the two chromatids are of different parental origins and thus not linked in the centromeric region, eventually segregate independently at anaphase II (Gruhn et al., 2019; Wartosch et al., 2021).

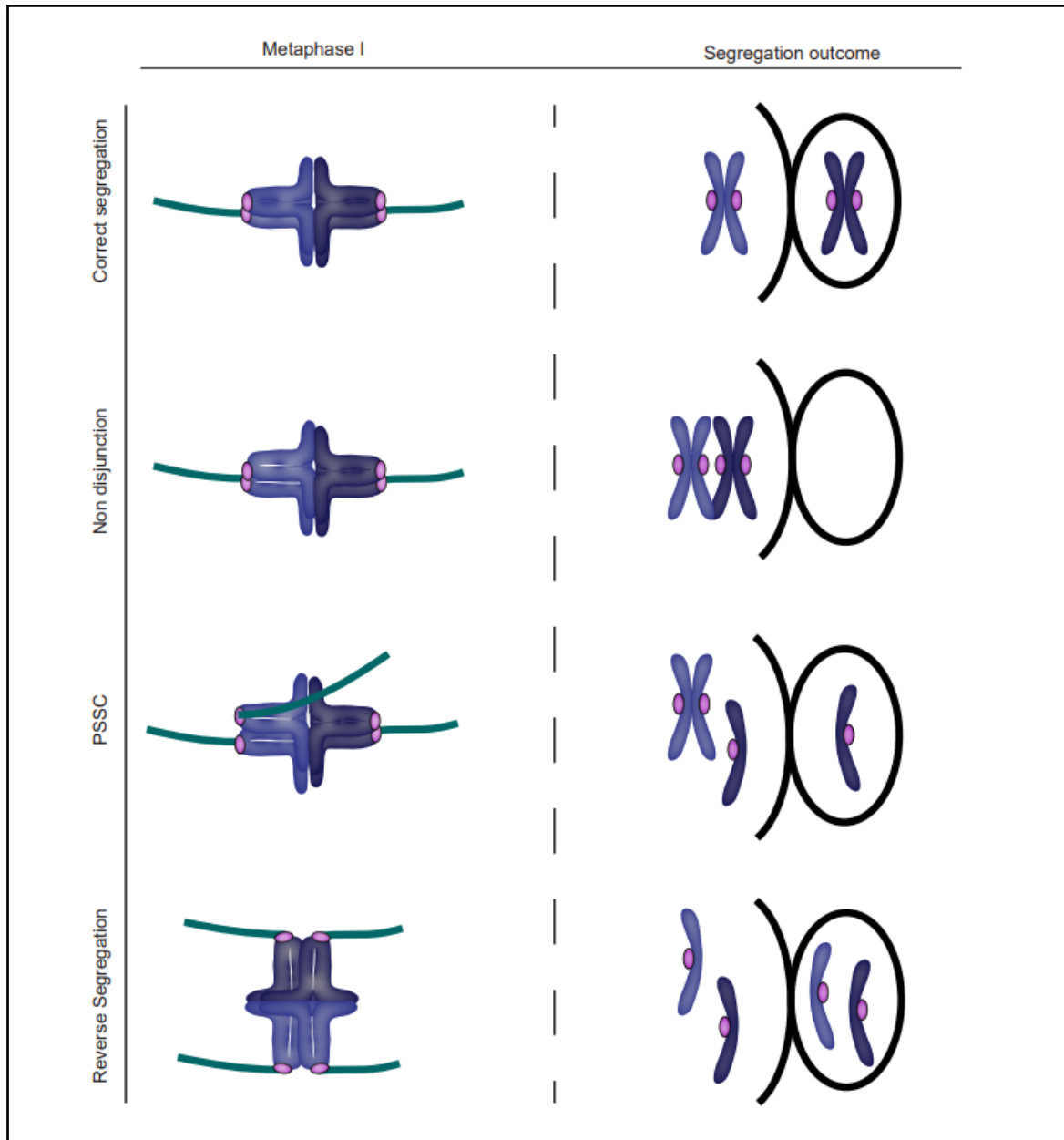


Figure 5: Types of chromosome segregation errors in meiosis I

For correct segregation in meiosis I, sister kinetochores orient towards the same spindle pole, and each homolog segregates to a different pole. If the bivalent fails to separate to the correct poles and the 4 chromatids segregate either to the oocyte or to the polar body, the error is called NDJ. Loss of cohesin in combination with incorrect attachments can lead to the missegregation of a sister chromatid and give rise to PSSC. Last, if the bivalents orient in the metaphase plate rotated by 90 degrees and the sister kinetochores are facing opposite poles, then this can lead to reverse segregation.

1.9 Types of errors in meiosis II

Apart from errors in meiosis I, errors can occur in meiosis II. This will result in the gain or loss of one chromatid. When the two sister chromatids fail to separate in meiosis II both will end up at the same pole. This will lead to MII non-disjunction (MII-NDJ) (Hassold & Hunt, 2001; Wartosch et al., 2021). Errors in MII can either lead to aneuploidy or have a beneficial outcome. The beneficial outcome will happen only if an error that occurred in MI, is balanced by a second error in MII that will bring balance in the number of chromatids in the cell (Magli et al., 2012).

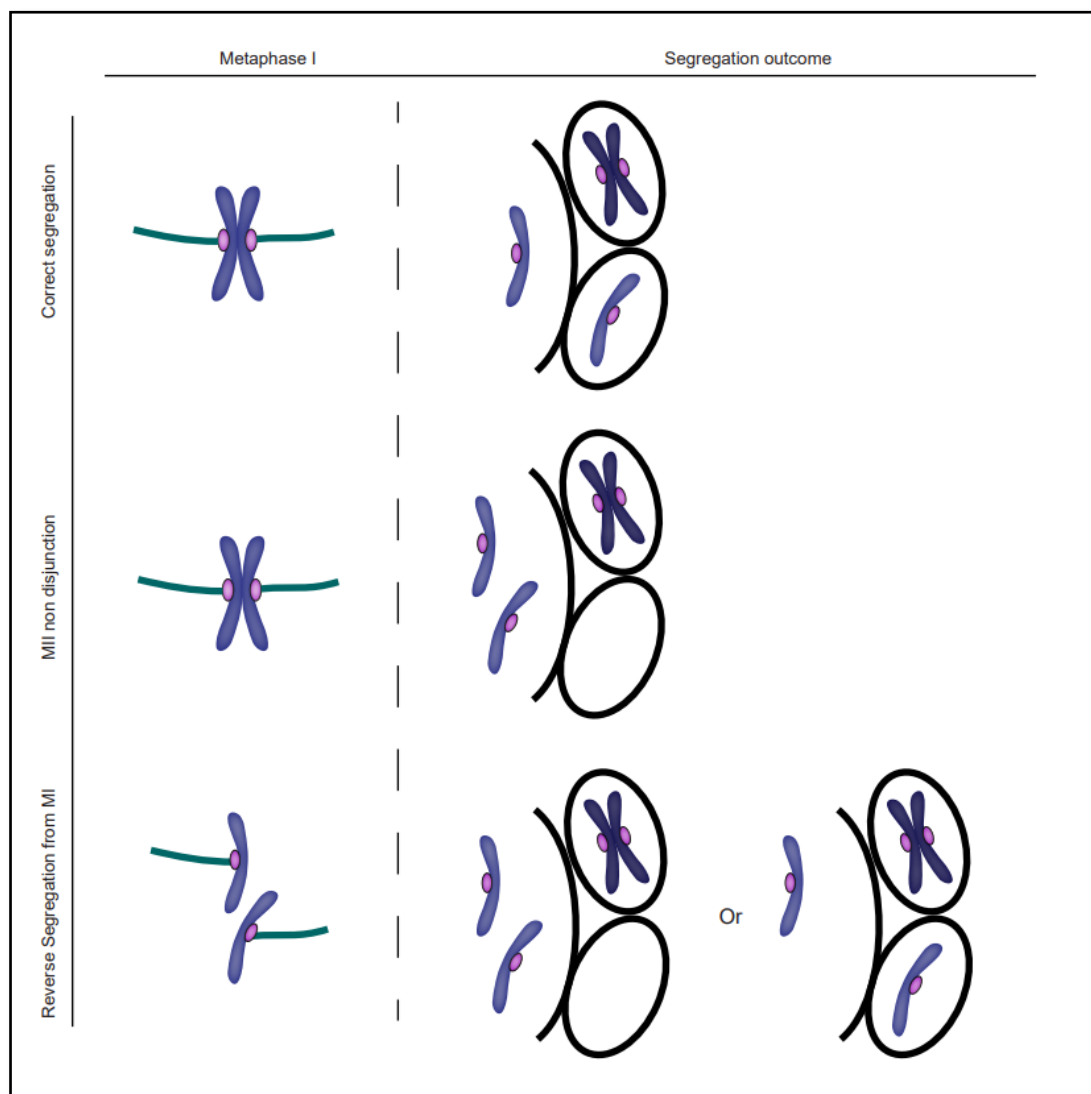


Figure 6: Types of chromosome segregation errors in meiosis II

For correct chromosome segregation in meiosis II, the sister kinetochores orient towards different spindle poles and separate one in the oocyte and one in the polar body. MII non-disjunction occurs when the sister chromatids fail to separate and both of them segregate to the same pole, in the oocyte or the polar body. If reverse

segregation is happening in meiosis I, then the two non-sister chromatids are not paired in meiosis II. Because of that, they interact with the microtubules separately and segregate independently from each other. The segregation outcome is random and can lead to a segregation error or to a euploid cell.

1.10 Causes of aneuploidy in human eggs

Aneuploidy affects women of all ages. Women in their 20s have around ~25% of aneuploid eggs (Gruhn et al., 2019). This suggests that human oocytes are intrinsically primed to errors and aneuploidy. In recent years, the differences of the oocytes to the mitotic cells have been extensively investigated. Human oocytes are proven to have inherently unstable spindles (Holubcova et al., 2015). Moreover, they are allowed to progress in anaphase I even if not all chromosomes are correctly attached (Thomas et al., 2021). Lastly, suboptimal positions of chiasmata can cause weak associations between bivalents (Webster & Schuh, 2017).

1.10.1 Spindle instability

Unlike mitotic cells and mouse oocytes human oocytes lack microtubule-organizing centers and nucleate microtubules from chromosomes (Holubcova et al., 2015). Nucleated microtubules undergo reorganization and eventually assembly into a spindle. However, human oocyte spindles are often multipolar and unstable. They often undergo repeated spindle remodeling, forming transient apolar or multipolar spindles (Holubcova et al., 2015). Multipolar spindles promote merotelic attachments and often chromosomes will remain merotelically attached even after pole clustering in a bipolar spindle (Holubcova et al., 2015; Silkworth et al., 2009). It was recently identified that human oocytes lack the KIFC1 protein and this results in spindle instability (So et al., 2022).

1.10.2 Spindle assembly checkpoint

Accurate chromosome segregation relies on correct kinetochore-microtubule attachments. In mice it has been observed that kinetochores in meiosis I form incorrect kinetochore-microtubule attachments and undergo multiple error-correction events (Kitajima et al., 2011). The multipolar spindle intermediates of human oocyte spindles increase the frequency of missegregation and enhance the probability of creating erroneous attachments (Holubcova et al., 2015). Cells have developed mechanisms that sense the incorrect attachments and replace them, and they can also delay the anaphase onset until all the chromosomes are correctly attached. SAC has been proven to recognize unattached kinetochores in oocytes. However, it is not as efficient as in mitosis, in which it can delay anaphase onset even if a single kinetochore is unattached (Touati & Wassmann, 2016). Oocytes are the largest cells in the human body and it has been shown that the large oocyte cytoplasm is responsible for the poor response of the mechanism to the signal from unattached kinetochores (Kyogoku & Kitajima, 2017; Lane & Jones, 2017).

1.10.3 Position of chiasmata

Crossovers are important to hold the bivalents together and ensure the reductional segregation in meiosis I. Each bivalent should have at least one crossover, but more than one is also possible (Herbert et al., 2015). It has been observed that 10% of the oocytes have at least one achiasmate bivalent (Nagaoka et al., 2012) and that bivalents with only one chiasma are at higher risk of missegregation (Lamb et al., 1996). Chiasmata are held together by arm cohesin. Some positions on the chromosome arm are less optimal for forming chiasmata and this includes positions in the pericentromeric region and close to the chromosomes edges (Webster & Schuh, 2017). Chiasmata close to the chromosome edges have little distal cohesin that holds the chromosomes together. Thus, it is easier to be resolved because of cohesin loss during the prolonged dictyate arrest. This would result in two separate univalents aligning on the MI spindle (Lamb et al., 1996). On the other hand chiasmata close to the

centromeres are associated with MI non-disjunction, as its formation close to the centromere will disrupt centromeric cohesin. This will lead to premature separation of sister chromatids, which will be randomly segregated during anaphase II (Hassold & Hunt, 2001; Lamb et al., 1996).

1.11 Causes of age-related aneuploidy in human eggs

Many evidence have shown that chromosome architecture is compromised in oocytes from both mouse and humans with advanced maternal age (Chiang et al., 2010; Patel et al., 2015; Sakakibara et al., 2015; Zielinska et al., 2015). The two major problems that arise are the separation of sister kinetochores and the split of bivalents into two univalents. It is well established now that the protein complex responsible for the compromised chromosome architecture is the cohesin complex (Chiang et al., 2010; Hodges et al., 2005). Cohesin is loaded on the chromosomes during early stages of development and remains there for all the protracted period of the dictyate arrest without being replenished (Burkhardt et al., 2016; Tachibana-Konwalski et al., 2010). On top of that, the amount of cohesin on chromosomes declines with increasing female age and the same happens for the pericentromeric protector of cohesion, Sgo2 (Chiang et al., 2010; Lister et al., 2010).

1.11.1 Sister kinetochore separation

Evidence in mouse oocytes shows that with advanced female age, the distance between the two sister kinetochores increases (Chiang et al., 2010). Surprisingly in human oocytes, the sister kinetochores has been shown to separate even in younger women (Patel et al., 2015; Zielinska et al., 2015). Sister kinetochores are expected to function as a single unit in meiosis I, ensuring the separation of homologous chromosomes. However, loosely associated sister kinetochores can function independently and interact separately with microtubules. This makes them more susceptible to merotelic attachments (Zielinska et al., 2015).

1.11.2 Bivalents split into univalents

Cohesion loss from chromosome arms can also compromise the integrity of the bivalents. Arm cohesion stabilizes the chiasmata and holds bivalents together (Petronczki et al., 2003). Loss of cohesion leads to prominent gaps between the two homologous chromosomes in both aged mouse and human oocytes. In some cases, it can lead to complete separation into two univalents (Sakakibara et al., 2015; Zielinska et al., 2015). The univalents will be able to act as two independent units and align on the spindle in a mitotic way (Kouznetsova et al., 2007; Sakakibara et al., 2015; Zielinska et al., 2015).

1.12 Not all chromosomes are equally affected by aneuploidy

As described in the previous paragraphs there are major differences between oocytes and mitotic cells that prime the female gametes to aneuploidy. The majority of meiotic errors arise during meiosis I (Handyside et al., 2012). Even though some errors are detected in meiosis II, they originated from errors in meiosis I (Handyside et al., 2012). For example, split sister chromatids in meiosis I can segregate correctly and give rise to a meiosis II spindle with correct number of chromosomes. However, the two sister chromatids will behave as two independent units in meiosis II and can give rise to an error. Such an example is Reverse Segregation (Gruhn et al., 2019; Ottolini et al., 2015).

Error types have been shown to be age-dependent. Female fertility follows a U-curve, with the very young and older women at higher risk of aneuploidy (Gruhn et al., 2019). The most common age-related error is PSSC, which increases linearly with maternal age (Gruhn et al., 2019; Handyside et al., 2012). Reverse segregation is also elevated in older women. However, a recent study showed that the most common error type in younger women is NDJ (Gruhn et al., 2019).

Another important observation is that meiotic errors are also chromosome-dependent (Gruhn et al., 2019; Ottolini et al., 2015). Even though humans have 23 chromosomes, many cytogenetic studies over the years have shown that not all 23 chromosomes missegregate at the same frequency. More

specifically, from cytogenetic studies in the oocytes and the two polar bodies chromosomes 15, 16, 21, and 22 are the chromosomes with the highest missegregation frequency (Fragouli et al., 2011; Fragouli et al., 2010; Gabriel et al., 2011; Gruhn et al., 2019; Handyside et al., 2012; Hassold et al., 1996; Ottolini et al., 2015). Embryo biopsies from different embryonic stages have also shown that the same four chromosomes (15, 16, 21, 22) are the most commonly missegregated in the embryos (Franasiak et al., 2014; Nakhuda et al., 2018; Shahbazi et al., 2020). Errors in embryos can be of maternal or paternal origin or they can result from the first embryonic divisions. Some studies in embryos that assigned the errors to their parental origin, further indicate that chromosomes 15, 16, 21, 22 are missegregated as whole chromosomes (Franasiak et al., 2014) and are mainly missegregated to the embryo from the mother (McCoy et al., 2015; Tsuiko et al., 2021).

Humans have a wide variety of different chromosome morphologies, with different sizes and positions of the kinetochore. Depending on the position of kinetochore on the chromosome arm, chromosomes are categorized into four groups: 1) metacentric when the kinetochore is in the middle of the chromosome arm, 2) submetacentric when the two arms are unequal, 3) acrocentric when it is close to the edge and 4) telocentric when it is exactly at the distal part of the chromosome ("A proposed standard system of nomenclature of human mitotic chromosomes (Denver, Colorado)," 1960).

Humans have 17 metacentric and 5 acrocentric chromosomes. The acrocentric chromosomes are 13, 14, 15, 21 and 22. As it can also be seen from the data above chromosomes 15, 21, and 22 are the 3 out of 4 most missegregated chromosomes, and they belong in the group of acrocentric. Acrocentric chromosomes as a group have been reported as the most missegregated chromosome group in human meiosis (Franasiak et al., 2014; Gruhn et al., 2019). Even though a lot of studies indicate that acrocentric chromosomes are often missegregated the mechanism that this happens is not yet clear.

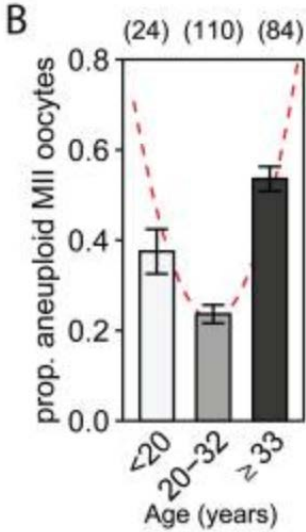


Figure 7: Aneuploidy in human oocytes follows a U-curve according to the female age

Human oocytes are significantly aneuploid throughout the reproductive life span of a human. However, aneuploidy rates peak in very young and older women. This creates a U-shaped curve of aneuploidy in humans during their reproductive life span. Graph taken from (Gruhn et al., 2019).

2. Objectives

Aim of manuscript 1

Studies of biopsies in human polar bodies and zygotes have shown that aneuploidy rates differ for different chromosomes during in human oocytes. Humans have a karyotype with a wide variety of chromosome morphologies, and current data indicate that the most vulnerable chromosome group is the acrocentric group. The goal of my PhD is to examine the behaviours of different chromosome subclasses during meiosis I, and to identify if there is a bias that primes one class of chromosomes to missegregate more than the other. However, human oocytes are only available in limited numbers. Therefore, I used porcine oocytes as a model to examine the behaviour of chromosome subclasses.

To this end, I collaborated with another PhD student in our lab (Agata Zielinska) in establishing a way of labelling the two chromosome groups in porcine cells. Moreover, I identified suitable markers for labelling different chromosomal regions in porcine oocyte. Then I confirmed that porcine oocytes are an appropriate system and that the chromosome classes interact with microtubules in the same way as in the human oocytes. Having established those tools, I was able to perform different types of imaging assays and to examine the behaviour of chromosomes live, during chromosome alignment, and during anaphase. Once the differences in behaviour were clear, I examined where those differences stem from and performed a morphological characterization of the bivalent structure. To address these questions, I used confocal and light-sheet microscopy for live experiments and super-resolution techniques such as airyscan confocal and 3D STED microscopy for fixed experiments.

Aim of manuscript 2

Manuscript 2 was an outcome of another collaboration with my colleague Agata Zielinska. The aim of her project was to identify how aging affects the centromere and kinetochore architecture and how those changes impact chromosome segregation. My contribution to the manuscript was to prove that Trim-Away of REC8 efficiently depletes cohesin in young mice by performing chromosome spreads in mouse oocytes, and to compare the efficiency of progression through meiosis between young and old mice. My data are shown in Figs. S2B and S3A-S3C of the manuscript.

3. Manuscript 1

(in preparation for submission)

Title: Bivalent architecture contributes to chromosome-specific aneuploidy in mammalian oocytes

Authors: Eirini Bellou¹, Agata P. Zielinska¹, Antonio Z. Politi¹, Eike Moennich¹, Antonina Wellecke¹, Katerina Menelaou¹, Claus Sibold², Andreas Tandler-Schneider², Melina Schuh^{1*}

Affiliations:

¹ Department of Meiosis, Max Planck Institute for Multidisciplinary Sciences, Göttingen, Germany

² Fertility Center Berlin, Berlin, German

*Corresponding author. Email: melina.schuh@mpinat.mpg.de

Title: Bivalent architecture contributes to chromosome-specific aneuploidy in mammalian oocytes

Authors: Eirini Bellou¹, Agata P. Zielinska¹, Antonio Z. Politi¹, Eike Moennich¹, Antonina Wellecke¹, Katerina Menelaou¹, Claus Sibold², Andreas Tandler-Schneider², Melina Schuh^{1*}

Affiliations:

¹ Department of Meiosis, Max Planck Institute for Multidisciplinary Sciences, Göttingen, Germany

² Fertility Center Berlin, Berlin, German

*Corresponding author. Email: melina.schuh@mpinat.mpg.de

Abstract:

Aneuploidy in human oocytes is a leading cause of miscarriages, infertility and genetic disorders such as Down Syndrome. Aneuploidy rates during meiosis are highly variable between individual chromosomes. The reason for this variability is unknown. Here, we show that both in human and porcine oocytes, acrocentric chromosomes are biased towards high aneuploidy due to their unique architecture during meiosis I. By devising methods to identify acro- and metacentric chromosomes in live and fixed oocytes, we demonstrate that acrocentric chromosomes often missegregate during meiosis I because they are incorrectly attached to spindle microtubules. Incorrect attachments are linked to local shielding of kinetochores by the small arm of acrocentric chromosomes, which does not recombine, and hence protrudes from the kinetochore region during meiosis I. This shielding hinders the formation of end-on kinetochore-microtubule attachments, providing an explanation for particularly high aneuploidy rates of acrocentric chromosomes during both female and male meiosis.

Introduction

For embryos to develop properly, they have to inherit the correct number of chromosomes from both parents. Human eggs frequently contain incorrect number of chromosomes, a condition known as aneuploidy (Herbert et al., 2015). Aneuploidy in human eggs increases with maternal age and follows a U-shaped curve that elevates from 25% in women in their early twenties to 50% above the age of 33 (Gruhn et al., 2019).

Aneuploidy in eggs frequently arises from chromosome segregation errors during meiosis I, which is error-prone in humans (Holubcova et al., 2015). In meiosis I, homologous chromosomes pair with each other to create a unique structure called the bivalent (Herbert et al., 2015; Webster & Schuh, 2017). Human oocytes often assemble unstable spindles that lead to chromosome missegregation (Holubcova et al., 2015). Interestingly, different chromosomes are missegregated at different frequencies (Gruhn et al., 2019; Ottolini et al., 2015). Humans have 23 chromosomes with different morphologies, including the size and the position of the kinetochore. Based on the kinetochore position, we separate the chromosomes into four categories: metacentric, submetacentric, acrocentric and telocentric ("A proposed standard system of nomenclature of human mitotic chromosomes (Denver, Colorado)," 1960).

Previous studies looking at segregation of individual chromosomes segregation in human eggs show that the most commonly missegregated chromosomes are chromosomes 15, 16, 21, and 22 (Fragouli et al., 2011; Fragouli et al., 2010; Gabriel et al., 2011; Gruhn et al., 2019; Handyside et al., 2012; Hassold et al., 1996; Ottolini et al., 2015). Chromosome 15, 21, and 22 are characterised as acrocentric chromosomes.

Similarly, data from embryo biopsies show that the same four chromosomes are the most missegregated in the embryos (Franasiak et al., 2014; Nakhuda et al., 2018; Shahbazi et al., 2020). It is further suggested, that these four are often missegregated as whole chromosomes (Franasiak et al., 2014) and are of maternal origin (McCoy et al., 2015; Tsuiko et al., 2021). Acrocentric chromosomes

are also missegregated at a high frequency in human spermatocytes (Bell et al., 2020; Soares et al., 2001). Together, these studies indicate that acrocentric chromosomes are the most frequently missegregated chromosomes in meiosis.

In contrast, chromosomes 1, 2, 3, 9, and X, but not the acrocentric chromosomes, are more often missegregated in mitosis (Dumont et al., 2020; Tovini & McClelland, 2019; Worrall et al., 2018). This difference between mitosis and meiosis leads us to the hypothesis that the meiosis-specific bivalent morphology of acrocentric chromosomes plays a role in chromosome segregation fate during the meiotic divisions.

Human oocytes are limited in availability. To perform in-depth characterization of chromosomes from different morphological groups, we utilized the porcine model system. Porcine oocytes have a human-like karyotype that includes both metacentric and acrocentric chromosomes (Hansen, 1977). Furthermore, porcine karyotype has a preserved pericentromeric region for all acrocentric chromosomes and a distinct but preserved pericentromeric region for the majority of metacentric chromosomes (Rogel-Gaillard et al., 1997). This makes it possible to establish pericentromeric fluorescent labelling for each chromosome class separately, using TALEs. TALEs fused with a fluorophore have previously been used successfully for live-cell imaging of chromosomes in other model systems (Miyanari et al., 2013).

In this study, we found that bivalent morphology influences the interaction between spindle microtubules and kinetochores. We analysed the behaviour of the acrocentric chromosomes during meiosis in porcine and human oocytes, and found that acrocentric chromosomes are more often erroneously attached to microtubules than metacentric chromosomes. Sterical hindrance of the small arm of the acrocentric chromosomes, which often localizes on top of the kinetochore, obstruct end-on interaction with the microtubule. As a consequence of incorrect attachments, acrocentric chromosomes missegregate more often than the metacentric in meiosis I in both porcine and human eggs.

Results

Human acrocentric chromosomes are prone to erroneous kinetochore-microtubule attachments

Acrocentric chromosomes have their kinetochores close to the edge of their chromosome arm. Thus, because the one arm is so short their kinetochores are in proximity to their telomeres (Fig. 1A). This morphological feature allowed us to separate acrocentric and metacentric chromosomes (Fig 1B) and investigate how they interact with microtubules. Analysis of attachments in human oocytes was separated into the 3 following categories: end-on, unattached, and lateral/merotelic (Fig. 1C).

Kinetochores of acrocentric chromosomes formed significantly fewer end-on attachments and more lateral/merotelic attachments compared to metacentric chromosomes. (Fig. 1D). Together these data indicate that acrocentric chromosomes are more prone to form erroneous microtubule attachments than the metacentric chromosomes.

Porcine acrocentric chromosomes are prone to erroneous attachment creation

Studies in human oocytes are limited by sample scarcity. Porcine oocyte meiosis resemble meiosis in human oocytes (So et al., 2022; Zielinska et al., 2019) and are easily accessible. Furthermore, porcine oocytes have a human-like karyotype that includes both acrocentric and metacentric chromosomes (Hansen, 1977). This makes porcine oocytes an ideal model for the characterization of the behavior of each chromosome group.

Porcine karyotype has a similar pericentromeric sequence repeat for each of the two chromosome groups (Rogel-Gaillard et al., 1997). This allowed us to selectively label the two chromosome classes by creating fluorescently labelled Transcription Activator Like Effectors (TALEs) (Fig. 2A) (Miyanari et al., 2013). Injection of the cells with the fluorescent TALE for the acrocentric chromosomes (Acrocentric-TALE) separates the chromosomes in the two experimental groups: The labelled group of acrocentric chromosomes and the unlabelled group of metacentric chromosomes. These two groups will be henceforth referred to as “Acro-labelled” and “Meta” (Fig S2A). A Metacentric-TALE that only

labels a fraction of the metacentric chromosomes (6/12) was also created. It was used as a control to verify that the presence of the Acrocentric-TALE is not responsible for the phenotypes observed in the acrocentric chromosomes (Fig. S2A). This labelled group is referred to as “Meta-labelled”. The remaining unlabelled chromosomes is a mix of acrocentric and metacentric chromosomes and was not used for quantifications. Examples of labelled chromosomes with the Acrocentric and Metacentric Tale are shown for Metaphase I and II spindles of intact cells (Fig. S2B and C).

Similar to our observations in human oocytes, we found that kinetochores of Acro-labelled chromosomes formed significantly fewer end-on attachments and significantly higher lateral/merotelic than that of Meta- and Meta-labelled chromosomes. (Fig.2B and 2D). This suggests that the two classes of chromosomes behave similarly in humans and in pigs, prompting us to investigate their behaviors in porcine oocytes further.

Additionally, we performed the same analysis of attachment types in cold-treated metaphase II porcine spindles (Fig 2C). No difference is observed between the two morphological groups in Metaphase II in porcine oocytes. Furthermore, the vast majority of kinetochores is attached end-on to the spindle microtubules (Fig 2E). These data confirm our initial hypothesis that specifically the morphology of the bivalents in meiosis I influences the interaction of the acrocentric chromosomes to the microtubules.

Acrocentric chromosomes are lagging during anaphase and misalign during late metaphase more often than the metacentric

To characterize the behavior of the two subclasses during anaphase I we co-expressed the Acrocentric-TALE or the Metacentric-TALE with the kinetochore marker CENPC and performed live-cell imaging at late metaphase I stage. In most cases, the cause for misaligned and lagging chromosomes is the formation of erroneous attachments, specifically lateral/merotelic microtubule attachments (Cimini et al., 2004; Thompson & Compton, 2011). Of the cells examined, 23% failed to segregate the chromosomes properly during meiosis I, resulting in an aneuploid egg. The missegregation frequency

for the Acro-labelled chromosomes was 8% and only 1% of the metacentric chromosomes were missegregated (Fig 3A and B). Following this, 85% of the missegregated chromosomes had an acrocentric morphology (Fig. S3A).

As previously described, lagging chromosomes can be an outcome of incorrect microtubule attachments, but not all lagging chromosomes lead to aneuploidy (Cimini et al., 2004; Mihajlovic et al., 2021). We found that there were two different types of missegregating chromosomes in porcine oocytes: the anaphase lagging chromosomes and the severely misaligned chromosomes. The two ways of missegregation contributed 66% and 33% to aneuploidy, respectively (Fig. 3C). Because the majority of errors come from lagging chromosomes, we further quantified the status of lagging chromosomes during anaphase. Examples of the different missegregation types can be seen in Figure 3D. Mildly misaligned chromosomes were considered chromosomes that were lagging 12 min after anaphase onset and severely misaligned chromosomes lagging 20 min after anaphase onset. We found that acro-labelled chromosomes were four times more likely to be mildly lagging, and six times more likely to be severely lagging when compared to Meta-labelled chromosomes (Fig. 3E and F). Meta-labelled chromosomes behaved similarly to Meta chromosomes, confirming that the presence of TALE did not alter chromosome behavior (Fig. 3B, E and F).

To further investigate chromosome behaviour before anaphase I onset, we imaged chromosome congression at high spatiotemporal resolution using lightsheet microscopy and performed kinetochore tracking (Fig. 3G) similar to previous studies (Kitajima et al., 2011). From these images, we measured the angle of the bivalent axis towards the spindle axis by calculating the dot product. The majority of the correctly attached chromosomes before anaphase are oriented parallel to the spindle axis which results in a dot product of 1. We observed that acrocentric chromosomes underwent 3 distinct rounds of rearrangement of their angle towards the spindle axis in the last 2.5 h before anaphase onset (Fig. 3H and I). We further observed that during their alignment to the metaphase plate, the acrocentric chromosomes occupy positions $\sim 1 \mu\text{m}$ outside of the metaphase plate. In contrast, the metacentric

chromosomes are located in the center of the spindle axis (Fig. 3J, K and S3B). Together, our data suggest that acrocentric chromosomes are more likely to be found outside the metaphase plate, to be tilted during alignment and to lag behind during anaphase compared to metacentric chromosomes.

Acrocentric chromosomes missegregate more often than the metacentric

Next, we examined the aneuploidy and missegregation rates by kinetochore counting in fixed MII porcine eggs (Fig. 4A). We found that 26% of the eggs were aneuploid (Fig 4B). Out of all the chromosomes examined in each group, acrocentric and metacentric chromosomes missegregated at a frequency of 7% and 1%, respectively (Fig 4C). The results obtained are similar to the live data and confirm the higher missegregation frequency of the acrocentric chromosomes.

The small arm of acrocentric chromosomes hinders the end-on microtubule attachment creation

We next investigated if there are morphological differences in the acrocentric chromosomes that can explain the higher rate of erroneous microtubule attachments. Metacentric chromosomes have two equally sized arms and usually form chiasmata in both. The presence of the chiasmata will link the two arms together and prevent obstruction of the kinetochore, leaving it easily accessible for the spindle microtubules, vertical to the spindle axis. Acrocentric chromosomes, however, have the kinetochore very close to the chromosome edge because of the small (p) arm on which usually no chiasmata form. The fact that the short arm is not folded backwards, towards bivalent center, could cause differences in the kinetochore angle. The lack of tension from one side could affect the angle of the kinetochores towards the spindle axis. To measure the angle of the kinetochores and the spindle axis, we performed isotropic 3D-STED imaging, followed by automated segmentation of the kinetochore signal (Fig.5A and B). The angle of each kinetochore was compared by measuring the dot product (Fig. 5C). We found that kinetochores of acro-labelled chromosomes are more often oriented parallel to the spindle axis, while those of Meta and the Meta-labelled chromosomes were predominantly oriented horizontally to it (Fig. 5D). From the distribution of the angles in the different groups, we could observe that the angles of the acro-labelled chromosomes are distributed across the entire spectrum while the meta

and the meta-labelled are mostly centered around 0.25 units (Fig. 5E). The orientation of kinetochores of acrocentric chromosomes might reflect that they are less accessible to microtubules and hence, less likely to form end-on attachments.

The short arm of acrocentric chromosomes renders the telomeres in close proximity to their kinetochores. Thus, in addition to the angle of the kinetochore to the spindle axis, another factor that could interfere with kinetochore-microtubule attachments is the position of the small arm. To test this possibility, we examined the relative positions of the kinetochores and small arms for acrocentric chromosomes using the positions of telomeres as a proxy. We found that there are two distinct orientations of small arms relative to the kinetochores. 20% of the kinetochores had the small arms on-top and 80% of the kinetochores had the small arms on the side (Fig 5F and Fig S5A).

To investigate the impact of the different orientations of the small arm in the creation of microtubule attachments, we performed a cold stable assay with labelled telomeres and we quantified the types of attachments for the two different morphologies of acrocentric chromosomes (Fig 5H). We identified the acro-labelled chromosomes by the presence of telomeres next to the kinetochores. We found that the kinetochores with the telomeres on top rarely form correct attachments, with only 7% being attached end-on. The remaining 93% of those kinetochores were either unattached or attached laterally/merotelically in equal percentages. This is in contrast to the other group of kinetochores with telomeres on the side where 60% of kinetochores were able to form end-on attachments (Fig. 5G). Next, we analyzed if the two types of small arm configurations changes over the course of meiosis. To this end, we performed the analysis in both early and late metaphase spindles, which were different in terms of spindle pole morphology and chromosome alignment. We observed that kinetochores with the on-top configuration were 26% and 13% in early and late metaphase, respectively (Fig. 5I). This suggests that the small arm can take two different configurations and the position of the arm affects the creation of end-on attachments.

The two acrocentric small arm configurations could also be observed in human oocytes (Fig 5J). The distribution of microtubule attachments to the different configurations was similar to the one in porcine oocytes. In human acrocentric chromosomes with on-top telomere-kinetochore configuration 30% had end-on attached microtubules and the rest 70% had equal amount of unattached and lateral/merotelic attachments. On the other hand, the kinetochores with the telomeres on the side were 70% end-on attached and 30% were distributed between unattached and lateral/merotelic attachments (Fig 5K). Overall, our data suggest that the small arm of the acrocentric chromosomes could affect the orientation of the kinetochore and hinder correct microtubule interaction.

Pig acrocentric chromosomes have on average less cohesin than metacentric chromosomes

Acrocentric chromosomes are also susceptible to age-related aneuploidy (Gruhn et al., 2019). The major mechanism involved in age-related aneuploidy is the premature separation of sister chromatids (PSSC) (Gruhn et al., 2019) and the key player of age-related aneuploidy is pericentromeric cohesin loss (Chiang et al., 2010; Lister et al., 2010; Tsutsumi et al., 2014). We asked whether the acrocentric and metacentric chromosomes also differ in the levels of pericentromeric cohesin. We first measured the interkinetochore distance between the sister chromatids in meiosis II. We found that the group of acrocentric chromosomes had on average an interkinetochore distance of 1.09 μm , while the Meta and Meta-labelled had 0.96 μm and 0.97 μm respectively (Fig 6A and B). From the microtubule attachment analysis in MII we know that there is no difference between acrocentric and metacentric chromosomes and 95% of kinetochores are end-on attached (Fig 2E). Since the interkinetochore distance was not due to different attachment types, we reasoned that the difference is likely a result of unequal cohesin levels.

During meiosis I the bivalents are held together with the pericentromeric cohesin and the arm cohesin. The second will be cleaved at anaphase I onset while the centromeric cohesin will remain to hold the sister chromatids together during meiosis II (Gomez et al., 2007; Llano et al., 2008). To investigate whether cohesin is responsible for the difference in the interkinetochore distance we

measured the centromeric cohesion in intact MII eggs. Cells were stained with anti-SMC3, a universal cohesin subunit (Fig. 6C). The intensity of SMC3 was measured between the two sister kinetochores. Acro-labelled chromosomes had on average 0.8 units of centromeric cohesion while Meta and Meta-labelled had on average 1.07 units (Fig. 6D). To complement the above finding, we also measured the level of centromeric cohesin of bivalents in MI by staining with anti-REC8. An identical sphere of 1 μ m radius was created from the center of each kinetochore (Fig. 6E). The cohesion in the pericentromeric region of acro-labelled, Meta, and Meta-labelled bivalents was similar to the levels observed in MII (Fig. 6F). Thus we conclude that Acro-labelled chromosomes have on average less pericentromeric cohesion than the Meta both in MI and in MII.

If the acrocentric chromosomes have lower cohesin levels, we would expect these chromosomes to separate first after acute cohesin depletion. To test this hypothesis, we depleted REC8 in MII porcine eggs in the presence of the acrocentric and the metacentric TALEs. This allows for better identification and direct comparison of the six labelled chromosomes in each group. We used the TRIM-away method for acute protein depletion (Clift et al., 2017). The first chromosome that separates after depletion of REC8 was 9/10 times an acrocentric chromosome (Fig. S6A). We also compared the time of separation for each of the six acro-labelled and meta-labelled chromosomes. Acro-labelled chromosomes were usually faster than the metacentric in each separation event. However, the high discrepancy of the timings indicates differences in the levels of cohesion within each group (Fig. S6B). This suggests that the acro-labelled chromosomes in porcine oocytes have on average less cohesin than the meta-labelled, but there are also differences among the individual chromosomes.

Discussion

Our study revealed that, in meiosis I, acrocentric chromosomes formed less end-on microtubule attachments and were more prone to missegregation than metacentric chromosomes. We observed

this both in human and porcine oocytes. We propose that the morphology of acrocentric bivalents and the geometrical constraint imposed by their small arms make this group of chromosomes more likely to missegregate during the first meiotic division. Furthermore, kinetochores of acrocentric chromosomes are more often oriented parallel to the spindle axis compared to the metacentric chromosomes. This, in addition to the small arm sterically obstructing the kinetochore, interferes with the creation of end-on microtubule attachments. We show, for the first time, that the small arm of acrocentric chromosomes has two different configurations: either on top of the kinetochore or on the side. An on-top configuration negatively affects the establishment of the correct microtubule attachments both in humans and in porcine oocytes.

We further compared the behaviours of acrocentric and metacentric chromosomes in live porcine oocytes. We demonstrated that acrocentric chromosomes were more often misaligned and lag during anaphase I and thus more often missegregate in meiosis I. Lagging chromosomes is a common outcome of improper kinetochore-microtubule attachments as it has been shown previously (Cimini et al., 2004; Mihajlovic et al., 2021; Thompson & Compton, 2011).

Chromosome specific aneuploidy has been observed both in meiosis (Bell et al., 2020; Fragouli et al., 2011; Fragouli et al., 2010; Franasiak et al., 2014; Gruhn et al., 2019; Handyside et al., 2012; McCoy et al., 2015; Nakhuda et al., 2018; Ottolini et al., 2015; Shahbazi et al., 2020; Soares et al., 2001; Tsuiko et al., 2021) and mitosis (Dumont et al., 2020; Tovini & McClelland, 2019; Worrall et al., 2018). However, the chromosomes affected differ between the two divisions. This difference between mitosis and meiosis further supports our hypothesis that the meiosis-specific bivalent morphology (of acrocentric chromosomes) plays a role in chromosome segregation in meiosis. Our data that the acrocentric chromosomes are highly missegregated in meiosis I are in line with previous work in the field. However, this is the first time that the bivalent morphology is linked to the error prone nature of acrocentric chromosomes and the high frequency of incorrect kinetochore-microtubule attachments.

In mitosis more than one mechanism seem to play a role in chromosome missegregation (Worrall et al., 2018). Chromosomes with low abundance of DNA-dependent centromeric components like chromosomes 3, 6, and X, are more prone to missegregate (Dumont et al., 2020) and large chromosomes are generally more susceptible to missegregation under impaired CENPE function (Tovini & McClelland, 2019). Missegregation of chromosomes 1 and 2 is particularly increased by microtubule poisons (Worrall et al., 2018) and that of 1, 9, and 16 by heterochromatin hypomethylation (Fauth et al., 1998). Aneuploidy is a basic cause of cancer with certain chromosome aneuploidies being tumor-specific. Generally, solid tumors present a higher loss of small chromosomes (Duijf et al., 2013) while primary glioblastoma cells present a higher missegregation of large chromosomes into micronuclei (Bochtler et al., 2019). In contrast to meiosis, acrocentric chromosomes have not been shown to missegregate in mitosis. In mitosis the sister chromatids biorient to the two different spindle poles to achieve that chromosomes are vertically aligned to the spindle axis. Thus, differences in arm length should not affect the orientation of the kinetochore or the exposure of the kinetochore to the microtubules. For this reason, morphological differences between chromosomes may not influence chromosome segregation in mitosis. Nevertheless, individual kinetochore characteristics play a major role in chromosome-specific missegregation in mitosis, yet with lower aneuploidy rates compared to meiosis. We do not exclude the possibility that apart from the bivalent morphology, these parameters also contribute in chromosome-specific aneuploidy in meiosis.

Multiple factors contribute to the high aneuploidy rates in human oocytes, including spindle instability (Holubcova et al., 2015; So et al., 2022) and split kinetochores (Zielinska et al., 2015). In this study, we add an additional factor, and we show how the bivalent morphology makes some chromosomes more susceptible to missegregation. Different species have different chromosomes morphologies. Unlike pigs that have a human-like karyotype, cows do not have metacentric chromosomes. In line with our hypothesis, cow oocytes present a higher level of aneuploidy compared to pigs (So et al., 2022).

In human sperm, meiosis lasts 50-70 days, which is a much shorter period compared to the protracted dicyate arrest of oocytes (Neto et al., 2016). Thus, spermatocytes are not affected in the same way by age-related aneuploidy. However, even though the total aneuploidy rate is lower, acrocentric chromosomes are shown to missegregate more than the metacentric chromosomes in human spermatocytes (Bell et al., 2020; Soares et al., 2001). This further supports our hypothesis that the bivalent morphology indeed affects the segregation outcome of meiosis I.

The distribution of the acrocentric small arm configurations differed between early and late metaphase, where the number of “on-top” configurations decreased in late compared to early metaphase I. As the creation of more end-on attachments is correlated with fewer on-top configurations, we speculate that there might be a competition between the microtubules and the small chromosome arms for the establishment of end-on attachments. The length of the small arm might vary between the acrocentric chromosomes of different species. Thus, there could be species-specific differences in the amount of interference that it causes.

Acrocentric chromosomes show increased missegregation with aging in humans (Gruhn et al., 2019). Cohesin loss is the major contributor to age-related aneuploidy (Chiang et al., 2010; Lister et al., 2010; Tsutsumi et al., 2014). We examined the levels of cohesin in acrocentric chromosomes compared to metacentric chromosomes in porcine oocytes. Our findings show that in the porcine system, acrocentric chromosomes have on average less cohesin than the metacentric, which could make them more vulnerable to age-related cohesin loss. However, differences in the levels of cohesin of individual chromosomes within each group can further influence the age-related susceptibility. It remains to be investigated whether the difference in cohesion levels between chromosomes of different morphology is the case also in human oocytes. However, it has been shown that acrocentric chromosomes are contributing to age-related aneuploidy and are particularly prone to reverse segregation while aging (Gruhn et al., 2019).

References

- Bajar, B. T., Wang, E. S., Lam, A. J., Kim, B. B., Jacobs, C. L., Howe, E. S., Davidson, M. W., Lin, M. Z., & Chu, J. (2016). Improving brightness and photostability of green and red fluorescent proteins for live cell imaging and FRET reporting. *Sci Rep*, *6*, 20889. <https://doi.org/10.1038/srep20889>
- Bell, A. D., Mello, C. J., Nemes, J., Brumbaugh, S. A., Wysoker, A., & McCarroll, S. A. (2020). Insights into variation in meiosis from 31,228 human sperm genomes. *Nature*, *583*(7815), 259-264. <https://doi.org/10.1038/s41586-020-2347-0>
- Bindels, D. S., Haarbosch, L., van Weeren, L., Postma, M., Wiese, K. E., Mastop, M., Aumonier, S., Gotthard, G., Royant, A., Hink, M. A., & Gadella, T. W., Jr. (2017). mScarlet: a bright monomeric red fluorescent protein for cellular imaging. *Nat Methods*, *14*(1), 53-56. <https://doi.org/10.1038/nmeth.4074>
- Bochtler, T., Kartal-Kaess, M., Granzow, M., Hielscher, T., Cosenza, M. R., Herold-Mende, C., Jauch, A., & Kramer, A. (2019). Micronucleus formation in human cancer cells is biased by chromosome size. *Genes Chromosomes Cancer*, *58*(6), 392-395. <https://doi.org/10.1002/gcc.22707>
- Bucevicius, J., Kostiuk, G., Gerasimaite, R., Gilat, T., & Lukinavicius, G. (2020). Enhancing the biocompatibility of rhodamine fluorescent probes by a neighbouring group effect. *Chem Sci*, *11*(28), 7313-7323. <https://doi.org/10.1039/d0sc02154g>
- Cavazza, T., Takeda, Y., Politi, A. Z., Aushev, M., Aldag, P., Baker, C., Choudhary, M., Bucevicius, J., Lukinavicius, G., Elder, K., Blayney, M., Lucas-Hahn, A., Niemann, H., Herbert, M., & Schuh, M. (2021). Parental genome unification is highly error-prone in mammalian embryos. *Cell*, *184*(11), 2860-2877 e2822. <https://doi.org/10.1016/j.cell.2021.04.013>
- Cermak, T., Starker, C. G., & Voytas, D. F. (2015). Efficient design and assembly of custom TALENs using the Golden Gate platform. *Methods Mol Biol*, *1239*, 133-159. https://doi.org/10.1007/978-1-4939-1862-1_7
- Chiang, T., Duncan, F. E., Schindler, K., Schultz, R. M., & Lampson, M. A. (2010). Evidence that weakened centromere cohesion is a leading cause of age-related aneuploidy in oocytes. *Curr Biol*, *20*(17), 1522-1528. <https://doi.org/10.1016/j.cub.2010.06.069>
- Cimini, D., Cameron, L. A., & Salmon, E. D. (2004). Anaphase spindle mechanics prevent mis-segregation of merotelically oriented chromosomes. *Curr Biol*, *14*(23), 2149-2155. <https://doi.org/10.1016/j.cub.2004.11.029>

- Clift, D., McEwan, W. A., Labzin, L. I., Konieczny, V., Mogessie, B., James, L. C., & Schuh, M. (2017). A Method for the Acute and Rapid Degradation of Endogenous Proteins. *Cell*, *171*(7), 1692-1706 e1618. <https://doi.org/10.1016/j.cell.2017.10.033>
- Duijf, P. H., Schultz, N., & Benezra, R. (2013). Cancer cells preferentially lose small chromosomes. *Int J Cancer*, *132*(10), 2316-2326. <https://doi.org/10.1002/ijc.27924>
- Dumont, M., Gamba, R., Gestraud, P., Klaasen, S., Worrall, J. T., De Vries, S. G., Boudreau, V., Salinas-Luybaert, C., Maddox, P. S., Lens, S. M., Kops, G. J., McClelland, S. E., Miga, K. H., & Fachinetti, D. (2020). Human chromosome-specific aneuploidy is influenced by DNA-dependent centromeric features. *EMBO J*, *39*(2), e102924. <https://doi.org/10.15252/emj.2019102924>
- Eijpe, M., Offenbergh, H., Jessberger, R., Revenkova, E., & Heyting, C. (2003). Meiotic cohesin REC8 marks the axial elements of rat synaptonemal complexes before cohesins SMC1beta and SMC3. *J Cell Biol*, *160*(5), 657-670. <https://doi.org/10.1083/jcb.200212080>
- Fauth, E., Scherthan, H., & Zankl, H. (1998). Frequencies of occurrence of all human chromosomes in micronuclei from normal and 5-azacytidine-treated lymphocytes as revealed by chromosome painting. *Mutagenesis*, *13*(3), 235-241. <https://doi.org/10.1093/mutage/13.3.235>
- Fragouli, E., Alfarawati, S., Goodall, N. N., Sanchez-Garcia, J. F., Colls, P., & Wells, D. (2011). The cytogenetics of polar bodies: insights into female meiosis and the diagnosis of aneuploidy. *Mol Hum Reprod*, *17*(5), 286-295. <https://doi.org/10.1093/molehr/gar024>
- Fragouli, E., Katz-Jaffe, M., Alfarawati, S., Stevens, J., Colls, P., Goodall, N. N., Tormasi, S., Gutierrez-Mateo, C., Prates, R., Schoolcraft, W. B., Munne, S., & Wells, D. (2010). Comprehensive chromosome screening of polar bodies and blastocysts from couples experiencing repeated implantation failure. *Fertil Steril*, *94*(3), 875-887. <https://doi.org/10.1016/j.fertnstert.2009.04.053>
- Franasiak, J. M., Forman, E. J., Hong, K. H., Werner, M. D., Upham, K. M., Treff, N. R., & Scott, R. T. (2014). Aneuploidy across individual chromosomes at the embryonic level in trophectoderm biopsies: changes with patient age and chromosome structure. *J Assist Reprod Genet*, *31*(11), 1501-1509. <https://doi.org/10.1007/s10815-014-0333-x>
- Gabriel, A. S., Thornhill, A. R., Ottolini, C. S., Gordon, A., Brown, A. P., Taylor, J., Bennett, K., Handyside, A., & Griffin, D. K. (2011). Array comparative genomic hybridisation on first polar bodies suggests that non-disjunction is not the predominant mechanism leading to aneuploidy in humans. *J Med Genet*, *48*(7), 433-437. <https://doi.org/10.1136/jmg.2010.088070>
- Gomez, R., Valdeolillos, A., Parra, M. T., Viera, A., Carreiro, C., Roncal, F., Rufas, J. S., Barbero, J. L., & Suja, J. A. (2007). Mammalian SGO2 appears at the inner centromere domain and

- redistributes depending on tension across centromeres during meiosis II and mitosis. *EMBO Rep*, 8(2), 173-180. <https://doi.org/10.1038/sj.embor.7400877>
- Gruhn, J. R., Zielinska, A. P., Shukla, V., Blanshard, R., Capalbo, A., Cimadomo, D., Nikiforov, D., Chan, A. C., Newnham, L. J., Vogel, I., Scarica, C., Krapchev, M., Taylor, D., Kristensen, S. G., Cheng, J., Ernst, E., Bjorn, A. B., Colmorn, L. B., Blayney, M., . . . Hoffmann, E. R. (2019). Chromosome errors in human eggs shape natural fertility over reproductive life span. *Science*, 365(6460), 1466-1469. <https://doi.org/10.1126/science.aav7321>
- Handyside, A. H., Montag, M., Magli, M. C., Repping, S., Harper, J., Schmutzler, A., Vesela, K., Gianaroli, L., & Geraedts, J. (2012). Multiple meiotic errors caused by predivision of chromatids in women of advanced maternal age undergoing in vitro fertilisation. *Eur J Hum Genet*, 20(7), 742-747. <https://doi.org/10.1038/ejhg.2011.272>
- Hansen, K. (1977). Identification of the chromosomes of the domestic pig (*Sus scrofa domestica*). An identification key and a landmark system. *Ann Genet Sel Anim*, 9(4), 517-526. <https://doi.org/10.1186/1297-9686-9-4-517>
- Hassold, T., Abruzzo, M., Adkins, K., Griffin, D., Merrill, M., Millie, E., Saker, D., Shen, J., & Zaragoza, M. (1996). Human aneuploidy: incidence, origin, and etiology. *Environ Mol Mutagen*, 28(3), 167-175. [https://doi.org/10.1002/\(SICI\)1098-2280\(1996\)28:3<167::AID-EM2>3.0.CO;2-B](https://doi.org/10.1002/(SICI)1098-2280(1996)28:3<167::AID-EM2>3.0.CO;2-B)
- Herbert, M., Kalleas, D., Cooney, D., Lamb, M., & Lister, L. (2015). Meiosis and maternal aging: insights from aneuploid oocytes and trisomy births. *Cold Spring Harb Perspect Biol*, 7(4), a017970. <https://doi.org/10.1101/cshperspect.a017970>
- Holubcova, Z., Blayney, M., Elder, K., & Schuh, M. (2015). Human oocytes. Error-prone chromosome-mediated spindle assembly favors chromosome segregation defects in human oocytes. *Science*, 348(6239), 1143-1147. <https://doi.org/10.1126/science.aaa9529>
- Jaffe, L. A., & Terasaki, M. (2004). Quantitative microinjection of oocytes, eggs, and embryos. *Methods Cell Biol*, 74, 219-242. [https://doi.org/10.1016/s0091-679x\(04\)74010-8](https://doi.org/10.1016/s0091-679x(04)74010-8)
- Jaqaman, K., Loerke, D., Mettlen, M., Kuwata, H., Grinstein, S., Schmid, S. L., & Danuser, G. (2008). Robust single-particle tracking in live-cell time-lapse sequences. *Nat Methods*, 5(8), 695-702. <https://doi.org/10.1038/nmeth.1237>
- Kitajima, T. S., Ohsugi, M., & Ellenberg, J. (2011). Complete kinetochore tracking reveals error-prone homologous chromosome biorientation in mammalian oocytes. *Cell*, 146(4), 568-581. <https://doi.org/10.1016/j.cell.2011.07.031>
- Legland, D., Arganda-Carreras, I., & Andrey, P. (2016). MorphoLibJ: integrated library and plugins for mathematical morphology with ImageJ. *Bioinformatics*, 32(22), 3532-3534. <https://doi.org/10.1093/bioinformatics/btw413>

- Lister, L. M., Kouznetsova, A., Hyslop, L. A., Kalleas, D., Pace, S. L., Barel, J. C., Nathan, A., Floros, V., Adelfalk, C., Watanabe, Y., Jessberger, R., Kirkwood, T. B., Hoog, C., & Herbert, M. (2010). Age-related meiotic segregation errors in mammalian oocytes are preceded by depletion of cohesin and Sgo2. *Curr Biol*, *20*(17), 1511-1521. <https://doi.org/10.1016/j.cub.2010.08.023>
- Llano, E., Gomez, R., Gutierrez-Caballero, C., Herran, Y., Sanchez-Martin, M., Vazquez-Quinones, L., Hernandez, T., de Alava, E., Cuadrado, A., Barbero, J. L., Suja, J. A., & Pendas, A. M. (2008). Shugoshin-2 is essential for the completion of meiosis but not for mitotic cell division in mice. *Genes Dev*, *22*(17), 2400-2413. <https://doi.org/10.1101/gad.475308>
- McCoy, R. C., Demko, Z. P., Ryan, A., Banjevic, M., Hill, M., Sigurjonsson, S., Rabinowitz, M., & Petrov, D. A. (2015). Evidence of Selection against Complex Mitotic-Origin Aneuploidy during Preimplantation Development. *PLoS Genet*, *11*(10), e1005601. <https://doi.org/10.1371/journal.pgen.1005601>
- Mihajlovic, A. I., Haverfield, J., & FitzHarris, G. (2021). Distinct classes of lagging chromosome underpin age-related oocyte aneuploidy in mouse. *Dev Cell*, *56*(16), 2273-2283 e2273. <https://doi.org/10.1016/j.devcel.2021.07.022>
- Miyanari, Y., Ziegler-Birling, C., & Torres-Padilla, M. E. (2013). Live visualization of chromatin dynamics with fluorescent TALEs. *Nat Struct Mol Biol*, *20*(11), 1321-1324. <https://doi.org/10.1038/nsmb.2680>
- Nakhuda, G., Jing, C., Butler, R., Guimond, C., Hitkari, J., Taylor, E., Tallon, N., & Yuzpe, A. (2018). Frequencies of chromosome-specific mosaicisms in trophoectoderm biopsies detected by next-generation sequencing. *Fertil Steril*, *109*(5), 857-865. <https://doi.org/10.1016/j.fertnstert.2018.01.011>
- Neto, F. T., Bach, P. V., Najari, B. B., Li, P. S., & Goldstein, M. (2016). Spermatogenesis in humans and its affecting factors. *Semin Cell Dev Biol*, *59*, 10-26. <https://doi.org/10.1016/j.semcdb.2016.04.009>
- Ottolini, C. S., Newnham, L., Capalbo, A., Natesan, S. A., Joshi, H. A., Cimadomo, D., Griffin, D. K., Sage, K., Summers, M. C., Thornhill, A. R., Housworth, E., Herbert, A. D., Rienzi, L., Ubaldi, F. M., Handyside, A. H., & Hoffmann, E. R. (2015). Genome-wide maps of recombination and chromosome segregation in human oocytes and embryos show selection for maternal recombination rates. *Nat Genet*, *47*(7), 727-735. <https://doi.org/10.1038/ng.3306>
- Parslow, A., Cardona, A., & Bryson-Richardson, R. J. (2014). Sample drift correction following 4D confocal time-lapse imaging. *J Vis Exp*(86). <https://doi.org/10.3791/51086>
- Politi, A. Z., Cai, Y., Walther, N., Hossain, M. J., Koch, B., Wachsmuth, M., & Ellenberg, J. (2018). Quantitative mapping of fluorescently tagged cellular proteins using FCS-calibrated four-dimensional imaging. *Nat Protoc*, *13*(6), 1445-1464. <https://doi.org/10.1038/nprot.2018.040>

- A proposed standard system of nomenclature of human mitotic chromosomes (Denver, Colorado). (1960). *Ann Hum Genet*, 24, 319-325. <https://doi.org/10.1111/j.1469-1809.1960.tb01744.x>
- Rogel-Gaillard, C., Hayes, H., Coullin, P., Chardon, P., & Vaiman, M. (1997). Swine centromeric DNA repeats revealed by primed in situ (PRINS) labeling. *Cytogenet Cell Genet*, 79(1-2), 79-84. <https://doi.org/10.1159/000134687>
- Schindelin, J., Arganda-Carreras, I., Frise, E., Kaynig, V., Longair, M., Pietzsch, T., Preibisch, S., Rueden, C., Saalfeld, S., Schmid, B., Tinevez, J. Y., White, D. J., Hartenstein, V., Eliceiri, K., Tomancak, P., & Cardona, A. (2012). Fiji: an open-source platform for biological-image analysis. *Nat Methods*, 9(7), 676-682. <https://doi.org/10.1038/nmeth.2019>
- Schuh, M., & Ellenberg, J. (2007). Self-organization of MTOCs replaces centrosome function during acentrosomal spindle assembly in live mouse oocytes. *Cell*, 130(3), 484-498. <https://doi.org/10.1016/j.cell.2007.06.025>
- Shahbazi, M. N., Wang, T., Tao, X., Weatherbee, B. A. T., Sun, L., Zhan, Y., Keller, L., Smith, G. D., Pellicer, A., Scott, R. T., Jr., Seli, E., & Zernicka-Goetz, M. (2020). Developmental potential of aneuploid human embryos cultured beyond implantation. *Nat Commun*, 11(1), 3987. <https://doi.org/10.1038/s41467-020-17764-7>
- So, C., Menelaou, K., Uraji, J., Harasimov, K., Steyer, A. M., Seres, K. B., Bucevicius, J., Lukinavicius, G., Mobius, W., Sibold, C., Tandler-Schneider, A., Eckel, H., Moltrecht, R., Blayney, M., Elder, K., & Schuh, M. (2022). Mechanism of spindle pole organization and instability in human oocytes. *Science*, 375(6581), eabj3944. <https://doi.org/10.1126/science.abj3944>
- So, C., Seres, K. B., Steyer, A. M., Monnich, E., Clift, D., Pejkovska, A., Mobius, W., & Schuh, M. (2019). A liquid-like spindle domain promotes acentrosomal spindle assembly in mammalian oocytes. *Science*, 364(6447). <https://doi.org/10.1126/science.aat9557>
- Soares, S. R., Vidal, F., Bosch, M., Martinez-Pasarell, O., Nogues, C., Egozcue, J., & Templado, C. (2001). Acrocentric chromosome disomy is increased in spermatozoa from fathers of Turner syndrome patients. *Hum Genet*, 108(6), 499-503. <https://doi.org/10.1007/s004390100521>
- Tischer, C., & Pepperkok, R. (2019). CATS: Fiji plugin for context aware trainable segmentation for big image data. <https://doi.org/10.5281/zenodo.2600293>
- Thompson, S. L., & Compton, D. A. (2011). Chromosome missegregation in human cells arises through specific types of kinetochore-microtubule attachment errors. *Proc Natl Acad Sci U S A*, 108(44), 17974-17978. <https://doi.org/10.1073/pnas.1109720108>
- Tovini, L., & McClelland, S. E. (2019). Impaired CENP-E Function Renders Large Chromosomes More Vulnerable to Congression Failure. *Biomolecules*, 9(2). <https://doi.org/10.3390/biom9020044>

- Tsuiko, O., Vanneste, M., Melotte, C., Ding, J., Debrock, S., Masset, H., Peters, M., Salumets, A., De Leener, A., Pirard, C., Kluyskens, C., Hostens, K., van de Vijver, A., Peeraer, K., Denayer, E., Vermeesch, J. R., & Dimitriadou, E. (2021). Haplotyping-based preimplantation genetic testing reveals parent-of-origin specific mechanisms of aneuploidy formation. *NPJ Genom Med*, 6(1), 81. <https://doi.org/10.1038/s41525-021-00246-0>
- Tsutsumi, M., Fujiwara, R., Nishizawa, H., Ito, M., Kogo, H., Inagaki, H., Ohye, T., Kato, T., Fujii, T., & Kurahashi, H. (2014). Age-related decrease of meiotic cohesins in human oocytes. *PLoS One*, 9(5), e96710. <https://doi.org/10.1371/journal.pone.0096710>
- Webster, A., & Schuh, M. (2017). Mechanisms of Aneuploidy in Human Eggs. *Trends Cell Biol*, 27(1), 55-68. <https://doi.org/10.1016/j.tcb.2016.09.002>
- Worrall, J. T., Tamura, N., Mazzagatti, A., Shaikh, N., van Lingen, T., Bakker, B., Spierings, D. C. J., Vladimirov, E., Fojer, F., & McClelland, S. E. (2018). Non-random Mis-segregation of Human Chromosomes. *Cell Rep*, 23(11), 3366-3380. <https://doi.org/10.1016/j.celrep.2018.05.047>
- Zielinska, A. P., Bellou, E., Sharma, N., Frombach, A. S., Seres, K. B., Gruhn, J. R., Blayney, M., Eckel, H., Moltrecht, R., Elder, K., Hoffmann, E. R., & Schuh, M. (2019). Meiotic Kinetochores Fragment into Multiple Lobes upon Cohesin Loss in Aging Eggs. *Curr Biol*, 29(22), 3749-3765 e3747. <https://doi.org/10.1016/j.cub.2019.09.006>
- Zielinska, A. P., Holubcova, Z., Blayney, M., Elder, K., & Schuh, M. (2015). Sister kinetochore splitting and precocious disintegration of bivalents could explain the maternal age effect. *Elife*, 4, e11389. <https://doi.org/10.7554/eLife.11389>

Acknowledgments: We are grateful to the patients who participated in this study. We thank the staff from the Live-Cell Imaging Facility at the Max Planck Institute for Multidisciplinary Sciences for technical assistance; the clinicians, nursing team, and embryology team at the Fertility Center Berlin for their support of this study; C. So, and L. Wartosch for help with human oocytes; T. Cavazza, C. So, and K. Harasimov for help to optimize the pig oocyte culture system; M. Daniel for help with the ovaries delivery; C. So for helpful discussions; C. So, for critical comments on the manuscript; S. Cheng, J. Ellenberg, and A. Webster for plasmids and A. Webster for antibody.

Funding: The research leading to these results was funded by the Max Planck Society and the DFG under a Leibniz Prize to M.S. (SCHU 3047/1-1).

Author Contributions:

MS conceived the study. APZ designed the TALEs, cloned the acrocentric-TALE, and established an initial protocol for porcine oocytes culture which was further developed by EB. EB and MS designed experiments. EB performed all the experiments apart from the fixation of MII oocytes for Fig. 4., which was performed by AW. EB and MS designed methods for data analysis with the exception of the STED analysis which was designed by AZP. EB performed all the analysis with the following exceptions: AZP analysed the data from STED microscopy in Fig. 5A-E. EM annotated the kinetochores for tracking in Fig. 3G. AW annotated the kinetochores in MII fixed cells used in Fig 4. AZP wrote the scripts for the analysis of the STED data. EM wrote the rest in-house imaris scripts. CS and ATS supervised the work in Berlin Fertility Center. EB and MS wrote the manuscript and prepared the figures with input from all authors. M.S supervised the study.

Competing interests: Authors declare that they have no competing interests.

Data availability: Plasmids are available from M.S. under a material transfer agreement with the Max Planck Society.

Figure 1

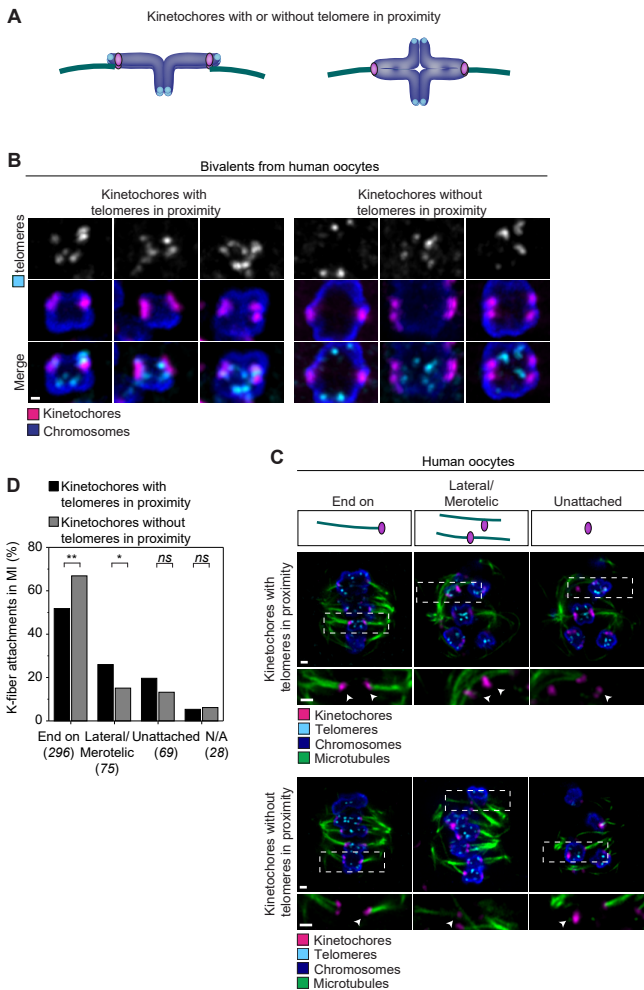
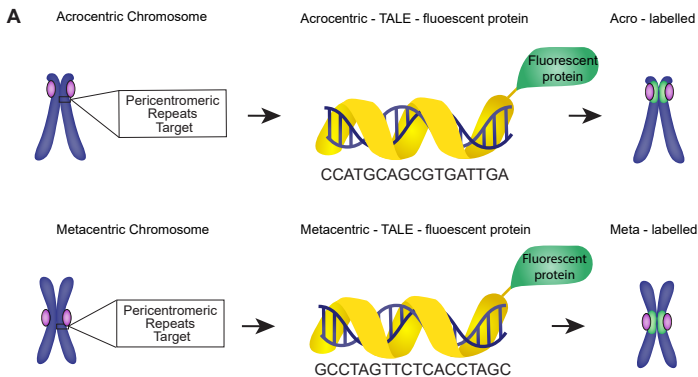
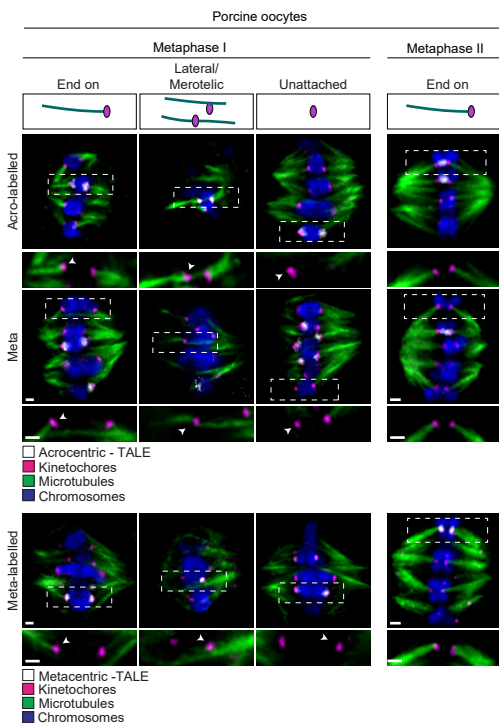


Fig.1 Human acrocentric chromosomes are prone to erroneous kinetochore-microtubule attachments. (A) Schematic representation of bivalents with kinetochores with telomeres in proximity and with kinetochores without telomere in proximity (chromosomes in blue; kinetochores in magenta; telomeres in cyan). **(B)** Representative examples of immunofluorescence airy scan images of human bivalents with kinetochores with telomeres in proximity and kinetochores without telomeres in proximity. Magenta, kinetochores, (ACA); cyan, telomeres, (TRF-2); blue, chromosome, (pH3); Scale bar, 0.5 μm . **(C)** Illustrations and representative immunofluorescent images of kinetochore-microtubule attachments from cold treated human oocytes in meiosis I. Overview images on the top row of a z-plane of the full spindle and insets of the attachments at the bottom row. Insets are magnifications of regions marked by dashed line boxes. Arrowheads indicate the specified attachment type. Magenta, kinetochores, (ACA); cyan, telomeres, (TRF-2); blue, chromosome, (pH3); green microtubules (a-tubulin); Scale bar, 1 μm for both overview and insets. **(D)** Quantification of the proportion of microtubule attachments to kinetochores with telomere in proximity and kinetochores without telomere in proximity. (Fisher's exact test) * $p < 0.05$, ** $p < 0.01$, and ns: non-significant.

Figure 2

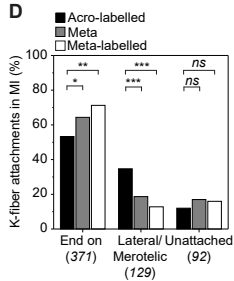


B



C

D



E

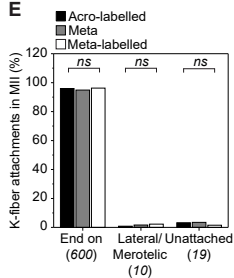


Fig 2. Porcine acrocentric chromosomes are prone to erroneous attachment creation. (A) Schematic representation of the labelling with the pericentromeric TALE in the porcine cells. The region recognized by each TALE is indicated for each chromosome type. TALEs are fused with a fluorescent protein. Labelled chromosomes are called acro-labelled and meta-labelled, respectively. blue, chromosomes; magenta, kinetochores; yellow, TALE; green, TALE on chromosomes. **(B)** Illustrations and representative immunofluorescent images of kinetochore-microtubule attachments from cold treated porcine oocytes in meiosis I. Overview images on the top row of a z-plane of the full spindle and insets of the attachments at the bottom row. Insets are magnifications of regions marked by dashed line boxes. Magenta, kinetochores, (ACA); gray, TALE, (anti-GFP); blue, chromosome, (Hoechst); green microtubules (α -tubulin); Scale bar, 1 μm for both overview and insets. **(C)** Illustrations and representative immunofluorescent images of end-on kinetochore-microtubule attachments from cold treated porcine oocytes in meiosis II. Overview images on the top row of a z-plane of the full spindle and insets of the attachments at the bottom row. Insets are magnifications of regions marked by dashed line boxes. Magenta, kinetochores, (ACA); gray, TALE, (anti-GFP); blue, chromosome, (Hoechst); green microtubules (α -tubulin); Scale bar, 1 μm for both overview and insets. **(D)** Quantification of the proportion of kinetochore-microtubule attachments for acro-labelled, meta, and meta-labelled chromosomes in meiosis I spindles in porcine oocytes. The number of attachments quantified per chromosome type is indicated in the brackets. (Fisher's exact test) * $p < 0.05$, ** $p < 0.01$, *** $p < 0.001$ and ns: non-significant. **(E)** Quantification of the proportion of kinetochore-microtubule attachments for acro-labelled, meta, and meta-labelled chromosomes in meiosis II spindles in porcine oocytes. The number of attachments quantified per chromosome type is indicated in the brackets. (Fisher's exact test) ns: non-significant.

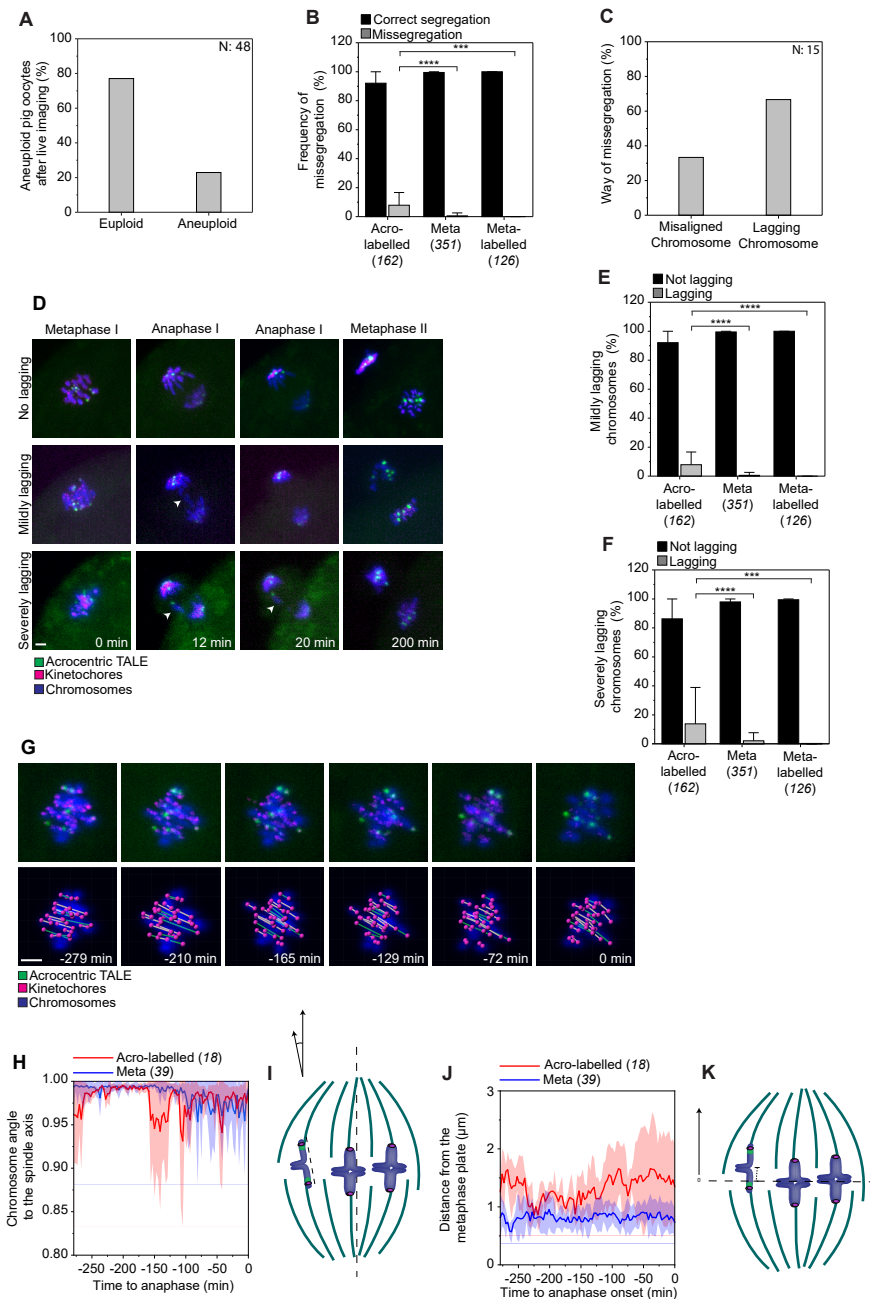


Fig. 3 Acrocentric chromosomes are lagging during anaphase and misalign during late metaphase more often than the metacentric (A) Proportion of euploid and aneuploid cells from the total number of cells imaged during anaphase. Euploidy status determined from the correct or not correct segregation outcome of the chromosomes during live imaging. **(B)** Frequency of missegregation per chromosome group. (Fisher's exact test) *** $p < 0.001$ and **** $p < 0.0001$. **(C)** Proportion of the different ways of missegregation from the total missegregated chromosomes. **(D)** Still images from a time-lapse movie of chromosome segregation from porcine oocytes. Images from metaphase I, anaphase I, and metaphase II. Time is indicated in minutes and timepoint 0 is the last frame before anaphase onset. Arrowheads indicate lagging chromosomes. Magenta, kinetochores (mScarlet-hCENPC); green, acrocentric label, (Acrocentric-TALE-GFP); blue, chromosomes, (H2B-SNAPf). Scale bar, 1 μm . **(E)** Frequency of mildly lagging chromosomes 12 min after anaphase onset from the total chromosomes examined. (Fisher's exact test) **** $p < 0.0001$. **(F)** Frequency of severely lagging chromosomes 20 min after anaphase onset from total chromosomes examined. (Fisher's exact test) *** $p < 0.001$ and **** $p < 0.0001$. **(G)** Still images from porcine chromosomes during alignment in the metaphase plate (top row) and the corresponding image from imaris with the tracking annotation (bottom row). Magenta, kinetochores (mScarlet-hCENPC); green, acrocentric label, (Acrocentric-TALE-GFP); blue, chromosomes, (H2B-SNAPf) top row and magenta, kinetochores; green line, pair of homologous acro-labelled kinetochores; white line, pair of homologous meta kinetochores. Scale bar, 1 μm . **(H)** Chromosome angle of the acro-labelled and meta bivalents compared to the whole spindle axis. Angle is defined by the dot product. **(I)** Schematic illustration of an acro-labelled bivalent that is tilted to the spindle axis and from vertical meta bivalents. Magenta; kinetochores; green, acrocentric-TALE; blue, chromosomes; green, spindle; **(J)** Distance of the acro-labelled and meta bivalents from the center of the metaphase plate. **(K)** Schematic that shows the acro-labelled chromosome aligning higher than the center of the metaphase plate and the meta chromosomes aligning in the middle of the metaphase plate. Magenta; kinetochores; light green, acrocentric-TALE; blue, chromosomes; dark

green, spindle; Number of chromosomes analyzed is indicated in brackets under each category and the number of cells of a graph is indicated with N.

Figure 4

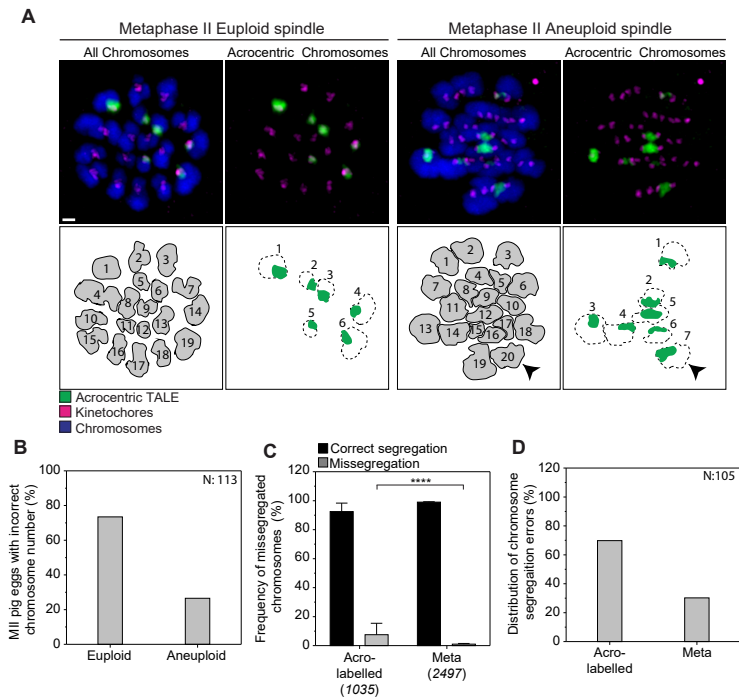


Fig. 4 Acrocentric chromosomes missegregate more often than the metacentric. (A) Representative images of a euploid and an aneuploid spindle from intact fixed metaphase II cells injected with the acrocentric-TALE at the top row. In the bottom row numbers within the gray illustrations indicate the total number of chromosomes and numbers next to the green illustrations indicate the total number of acro-labelled chromosomes in both the euploid and aneuploid spindle. The black arrowheads indicate the extra chromosome. Scale bar, 1 μm . **(B)** Proportion of aneuploid cells from the fixed metaphase II porcine oocytes. Aneuploid cells were identified from the total kinetochore count. **(C)** Frequency of missegregation for acro-labelled and meta chromosomes from the total chromosomes count in fixed metaphase II porcine spindles. (Fisher's exact test), **** $p < 0.0001$. **(D)** Proportion of each chromosome type in the total missegregated chromosomes. Number of chromosomes analyzed is indicated in brackets under each category and the number of cells of a graph is indicated with N.

Figure 5

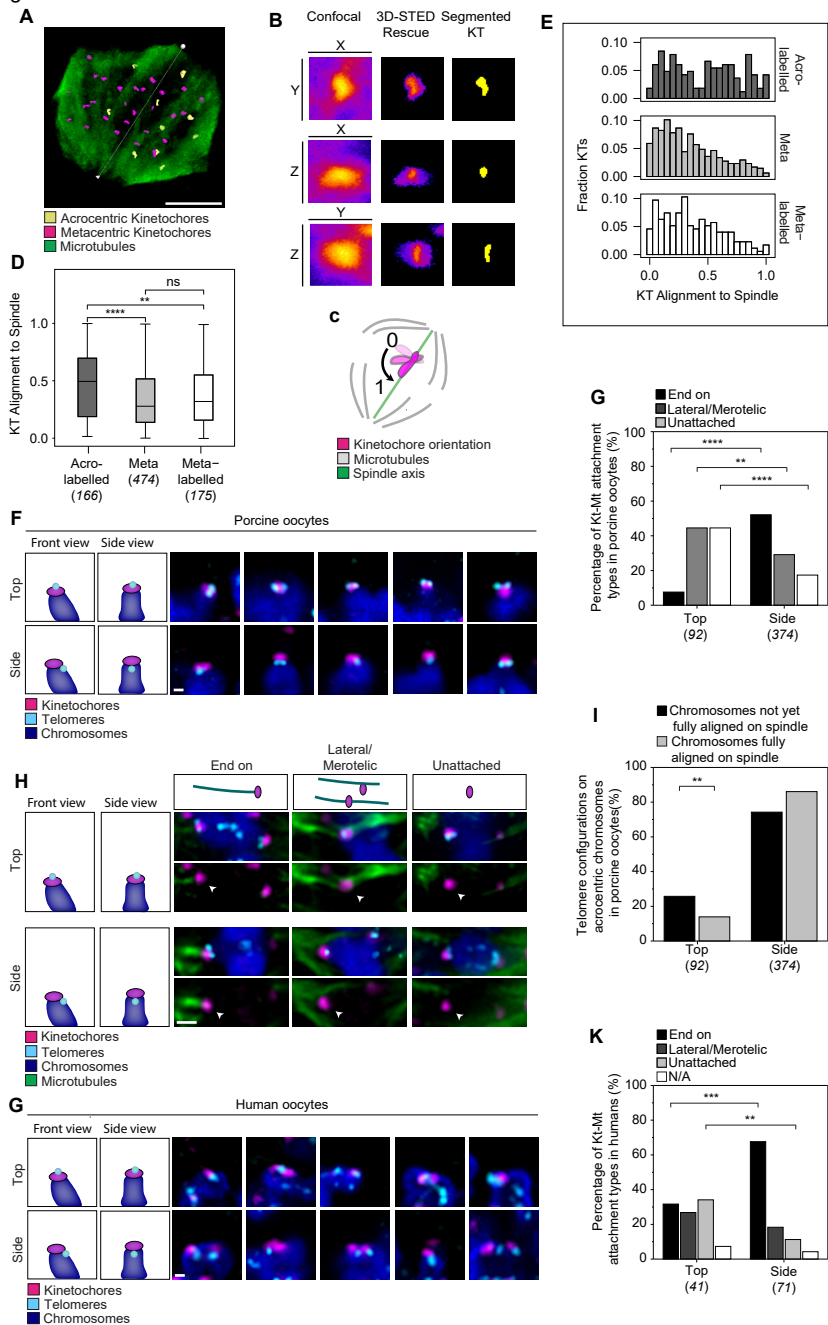


Fig 5. The small arm of acrocentric chromosomes hinders the end-on microtubule attachment creation. (A) 3D rendering of segmented acro-labelled kinetochores (yellow, TALE-labelled) and non-labelled kinetochores (magenta) in a meiotic metaphase spindle (MTs in green). The arrow indicates the spindle direction. Scale bar, 5 μm . **(B)** Magnification of KT showed in A, white square, and the corresponding confocal, 3D-STED, and segmented KT in a XY, XZ, and YZ views. Each tile is 2x2 μm . **(C)** KTs alignment to spindle is computed from the absolute value of the scalar product of the KT and spindle direction vectors. **(D)** Distribution of the KTs alignment to spindle for KTs labelled with acrocentric TALE (upper graph), non-labelled kinetochores (middle graph), and KTs labelled with metacentric TALE (lower graph). **(E)** Data from D showing the median, interquartile range, and outlier for the 3 KTs populations. Number above boxplots shows p -value of Wilcoxon two-tailed test. Number in the x-axis indicates the number of kinetochores from 17 acrocentric-TALE labelled cells, and 15 metacentric-TALE labelled cells. **(F)** Illustrations and representative airy scan immunofluorescent images with telomeres on top of the kinetochores (top row) and telomeres at the side of the kinetochores (bottom row) in porcine cells. Magenta, kinetochores, (ACA); cyan, telomeres, (TRF-2); blue, chromosomes, (Hoechst); Scale bar, 0.5 μm . **(G)** Quantification of the proportion of kinetochore-microtubule attachments for the two different telomere configurations in porcine oocytes. (Fisher's exact test) $**p < 0.01$, and $***p < 0.001$. **(H)** Illustrations and representative airy scan immunofluorescent images from the attachment types of kinetochores with telomeres on top and kinetochores with telomeres at the side in porcine cells. Arrowheads indicate the specified attachment type. Magenta, kinetochores, (ACA); cyan, telomeres, (TRF-2); blue, chromosomes, (Hoechst); green, microtubules, (α -tubulin); Scale bar, 1 μm . **(I)** Distribution of the top and side configuration on spindles with fully aligned chromosomes and spindles that have not yet aligned their chromosomes. (Fisher's exact test) $**p < 0.01$. **(J)** Illustrations and representative immunofluorescent images with telomeres on top of the kinetochores (top row) and at the side of the kinetochores (bottom row) from human cells. Magenta, kinetochores, (ACA); cyan, telomeres, (TRF-2); blue, chromosomes, (Hoechst); Scale

bar 0.5 μm . **(K)** Quantification of the proportion of kinetochore-microtubule attachments for the two different telomere configurations in human oocytes. (Fisher's exact test) ** $p < 0.01$, and *** $p < 0.001$.

Number of chromosomes analyzed is indicated in brackets under each category and the number of cells of a graph is indicated with N.

Figure 6

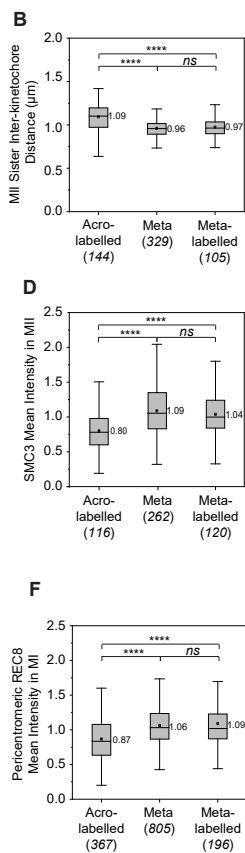
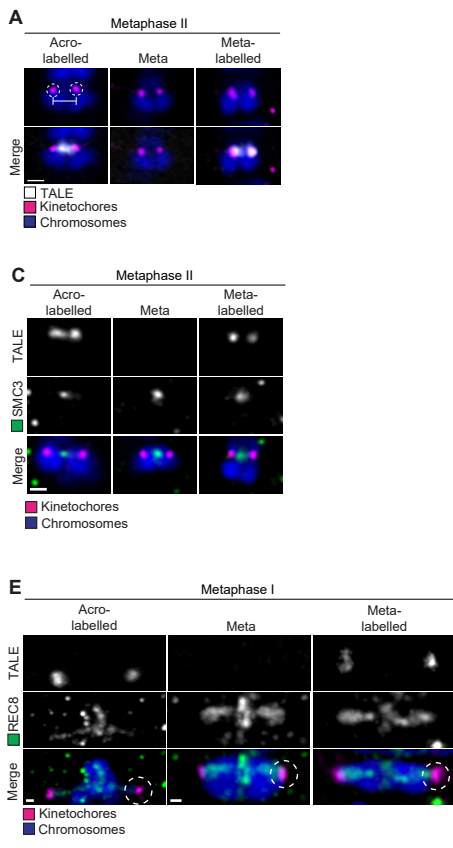


Fig 6. Pig acrocentric chromosomes have on average less cohesin than metacentric chromosomes.

(A) Representative airyscan immunofluorescent images of the measurements from the sister chromatids in the three different chromosome groups. Magenta, kinetochores, (ACA); gray, TALE (anti-GFP); blue, chromosomes, (Hoechst); Dashed circles indicate the sister kinetochores and white line indicates the distance measured. Scale bar, 1 μm . **(B)** Box plot showing measurements of the interkinetochore distance of sister chromatids on metaphase II intact spindles of porcine oocytes. (Two-sample t-test) **** $p < 0.0001$, ns: non-significant. **(C)** Representative airyscan immunofluorescent images of the SMC3 staining on chromosomes in metaphase II intact spindles of porcine eggs. Images from the three different chromosome groups. Magenta, kinetochores, (ACA); gray, TALE (anti-GFP); blue, chromosomes, (Hoechst); green, cohesion, (SMC3); Scale bar, 1 μm . **(D)** Box plot showing mean intensity measurements of SMC3 signal on chromosomes from metaphase II intact spindles of porcine eggs. (Two-sample t-test) **** $p < 0.0001$ and ns: non-significant. **(E)** Representative airyscan immunofluorescent images of the REC8 staining on chromosomes from metaphase I intact spindles of porcine oocytes. Images from the three different chromosome groups. Dashed circle indicates the area of the measurements. Magenta, kinetochores, (ACA); gray, TALE (anti-GFP); blue, chromosomes, (Hoechst); green, cohesion, (REC8); Scale bar, 0.5 μm . **(F)** Box plot of mean intensity measurements of REC8 intensity on chromosomes from metaphase I intact spindles of porcine oocytes. (Two-sample t-test) **** $p < 0.0001$ and ns: non-significant. Number of chromosomes analyzed is indicated in brackets under each category and the number of cells of a graph is indicated with N.

Supplementary Materials for

Bivalent architecture contributes to chromosome-specific aneuploidy in mammalian oocytes

Authors: Eirini Bellou, Agata P. Zielinska, Antonio Z. Politi, Eike Moennich, Antonina Wellecke, Katerina Menelaou, Claus Sibold, Andreas Tandler-Schneider, Melina Schuh*

*Corresponding author. Email: melina.schuh@mpinat.mpg.de

This file includes:

Materials and methods

Fig. S2 to S6

Material and Methods

Preparation and culture of porcine oocytes

Porcine ovaries from prepubertal animals were obtained from a local slaughterhouse and transported to the laboratory in a thermo-flask. Oocyte isolation and culture was performed using collection and maturation media from Cosmobio. In brief, dissection of antral follicles from the surface of porcine ovaries was performed in homemade M2 medium supplemented with 10 μ M RO-3306 (#SML0569) at 38.5°C. The follicular fluid was transferred to a 50 ml tube. Cumulus oocyte complexes (COCs) were allowed to sediment and then washed extensively with M2medium. In the final wash, COCs were transferred to porcine oocyte/embryo collection medium (POE-CM, Cosmobio, #CK020) supplemented with 10 μ M RO-3306. All handling and manipulations outside the CO₂ incubator were performed in POE-CM medium. Only oocytes with a homogeneous cytoplasm and at least 3-5 complete layers of compact cumulus cells were selected for experiments. The selected oocytes were transferred to basic medium for porcine maturation (POM, Cosmobio, #CK021) supplemented with 10 IU/ml equine chorionic gonadotropin (eCG), 10 IU/ml human chorionic gonadotropin (hCG), and 10uM RO-3306 for meiotic arrest. COCs were incubated in the media at 38.5°C in a 5% CO₂ incubator. After 6 h, COCs were partially denuded using a EZ-Grip denudation pipettor with a 135 μ m wide at an EZ-Grip denudation pipettor. All handlings outside the CO₂ incubator were performed in the POE-CM apart from live imaging which was performed in POM. To induce the resumption of meiosis, oocytes were washed in RO-3306-free medium. Complete denudation of the oocytes was performed before release from the RO-3306 induced arrest. For complete imaging of meiosis I, oocytes were transferred to the light sheet sample chamber immediately after release. For imaging of anaphase I, oocytes were transferred to the light sheet chamber or the confocal imaging dish 11 h after release. For immunofluorescence of metaphase I spindles, oocytes were fixed 12 h after release.

Expression constructs and mRNA synthesis

For the generation of the constructs for mRNA synthesis previously published coding sequences were fused with mClover3 (Bajar et al., 2016), mScarlet (Bindels et al., 2017). Acrocentric-TALE and Metacentric-TALE plasmids were generated by fusing the previously published sequences (Rogel-Gaillard et al., 1997) in pTALYM3 vector, described in more detail below. Acrocentric-TALE was subsequently inserted in a pGEHME-mclover and a pGEHME-mScarlet using pENTER/D-TOPO Gateway cloning (Invitrogen). pGEHME-mScarlet-hCENPC (Cavazza et al., 2021), pGEHME-mcherry-TRIM21 (Clift et al., 2017), pGEHME-H2B-SNAPf and pGEMHE-3xEGFP-TRF1 (gift from Jan Ellenberg) were also used. All mRNAs in this study were synthesized using HiScribe T7 ARCA mRNA kit (NEB# E2065S) according to the manufacturer's protocol and quantified using Qubit RNA HS Assay Kit (Thermo Fisher Scientific #Q32852).

Creation of fluorescent TALEs

Fluorescent TALEs were created according to previously published protocol (Cermak et al., 2015). RVDS plasmid were obtained from Addgene (Kit #1000000024). TALEs are assembled by Golden Gate cloning in Top10 competent cells (Thermo Fisher Scientific; C404010). The assembled TALEs were further subcloned into the destination vectors pGEHME-mclover3-N1 and pGEHME-mScarlet-N1 using the pENTER/D-TOPO cloning (Invitrogen).

Microinjection of porcine oocytes

Porcine oocytes were microinjected with 2.5 pl of mRNAs as previously described by (Jaffe & Terasaki, 2004; Schuh & Ellenberg, 2007) in a microinjection chamber created with two layers of double-sided sticky tape. Oocytes microinjection was performed after the partial denudation. mRNAs were injected at the following concentrations on the microinjection needle: H2B-SNAPf at 9 ng/ μ l, mScarlet-hCENPC at 10 ng/ μ l, Acrocentric-TALE at 50 ng/ μ l, Metacentric-TALE at 50 ng/ μ l, mcherry-TRIM21 at 150 ng/ μ l. After injection oocytes were allowed to express the mRNAs in medium supplemented with RO-3306 for 3 h before release.

TRIM-Away REC8 in MII porcine oocytes

REC8 antibody used for TRIM-away was generated in the lab using a previously characterized epitope (Eijpe et al., 2003). Antibodies were concentrated using Ultra 0.5mL Amicon 100kD centrifugal filters (Merck #UFCS510024). The concentrated antibodies were supplemented before injection with NP40 (Merck #492016) to a final concentration of 0.05% and centrifuged for 14.000 g for 10 min.

Trim-away was performed by injecting the mRNA at a final concentration of 150 ng/ μ l at the germinal vesicle (GV) stage with other mRNAs (H2B-SNAPf and the two TALEs). Cells were released after 3 h of expression and allowed to mature till metaphase II. Only oocytes with a polar body were selected for antibody injection. 34 h after release the MII cells were injected with the REC8 antibody. Only a few oocytes were injected at a time and immediately transferred to the light-sheet sample chamber for imaging. Imaging was performed at one-minute intervals until sister chromosome separation occurred in the cells.

Human oocytes culture and injection

The use of unfertilized human oocytes in this study was approved by the Ärztekammer Niedersachsen (Ethics Committee of Lower Saxony) under the reference 15/2016.

Oocytes were collected from patients who underwent ovarian stimulation for intracytoplasmic sperm injection (ICSI) as part of their assisted reproduction treatment at Fertility Center Berlin. Only oocytes that were immature at the time of ICSI and thus unsuitable for the procedure were vitrified for this study with Cryolock (FUJIFILM Irvine Scientific) using Vit Kit-Freeze (FUJIFILM Irvine Scientific). All patients gave informed consent for their surplus oocyte(s) to be used in this study. All human oocytes used in this study were vitrified oocytes collected from women undergoing assisted reproduction treatments after having obtained fully informed consent. Oocytes were thawed as previously described (So et al., 2022). Oocytes were injected with 3xEGFP-TRF1 mRNA at 200 ng/ μ l immediately after thawing. After that oocytes were cultured in G-MOPS medium (Vitrolife, #10129)

supplemented with 10% FBS (G S36817 S36817 S36817IBCO, #16000044) under mineral oil (Nidoil, Nidacon #NO-400K) at 37°C as described previously (Zielinska et al., 2019). To assess the maturation stage, the medium was supplemented with 10 nM 5-SiR-Hoechst DNA (Bucevicius et al., 2020) for chromosome staining (So et al., 2022). When chromosomes were largely aligned, oocytes were cold treated and fixed as described below.

Immunofluorescence

To obtain porcine oocytes metaphase I and metaphase II spindles, oocytes were fixed at 12 h and 24 h after release from RO-3306. Oocytes were matured at 39°C/ 5% CO₂ incubator before fixation. To obtain human metaphase I spindles, thawed human meiosis I oocytes were monitored every 30 min on the confocal LSM880 microscope at 38,5°C as described above. For human Metaphase II spindles, thawed human meiosis II oocytes were fixed 10 h after thawing.

Both porcine and human oocytes were fixed in 100 mM HEPES (pH 7.0, titrated with KOH), 50 mM EGTA (pH 7.0, titrated with KOH), 10 mM MgSO₄, 2% methanol-free formaldehyde and 0.5% triton X-100 (10% stock; Sigma Aldrich, 93443) at room temperature for 30 min. Fixed oocytes were extracted in phosphate-buffered saline (PBS) with 0.5% triton X-100 (PBT) overnight at 4°C and then blocked in PBT with 5% BSA (Fisher Scientific #BP1605) (PBT-BSA) overnight at 4°C. Lipid droplets in porcine oocytes were cleared before staining with primary antibodies as previously described (So et al., 2019). All primary antibody incubations were performed overnight at 4°C in PBT-BSA at the concentrations listed below. Secondary antibodies and Hoechst 33342 incubations were performed in PBT-BSA for 1 h at room temperature.

Primary antibodies used were human anti-centromere antibody (ACA) at 1:50 dilution (Antibodies Incorporated #15-234), rabbit anti-gfp (#A11122, Invitrogen), rat anti-alpha-tubulin (MCA78G, Bio-rad), mouse anti-TRF-2 (NB100-56506SS), goat anti-GFP (600-101-215; Rockland Immunochemicals), mouse anti-alpha-tubulin (#T6199, Merck), rabbit anti-pH3 (#9701, Cell Signaling Technology), rabbit

anti-REC8 generated in-house based on a published epitope (Eijpe et al., 2003), rabbit anti-SMC3 (#ab128919, abcam) at 1:100 dilution. Secondary antibodies used in this study were Alexa Fluor 405-, 488-, 568- or 647-conjugated anti-human IgG, goat IgG, mouse IgG, rabbit IgG, rat IgG all raised in donkey or goat (Thermo Fisher Scientific; 1:200). Hoechst 33342 was used at 100 μ M to stain the DNA (Molecular Probes; 20mM stock). For STED microscopy the secondaries used were STAR RED, -635, -580 or -ORANGE – conjugated to anti-human IgG and anti-goat IgG (abberior; 1:200).

Cold stable assay

Porcine metaphase I and II oocytes were incubated on ice for 9 min, while human metaphase I and metaphase II oocytes were incubated on ice for 5.5 min. Subsequently, they were fixed for immunofluorescence as described above.

Confocal and super-resolution microscopy

For live confocal imaging, oocytes were imaged in 5 μ l of M2 medium (for live porcine oocytes) under mineral oil (Light mineral oil, Irvine Scientific #9305) in a 35 mm dish with a #1.0 coverslip (#MAT-TEK). Just before imaging cells injected with H2B-SNAPf were incubated with 2 μ M SNAP-cell 637-SiR (NEB, S9102S) supplemented with 10 μ M Verapamil (Spirochrome; #SC007) for 1 h. Images were acquired on an LSM 880 confocal laser scanning microscope (Zeiss) equipped with an environmental incubator box and a 40 \times C-Apochromat 1.2 NA water-immersion objective. at 38,5°C. Automatic 3D tracking was implemented for time-lapse imaging with a temporal resolution of 4 min using MyPiC (Politi et al., 2018). mClover3 was excited with a 488 nm laser line and detected at 493 - 571 nm. mScarlet was excited with a 561 nm laser line and detected at 571 - 638 nm. SNAP-cell 647-SiR was excited with a 633 nm laser line and detected at 638 - 700 nm. Images of the control and experimental groups were acquired under identical imaging conditions on the same microscope. Noise was reduced with a Gaussian filter in ZEN (Zeiss).

Fixed samples were imaged in 2 μ l of PBS with 10% BSA under paraffin oil in a 35 mm dish with a #1.0 coverslip (#MAT-TEK). Images were acquired using the Airyscan module on LSM800, LSM880 or LSM900 confocal laser scanning microscopes (Zeiss) and processed in ZEN (Zeiss). Acquisition was performed at room temperature with a 40x C-Apochromat 1.2 NA water-immersion objective. Imaging conditions were carefully selected (laser power, pixel-dwell time and detector gain) to avoid phototoxicity (for live imaging), photobleaching or saturation. For the analysis of kinetochore-microtubule attachments and telomere orientations, oocytes were manually rotated with an unbroken microinjection needle such that the long axis of the spindle was parallel to the imaging plane.

STED microscopy

3D stimulation emission depletion microscopy (3D STED) of fixed porcine oocytes were performed on a STED Expertline scanning microscope (Abberior Instruments GmbH) equipped with 405, 488, 561, and 640 nm excitation lasers and a pulsed 775 nm STED laser. Imaging was performed using a 100x oil immersion objective lens (N.A. 1.4, Olympus). Fixed cells, stained with the abberior STAR secondary antibodies were mounted in a drop of Slow fade Glass Soft-set Antifade Mountant (Thermo Fisher Scientific; # S36817). STED Images were acquired with an isotropic 40 nm pixel size isotropically using the ADAPTIVE ILLUMINATION RESCUE function, to minimize laser exposure and reduce photobleaching. Two separate, sequential acquisitions have been performed for this experiment. The first acquisition was performed in fast confocal mode with a pixel size of 40 nm x 40 nm x 320 nm. 4 colour imaging was performed of DNA, kinetochores, microtubules and the TALE I to define the spindle axis and detect the acrocentric chromosomes. The second acquisition was performed by imaging the DNA in confocal mode and the kinetochores in STED mode using the RESCUE function with a pixel size of 40nm x 40nm x 40nm. The DNA and confocal kinetochores channels from both acquisitions were used to align the images in order to determine the angle of kinetochores to the spindle axis as described below in the analysis.

Light-sheet microscopy

Data used for the kinetochore tracking in figure 4 G, H, and I as well as most of the data for anaphase imaging in figure 4 A-F were acquired on a LS1 Live light sheet microscope system (Viventis). A customized script was used to track the sample in order to minimize the field of imaging and reduce phototoxicity.

Data analysis

Chromosome tracking

Homologous kinetochores were tracked and paired before anaphase using an in-house plugin for Imaris (Bitplane). Mixed Integer Linear Programming (MILP) is used to find the optimal set of tracks and pairings in concert. This produces better results than pairing after the tracks have been determined (Jaqaman et al., 2008). Furthermore, MILP allows constraint introduction in order to avoid mistakes.

Tracked Filament objects in Imaris (Bitplane) are used to represent homologous kinetochores and their tracks.

The script was written in Matlab R2018b and additionally uses IBM Cplex with an academic license to improve performance.

Tracks are weighted by the square of the distance traveled between frames. The distance is determined by the mean distance traveled of both kinetochores. All distances are relative to a reference frame determined by the center of mass of the chromosome signal.

Pairings are weighted by the chromosome signal on a line connecting the putative homologs. Furthermore, the angle between the line connecting the sisters and the spindle axis is minimized. The optimization is run iteratively and the spindle axis is determined by the mean direction of the

previously determined sister chromosomes. If all sister connecting lines in a frame are close to parallel, this factor is more important.

Additional weights with little influence, are the variance of the chromosome signal between sister chromosomes and a combination of the angle to the spindle axis with the interkinetochore distance to discourage far separated sisters being non-parallel.

Constraints are introduced setting a maximum distance between sisters and a maximum distance traveled between frames. Line segments connecting sisters must be at least a certain distance apart and there must be 19 sister pairs identified in each frame. Any missing sister pair is heavily penalized. There must be at least one kinetochore somewhere near any detected spot. The chromosome signal is segmented and at least one sister pair must be close to any connected component of this signal.

Depending on the number of spots and length of the time series, the script can take a few minutes to hours to finish. For this reason time series of more than a 100 frames are solved in smaller batches. The tracks can be easily stitched in Imaris. Manual corrections of tracks are fixed in Imaris as well. Corrections of pairings are performed by deleting erroneous ones in Imaris and adding new ones via a separate script.

Analysis of tracking

An analysis script was written for Imaris in Matlab R2018b to obtain data on tracked kinetochore pairs. This script exports positions and velocities of pairs and individual kinetochores relative to the chromosome mass and spindle axis from many Imaris files in one run.

The middle of the chromosome mass is determined from a reference frame that was created before using the tracking script. The spindle axis is determined by the average direction of the lines connecting

kinetochore pairs. More specifically, these lines are interpreted as 180-degree rotation vectors of length 1 and averaged using the Matlab function `meanrot`.

Positions of kinetochores and pairs are determined vertically, i.e. along the spindle axis and laterally, i.e. the distance from the spindle axis. Furthermore, the angle of the sister connecting lines with the spindle axis are exported.

Chromosome count in meiosis II

Airyscan images were used for chromosome count analysis after airyscan processing with the ZEN software. Analysis was done in arivis Vision4D software. The kinetochores were detected by automated thresholding of the kinetochore signal. The euploidy status of the cell was evaluated first independent of the presence of the TALE. A cell is considered euploid if 38 kinetochores were detectable and aneuploid if the number of kinetochores was deviating from 38. Subsequently, the two kinetochores of a pair were manually assigned to each DNA unit and annotated. Subsequently, the labelled kinetochores were identified from the presence of the TALE in the kinetochore proximity or not. Acrocentric chromosomes were the ones with the TALE in proximity and Metacentric the ones without.

Lagging chromosomes in anaphase

Three color imaging datasets of anaphase from either confocal or light sheet microscopy were used. Images were acquired every 3-4 min. Anaphase onset was defined as the first time point where the chromosomes started separating in the two anaphase masses. A small gap between the two masses is already visible at this stage. Chromosomes that are still present in the center of the spindle 12 and 20 min after anaphase onset were classified as lagging chromosomes and were assigned as mildly and severely lagging respectively. The mildly lagging group is not including the severely lagging chromosomes.

Analysis of kinetochore – Microtubule attachments

Microtubule-kinetochore attachments were analysed by 3D analysis of high resolution airyscan images of the whole spindle volume in Imaris software (Bitplane). Only oocytes with the spindle oriented parallel to the imaging plane were used in this analysis. For all quantifications of human or porcine spindles, the kinetochore-microtubule attachments were assessed in the same way. An attachment is classified as end-on if the k-fibre stopped just in front of the kinetochore surface. An attachment is classified as lateral if the k-fibre was extending past the kinetochore and as merotelic if two distinct k-fibres originating from different poles were interacting with the kinetochore. A kinetochore is considered unattached if there is no interaction with microtubule filaments. All kinetochores were annotated in Imaris 2D view and then classified in one of the above categories. The data used for this analysis were two types of 4-color images; oocytes stained for kinetochores, microtubules, TALE and DNA, and oocytes stained for kinetochores, microtubules, telomeres, and DNA. The quantification was done blindly for all kinetochores excluding the TALE and telomere channels from the analysis. Thus, the attachment type was assigned without knowing the chromosome category (acrocentric or metacentric) or the telomere configuration.

Analysis of STED microscopy

For the analysis, we use two image stacks acquired sequentially to preserve fluorescence. In stack1, we imaged, with isotropic sampling, the KT's using STED and confocal, and DAPI in confocal. In stack2, we imaged the KT's, TALE, MT's and Hoechst in confocal. The analysis has been performed in Fiji (Schindelin et al., 2012) using different publicly available plugins and own code.

KT's in the STED image (stack1) were segmented semantically using CATS, a trainable pixel classifier in Fiji (Tischer & Pepperkok, 2019) followed by a connected component analysis with MorphoLibJ (Legland et al., 2016). With Labkit (<https://imagej.net/plugins/labkit/>) we manually inspected the label mask and if necessary corrected the segmentation. Typical segmentation errors were merged

kinetochores and false positives. In 28/32 oocytes we correctly identified 38 kinetochores, in 4/32 we could identified 34-37 kinetochores.

To define TALE label masks we used the confocal images of the TALE and Hoescht/DNA channels from stack2. We wrote an ImageJ macro to perform instance segmentation of the bright TALE blobs within a mask defined by the DNA signal. Manual correction was done by inspecting TALE, kinetochore and DAPI channels Labkit. Overall we were able to correctly detect 12 TALE labels in 15/32 oocytes. In 17/32 oocytes we identified in median 10 labels (spread 8-13). To pair the KTs and TALE labels we first registered stack1 and stack2 by means of their respective confocal KTs signal using the ImageJ plugin *Correct 3D drift* (Parslow et al., 2014). The registration shifts are applied to the TALE label centroids and used to compute the shortest distance to KTs centroids. KTs centroids further away than 2 μm are considered as non-TALE labelled.

The main axis of each kinetochore label was computed using MorphoLibJ and corresponds to the longest ellipsoid axis. Spindle direction was defined using the MTs signal in stack2 and manually placed labels at each spindle pole. The absolute value of the scalar product between KT and spindle axis gives the kinetochore alignment to the spindle.

Analysis of telomere position

The position of telomere in respect to the kinetochore was evaluated by 3D analysis of high-resolution airyscan images of the whole spindle volume in Imaris software (Bitplane). Only oocytes with the spindle oriented parallel to the imaging plane were used in this analysis. First, the kinetochores that had a telomere in their proximity were identified and annotated. Then, using the 3 channels of kinetochore, telomere and DNA, the relative position was evaluated. A telomere is classified as on top when it was covering part of the upper surface of the kinetochore. In most cases for porcine oocytes, the telomeres with an on-top configuration were barely touching the DNA of the long arm. A telomere

position is classified as side if the upper surface of the kinetochore is free and the telomere is in contact with the chromosome mass.

Measurements of SMC3 Intensity MII

We used an in-house script to measure the intensity of SMC3 in the pericentromeric region of sister chromatids. Sister kinetochores were paired using the measurement points in Imaris 9.3. (Bitplane). The cohesin signal is measured in a round cylinder in the direction of the connecting filament between the two sister kinetochores.

All Imaris files within a folder are analyzed and the results are recorded in an excel sheet.

Measurements of REC Intensity MI

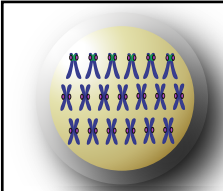
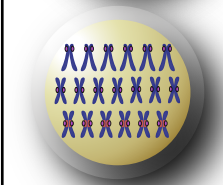
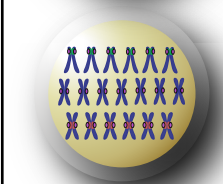
In order to measure the REC8 intensity in the pericentromeric region of MI bivalents, we wrote an in-house plugin for Imaris 9.3 (Bitplane) using Matlab R2018b. First the kinetochores were identified using the spots object. The plugin changes the size of spots. This allows us to use the inbuilt spot function in Imaris to detect the center of the signal of the kinetochore more easily, but measure the REC8 intensity in a larger radius covering the pericentromeric region that is identical for all the kinetochores analyzed.

Analysis of trim-away

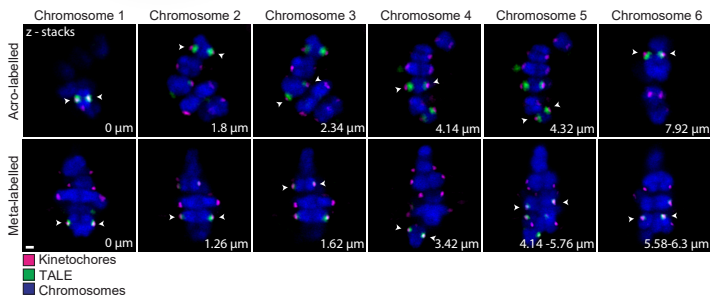
Oocytes were co-labelled with for DNA and the acrocentric- and metacentric-TALE. Analysis was performed after 3D reconstruction in Imaris 9.3 (Bitplane). The time that two sister chromatids were separated from one another was noted for all the labelled chromosomes. For all graphstime point zero marks the time of the first separation event for each cell.

Statistical analysis

Statistical significance based on unpaired, two-tailed Student's t-test (for absolute values) was calculated in OriginPro and two-tailed Fisher's exact test (for categorical values) in Prism (GraphPad). All box plots show median (horizontal black line), 25th and 75th percentiles (boxes) and 5th and 95th percentiles (whiskers). All data are from at least three independent experiments apart from the Cold stable assay in metaphase II of pig oocytes and the position of telomeres in mouse oocytes which are from two repetitions. P values are designated as *P < 0.05, **P < 0.01, ***P < 0.001 and ****P < 0.0001. Non-significant values are indicated as "N.S".

<p>A</p> 	<p><u>Experimental type 1</u></p> <ul style="list-style-type: none"> - Acrocentric chromosomes are labelled for DNA, kinetochores and with pericentromeric Acro-TALE (Acro-labelled) - Metacentric chromosomes are labelled for DNA and kinetochores only (Meta)
	<p><u>Experimental type 2</u></p> <ul style="list-style-type: none"> -All chromosomes are labelled for DNA and kinetochores -A subgroup of Metacentric chromosomes is labelled with the pericentromeric Meta-TALE (Meta-labelled)
	<p><u>Experimental type 3</u></p> <ul style="list-style-type: none"> - All chromosomes are labelled for DNA -All acrocentric chromosomes are labelled with the acro-Tale (Acro-labelled) -The subgroup of metacentric chromosomes is labelled with the Meta-TALE (Meta-labelled)

B Examples of acro- and meta-labelled chromosomes in metaphase I



C Examples of acro- and meta-labelled chromosomes in metaphase II

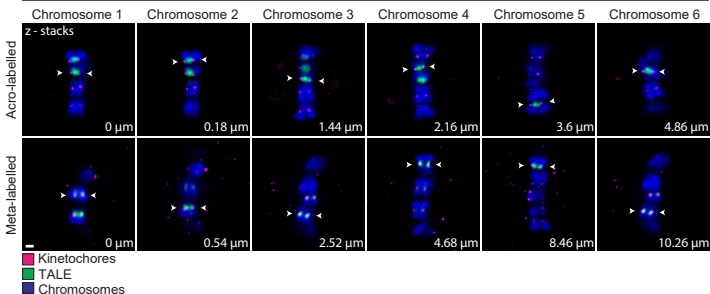


Fig S2. Porcine acrocentric chromosomes are prone to erroneous attachment creation (A) Illustration of the labelling system in the porcine oocytes for the 3 different types of experiments. Labelling with the acrocentric-TALE, labelling with the metacentric-TALE and labelling with both TALEs simultaneously. Explanation of what is labelled in each experiment and the respective nomenclature can be found on the left side of the table. Magenta, kinetochores; gray, acrocentric-TALE; orange, metacentric-TALE; blue, chromosomes; **(B)** Single z-planes of labelled chromosomes with the acrocentric-TALE (top row) and the metacentric TALE (bottom row) from meiosis I intact porcine cell injected with the respective TALE. Magenta, kinetochores, (ACA); green, TALE (anti-GFP); blue, chromosomes, (Hoechst); Scale bar, 1 μm . **(C)** Single z-planes of labelled chromosomes with the acrocentric-TALE (top row) and the metacentric TALE (bottom row) from meiosis II intact porcine cell injected with the respective TALE. Magenta, kinetochores, (ACA); green, TALE (anti-GFP); blue, chromosomes, (Hoechst); Scale bar, 1 μm .

Figure S3

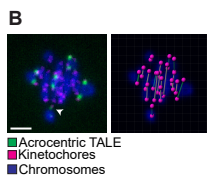
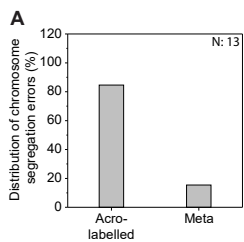


Fig. S3 Acrocentric chromosomes are lagging during anaphase and misalign during late metaphase more often than the metacentric (A) Proportion of the type of chromosomes in the total missegregated chromosomes. The number of missegregated chromosomes is indicated with N. **(B)** Still images from porcine chromosomes during alignment in the metaphase plate (left-hand side) and the corresponding image from imaris with the tracking annotation (right-hand side). White arrowhead indicates the misaligned acro-labelled chromosome. On the left, magenta, kinetochores (mScarlet-hCENPC); green, acrocentric label, (Acrocentric-TALE-GFP); blue, chromosomes, (H2B-SNAPf); and on the right magenta, kinetochores; green line, pair of homologous acro-labelled kinetochores; white line, pair of homologous meta kinetochores. Scale bar, 1 μ m.

Figure S5

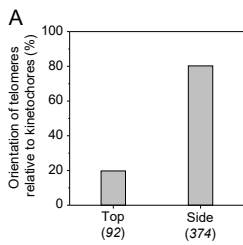
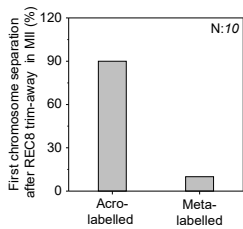


Fig S5. The small arm of acrocentric chromosomes hinders the end-on microtubule attachment creation. (A) Proportion of the configuration on top and the configuration on the side from the total kinetochores examined. Number of chromosomes analyzed is indicated in brackets under each category

Figure S6

A



B

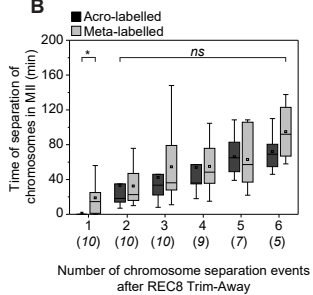


Fig S6. Pig acrocentric chromosomes have on average less cohesin than metacentric chromosomes

(A) Percentage of the first chromosome to separate after trim-away of REC8 in metaphase II porcine cells. **(B)** Time of separation for each of the six acro-labelled and meta-labelled chromosomes after trim-away of REC8 in porcine eggs. As time point zero in each cell is the time of the first chromosome separation. (two sample t-test performed between each separation event for acro-labelled and meta-labelled). * $p < 0.05$ and ns: non-significant. Number of chromosomes analyzed is indicated in brackets.

4. Manuscript 2

(published)

Title: Meiotic Kinetochores Fragment into Multiple Lobes upon Cohesin Loss in Aging Eggs

Authors: Agata P Zielinska ¹, **Eirini Bellou** ¹, Ninadini Sharma ¹, Ann-Sophie Frombach ¹, K Bianka Seres ², Jennifer R Gruhn ³, Martyn Blayney ⁴, Heike Eckel ⁵, Rüdiger Moltrecht ⁵, Kay Elder ⁴, Eva R Hoffmann ³, Melina Schuh ⁶

Affiliations:

¹Max Planck Institute for Biophysical Chemistry, Am Fassberg 11, Göttingen 37077, Germany.

²Max Planck Institute for Biophysical Chemistry, Am Fassberg 11, Göttingen 37077, Germany; Bourn Hall Clinic, High Street, Cambridge CB23 2TN, UK.

³DNRF Center for Chromosome Stability, Department of Cellular and Molecular Medicine, University of Copenhagen, Blegdamsvej 3, Copenhagen DK-2200, Denmark.

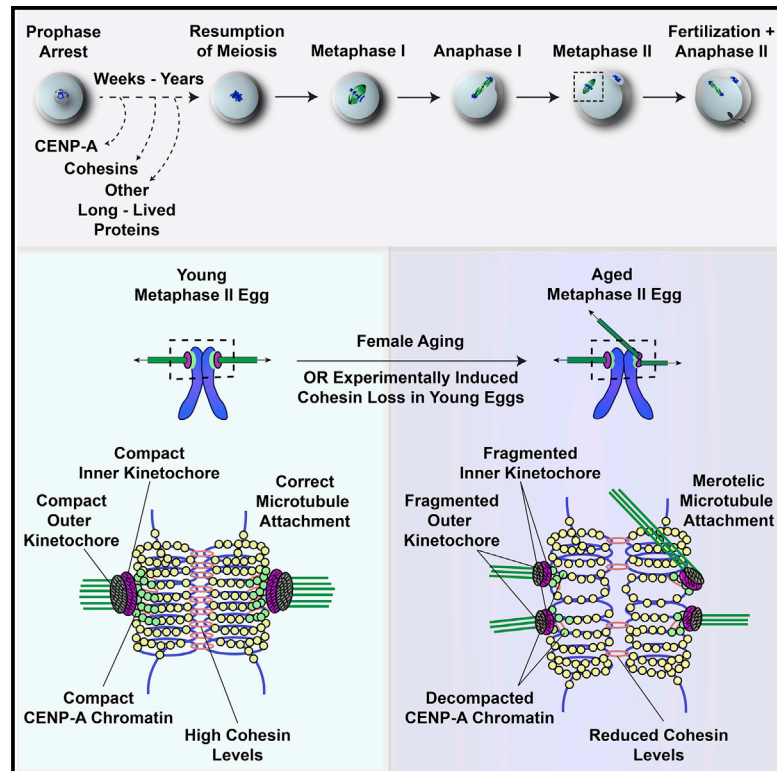
⁴Bourn Hall Clinic, High Street, Cambridge CB23 2TN, UK.

⁵Kinderwunschzentrum, Kasseler Landstraße 25A, Göttingen 37081, Germany.

⁶Max Planck Institute for Biophysical Chemistry, Am Fassberg 11, Göttingen 37077, Germany.
Electronic address: melina.schuh@mpibpc.mpg.de.

Meiotic Kinetochores Fragment into Multiple Lobes upon Cohesin Loss in Aging Eggs

Graphical Abstract



Authors

Agata P. Zielinska, Eirini Bellou, Ninadini Sharma, ..., Kay Elder, Eva R. Hoffmann, Melina Schuh

Correspondence

melina.schuh@mpibpc.mpg.de

In Brief

Aneuploidy in eggs increases dramatically as females age. Zielinska et al. show that aging affects the internal architecture of centromeres and kinetochores in mammalian eggs, including humans. As cohesin is lost, centromeric chromatin decompacts and kinetochores fragment, which is linked to incorrect chromosome-microtubule attachments.

Highlights

- Centromeric chromatin in oocytes decompacts as females age
- MI/MII kinetochores built on decompact centromeres fragment into multiple lobes
- A partial loss of cohesin is sufficient to mimic these changes in young eggs
- Fragmented kinetochores frequently interact incorrectly with spindle microtubules



Meiotic Kinetochores Fragment into Multiple Lobes upon Cohesin Loss in Aging Eggs

Agata P. Zielinska,¹ Eirini Bellou,¹ Ninadini Sharma,¹ Ann-Sophie Frombach,¹ K. Bianka Seres,^{1,2} Jennifer R. Gruhn,³ Martyn Blayney,² Heike Eckel,⁴ Rüdiger Moltrecht,⁴ Kay Elder,² Eva R. Hoffmann,³ and Melina Schuh^{1,5,*}

¹Max Planck Institute for Biophysical Chemistry, Am Fassberg 11, Göttingen 37077, Germany

²Bourn Hall Clinic, High Street, Cambridge CB23 2TN, UK

³DNRF Center for Chromosome Stability, Department of Cellular and Molecular Medicine, University of Copenhagen, Blegdamsvej 3, Copenhagen DK-2200, Denmark

⁴Kinderwunschzentrum, Kasseler Landstraße 25A, Göttingen 37081, Germany

⁵Lead Contact

*Correspondence: melina.schuh@mpibpc.mpg.de

<https://doi.org/10.1016/j.cub.2019.09.006>

SUMMARY

Chromosome segregation errors during female meiosis are a leading cause of pregnancy loss and human infertility. The segregation of chromosomes is driven by interactions between spindle microtubules and kinetochores. Kinetochores in mammalian oocytes are subjected to special challenges: they need to withstand microtubule pulling forces over multiple hours and are built on centromeric chromatin that in humans is decades old. In meiosis I, sister kinetochores are paired and oriented toward the same spindle pole. It is well established that they progressively separate from each other with advancing female age. However, whether aging also affects the internal architecture of centromeres and kinetochores is currently unclear. Here, we used super-resolution microscopy to study meiotic centromere and kinetochore organization in metaphase-II-arrested eggs from three mammalian species, including humans. We found that centromeric chromatin decompacts with advancing maternal age. Kinetochores built on decompacted centromeres frequently lost their integrity and fragmented into multiple lobes. Fragmentation extended across inner and outer kinetochore regions and affected over 30% of metaphase-II-arrested (MII) kinetochores in aged women and mice, making the lobular architecture a prominent feature of the female meiotic kinetochore. We demonstrate that a partial cohesin loss, as is known to occur in oocytes with advancing maternal age, is sufficient to trigger centromere decompaction and kinetochore fragmentation. Microtubule pulling forces further enhanced the fragmentation and shaped the arrangement of kinetochore lobes. Fragmented kinetochores were frequently abnormally attached to spindle microtubules, suggesting that kinetochore fragmentation could contribute to the maternal age effect in mammalian eggs.

INTRODUCTION

Chromosome segregation is driven by interactions between spindle microtubules and kinetochores, the macromolecular structures that assemble on centromeric nucleosomes containing the histone variant CENP-A [1–3]. These interactions allow the microtubule spindle to direct chromosome movement in space and time [4–6]. Failure to correctly attach all kinetochores generates cells with too many or too few chromosomes, a condition known as aneuploidy. Aneuploidy is particularly prominent in female meiosis: 20%–70% of human eggs carry an incorrect number of chromosomes, making chromosome segregation errors in oocytes a leading cause of pregnancy loss and human infertility [7–9].

Given the important role of kinetochores and centromeres in chromosome segregation, their structure has been studied extensively in mitosis [2, 10]. By contrast, our understanding of the internal architecture of centromeres and kinetochores in mammalian meiosis is still very limited. Studies in mice and humans have predominantly focused on the spacing between sister kinetochores during the two meiotic divisions [8, 9]. These studies revealed that the distance between sister kinetochores increases both in meiosis I [11–18] and meiosis II [17, 19–22] with advancing female age. This increase has been linked to an age-related loss of cohesin from chromosomes [23], as cohesins play an important role in sister kinetochore pairing and the cohesion between metaphase-I (MI) chromosomes and metaphase-II (MII) chromatids [11, 24–27]. In particular, centromeric cohesins pair sister kinetochores into a single functional unit during meiosis I, and physically link sister chromatids in meiosis II [28]. Cohesins are thought to be exceptionally long lived in oocytes and to gradually dissociate from chromosomes as females get older [12, 13, 23, 29, 30]. As cohesin levels decline, the space between sister kinetochores progressively increases. This has functional consequences for both meiosis I and meiosis II. Split meiosis-I sister kinetochores are more likely to form incorrect attachments to spindle microtubules [14, 17], and insufficient centromeric cohesion in meiosis II results in chromosomes separating prematurely into single chromatids [21, 31, 32] and aneuploidy [33–36]. However, although it is well established that sister kinetochores in oocytes separate



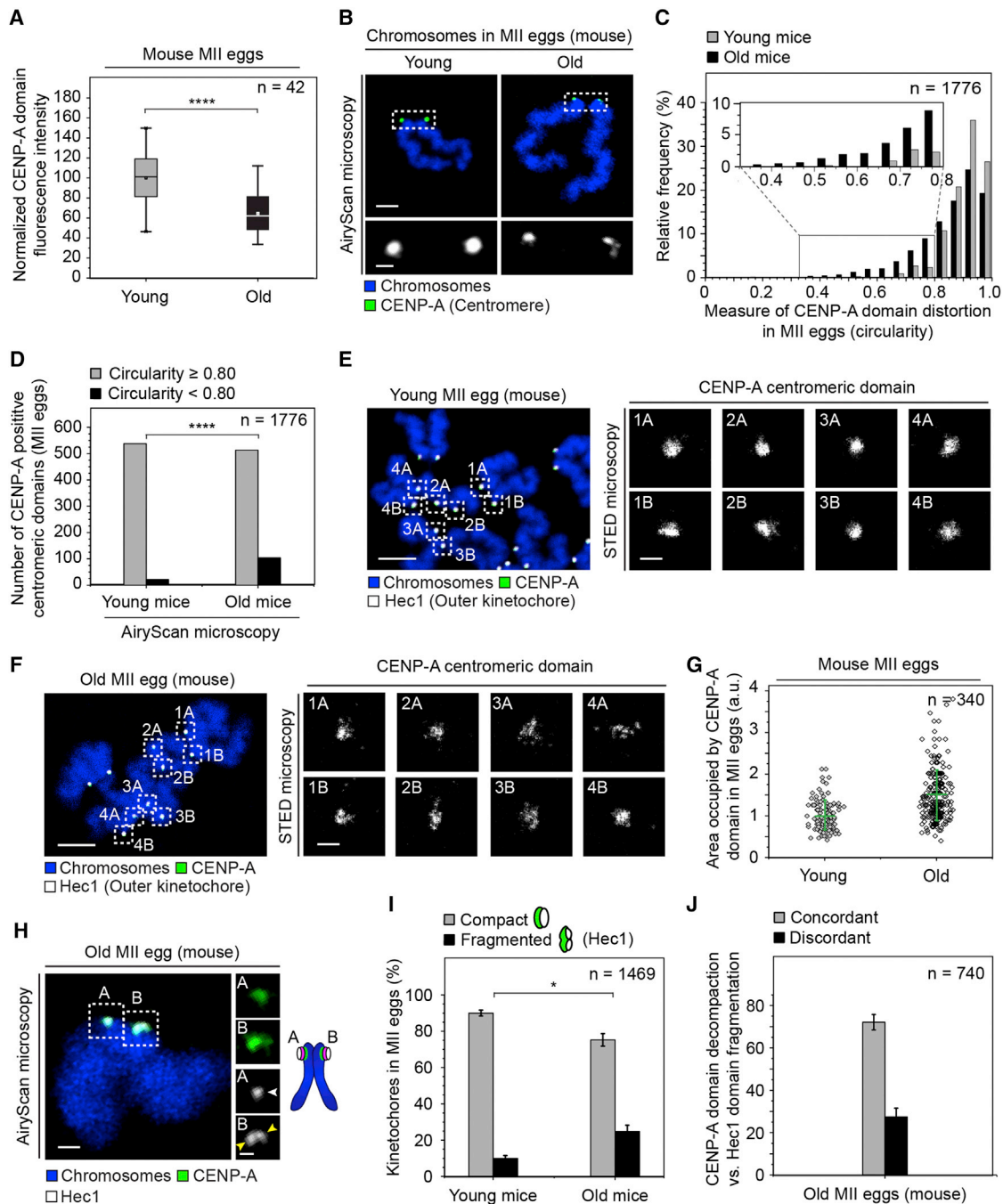


Figure 1. The Centromeric CENP-A Domain Decompacts as Oocytes Age and MII Kinetochores Built upon It Fragment into Lobes

(A) Centromeric CENP-A fluorescence intensity (integrated density of the centromeric region of interest [ROI] – mean background fluorescence \times ROI) in 42 mouse MII eggs (3 independent experiments). 100% was assigned to the mean intensity of young groups. Box plots show median (horizontal white lines), mean (small white squares), 25th and 75th percentiles (boxes), and 5th and 95th percentiles (whiskers).

(B) Representative metaphase-II chromosomes from a young and an old mouse egg (8- and 62-week-old females, respectively) visualized with Airyscan microscopy (z projections of 14–16 sections, acquired every 0.18 μm). Centromeres (green, CENP-A) and DNA (blue, Hoechst) are shown. Scale bars represent 2 μm in overviews, and 0.5 μm in insets.

(C) Quantification of MII centromere circularity across the two age groups. A circularity value of 1.0 indicates a perfect circle. 1,776 measurements from 14 young and 17 aged MII eggs, imaged as in (B).

(D) Age-related increase in centromere distortion (circularity < 0.80) in MII eggs from young and old mice, imaged as in (B).

(E) Representative chromosome spread of a young MII mouse egg. DNA signal (blue, Picogreen, confocal mode), outer kinetochore region (white, Hec1, confocal mode), and the centromeric signal (green, CENP-A, STED mode) are shown. Right: one centromere in each panel (STED microscopy, grayscale; A and B, sister centromeres).

(legend continued on next page)

from each other as females age, we still know very little about the internal architecture of centromeres and kinetochores in aging mammalian oocytes.

Given the importance of the kinetochore in chromosome segregation, it is conceivable that changes in the internal architecture of centromeres and kinetochores could contribute to aneuploidy in aging oocytes. This seems plausible because oocyte kinetochores are built on a centromeric chromatin scaffold that can be several decades old at the time of chromosome segregation [37]. If and how centromeric chromatin changes with age, and whether this affects the architecture of the kinetochores that are built upon it, are currently unclear.

We therefore analyzed whether the internal organization of the meiotic centromere and kinetochore change as females age. In particular, we used quantitative super-resolution microscopy to analyze the architecture and function of 35,700 meiotic kinetochores in three mammalian species, including humans. In most experiments, we studied the internal architecture of kinetochores during metaphase of meiosis II, as sister kinetochores are spatially separated from each other during this stage, which greatly facilitates the analysis of individual kinetochores. By contrast, sister kinetochores are predominantly fused during metaphase I [38], which impedes the assessment of individual kinetochores and makes this stage less suitable for studies of internal kinetochore architecture.

Our analysis suggests that the centromeric CENP-A domain, on which the kinetochore is assembled, becomes decompact with advancing female age. This was accompanied by fragmentation of inner and outer kinetochore regions into multiple lobes in over 30% of metaphase-II kinetochores of women and aged mice. An acutely induced loss of cohesin in eggs from young mice was sufficient to trigger the decompaction of CENP-A-containing chromatin, as well as kinetochore fragmentation, causing changes to the morphology of centromeres and kinetochores that closely resembled those in eggs from naturally aged females. Microtubule pulling further enhanced kinetochore fragmentation and shaped the pattern of the kinetochore lobules. Based on these data, we propose a model whereby the age-related cohesin loss not only favors aneuploidy by inducing a premature loss of cohesion within meiosis-I bivalents and meiosis-II chromosomes but also disrupts the organization of centromeric chromatin and thereby destabilizes the meiotic kinetochore in females.

RESULTS

The Centromeric CENP-A Domain Decompacts as Oocytes Age

To investigate whether aging affects the organization of centromeres, we used immunofluorescence microscopy to assess metaphase-II-arrested (MII) eggs from mice of different ages. In particular, we compared 8-week-old and 60- to 64-week-old FVB-N mice, which correspond to reproductively young and old females, as evident from a strong increase in aneuploidy in the aged group (Figure S1A).

MII centromeres in the aged group had strongly decreased levels of the centromere-specific histone variant CENP-A (Figure 1A), consistent with observations in prophase-arrested oocytes [39]. Strikingly, the centromeres also differed in their architecture. Whereas young centromeres had a compact CENP-A signal when visualized with Airyscan microscopy (Figure 1B, left panel), aged centromeres were often organized into multiple CENP-A subunits (Figure 1B, right panel) and frequently appeared decompact (Figures 1C and 1D).

Stimulated emission depletion (STED) microscopy, which has greater resolving power [40], revealed multiple clustered CENP-A foci within the aged centromeric domain (Figures 1F and S1B). This was in contrast to the compact appearance of centromeres in young eggs (Figures 1E and S1B). Consistent with age-related decompaction, the CENP-A domain was distributed over a larger surface area in eggs from older mice (Figure 1G). Decompaction of individual centromeres into multiple subunits was also evident in meiosis-I bivalents (Figure S1C, yellow arrowheads), suggesting that it is a general feature of aged meiotic centromeres. Altogether, these results establish that centromeric chromatin in oocytes and eggs decompacts as females age.

Kinetochores Built on Decompacted Centromeres Fragment into Lobes

Next, we asked whether kinetochores, which assemble upon centromeres, also show age-related changes in mammalian eggs. We first examined the outer kinetochore components on chromosome spreads. The outer kinetochore Hec1 domain that directly interacts with spindle microtubules appeared distorted in aged mouse eggs, and was frequently fragmented into two prominent lobes (Figures 1H, 1I, and S1D). In 75% of cases, the centromeric CENP-A region and the Hec1 kinetochore domain were concordant, with both appearing either

(F) Representative chromosome spread of an MII egg from an old mouse (63 weeks), labeled as in (E).

(G) Surface area of CENP-A centromeric domains in MII eggs from young and aged mice, acquired as in (E) and (F). Distortion of the centromeric domain was measured as the surface area of the smallest circle encompassing the CENP-A signal (119 young and 221 aged centromeres analyzed). Mean and SD are shown.

(H) Representative Airyscan-imaged metaphase-II chromosome from an aged mouse egg (61-week-old female). Outer kinetochores (white, Hec1), centromeres (green, CENP-A), and DNA (blue, Hoechst) are shown. Scale bars represent 1 μm in overview, and 0.5 μm in insets.

(I) Quantification of kinetochore configurations visualized with Airyscan microscopy, based on the outer Hec1 signal in 37 MII mouse eggs (3 experiments), labeled as in (H).

(J) Quantification of how frequently the MII outer kinetochore pattern follows changes in the underlying centromeric domain. Concordant indicates centromere/outer kinetochore pairs where the CENP-A/Hec1 signals were both either compact or fragmented. 740 centromeres and their corresponding kinetochores from 19 old MII mouse eggs (3 experiments), labeled as in (B) and (H).

Young MII eggs: 8-week-old females; aged eggs (12 animals): 60- to 64-week-old females. Scale bars represent 4 μm in overviews, and 0.5 μm in insets in (E) and (F). p values are designated as *p < 0.05 and ****p < 0.0001. p values were calculated with Student's t test (I) and Fisher's exact test (D). In (A), mean fluorescence measurements per egg were compared by one-way ANOVA followed by Tukey's test. Error bars show SEM. White arrows point to compact kinetochores, and yellow arrows point to lobes within a fragmented MII kinetochore.

See also Figure S1.

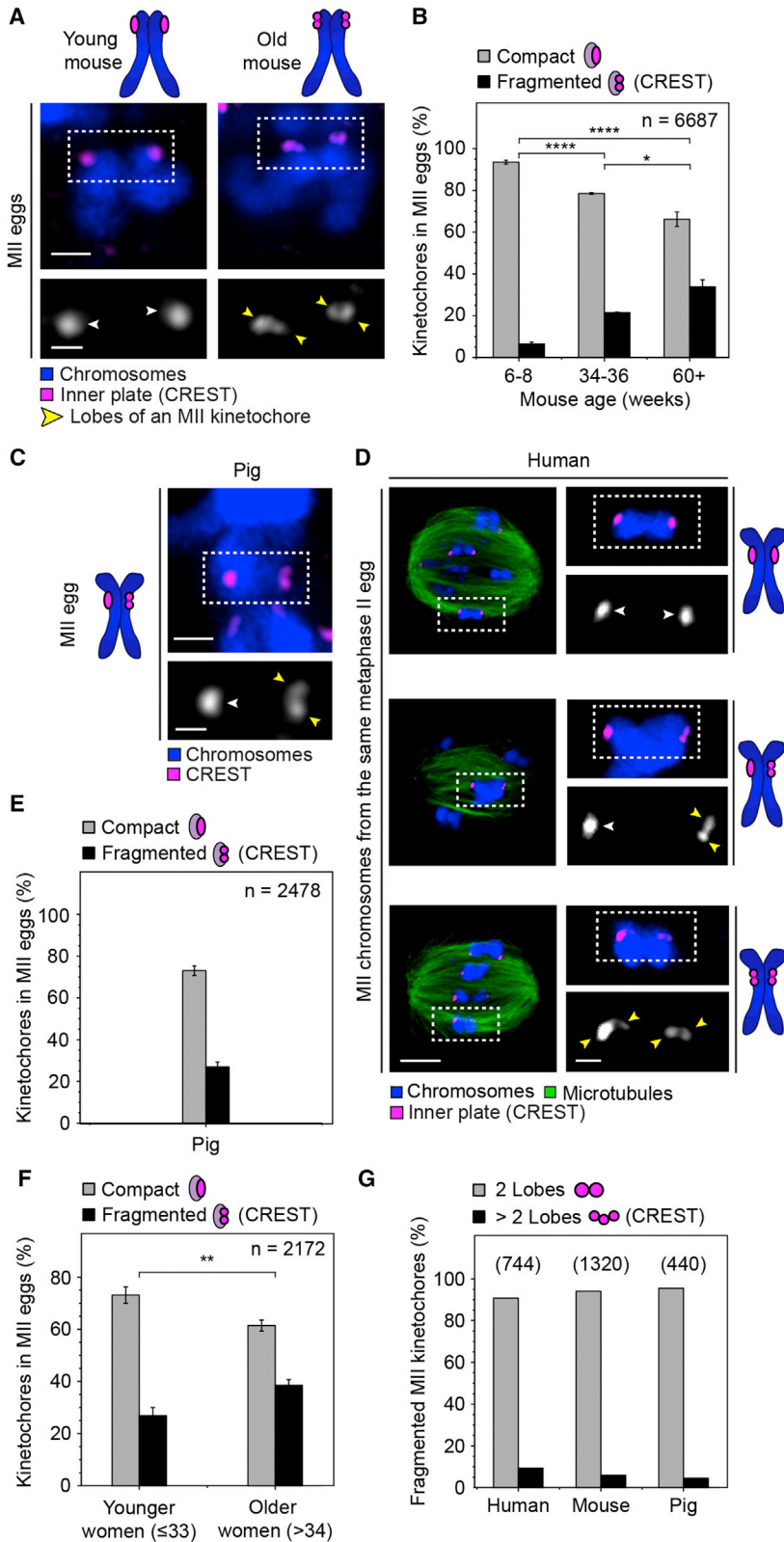


Figure 2. Kinetochores Fragmentation Is Conserved across Various Mammalian Species

(A) Examples of kinetochores in MII eggs from young (8 week) and aged (≥ 60 week) mice. (B) Kinetochore configurations shown in (A) and their occurrence in 176 MII eggs from mice of different ages (6 experiments; aged eggs originated from 29 mice). (C) Representative pig metaphase-MII chromosome and its corresponding kinetochores. (D) Three representative human MII chromosomes from the same egg (33-year-old donor). Scale bars represent $4 \mu\text{m}$ in overview, and $0.5 \mu\text{m}$ in insets. (E) Kinetochore configurations shown in (C) and their occurrence in 63 pig MII eggs (8 experiments). (F) Kinetochore configurations shown in (D) and their occurrence in 17 MII eggs from young (≤ 33 years old) and 32 MII eggs from older (>34 years old) women. (G) Multi-lobular kinetochore configurations (2 or >2 distinct lobes) and their occurrence in MII eggs from humans, pigs, and aged mice. Kinetochores (magenta, CREST) and DNA (blue, Hoechst) are shown in (A), (C), and (D). In (D), microtubules are additionally labeled (green, α -tubulin). Chromosomes were fixed on intact spindles at the metaphase-II stage and imaged with Airyscan microscopy. Scale bars represent $1 \mu\text{m}$ in overview, and $0.5 \mu\text{m}$ in insets in (A) and (C). p values are designated as *p < 0.05, **p < 0.01, and ****p < 0.0001. All p values were calculated with Student's t test. Error bars show SEM. White arrows point to compact kinetochores, and yellow arrows point to lobes within a fragmented MII kinetochore. See also Figure S2.

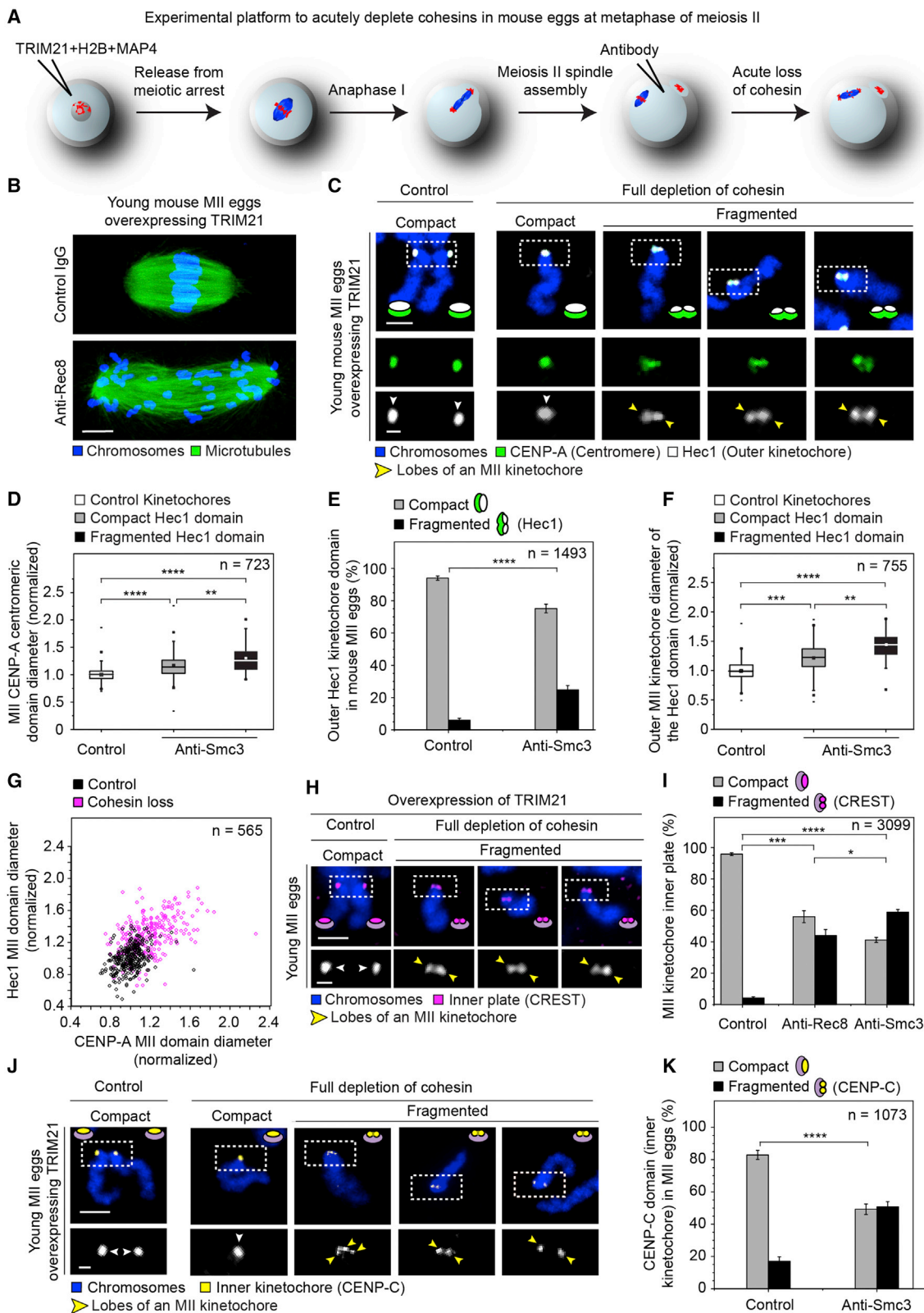


Figure 3. Cohesin Loss Causes Decompaction of Centromeric Chromatin and Fragmentation of Meiotic Kinetochores

(A) Scheme of Trim-Away experiments to acutely degrade cohesins in mouse metaphase-II eggs. Trim-Away is a protein depletion tool, which uses antibodies to rapidly remove unmodified, native proteins via the antibody receptor/E3 ubiquitin ligase TRIM21 and the endogenous protein degradation machinery.

(legend continued on next page)

compact or fragmented (Figure 1J). Centromere decompaction hence correlates with the fragmentation of the outer kinetochore domain, and both are increased in aged mouse eggs.

We then tested whether the age-related changes in centromere and kinetochore architecture are also evident in intact eggs, in which the three-dimensional arrangement of chromosomes on the spindle is preserved. Because the majority of super-resolution techniques are not compatible with the size of mammalian oocytes, we employed Airyscan microscopy to establish whether the bilobed appearance is evident across the kinetochore complex. We labeled inner kinetochore plates (Figure S2A) with CREST antisera (Figure 2A), which mark predominantly CENP-B [41]. Consistent with the observations for Hec1, CREST-labeled inner kinetochore plates appeared as fragmented foci in 6% and 21% of MII eggs from mice aged 8 weeks and 34–36 weeks, respectively (Figure 2B, left and middle panels). The frequency of kinetochore fragmentation further increased to over 33% in eggs from mice older than 60 weeks (Figure 2B, right panel). The changes in MII kinetochore architecture between young and aged eggs could not be attributed to differences in the time required for the oocytes to progress through meiosis I (Figure S2B). They were also not an artifact of the imaging conditions that we used, because mitotic kinetochores under identical conditions appeared as single compact structures (Figures S2C and S2D). Together, these data suggest that inner and outer kinetochore regions fragment into lobes in aged mouse eggs.

Kinetochore Fragmentation Is Conserved across Various Mammalian Species

To establish whether fragmented kinetochores are also present in other species, we examined eggs from humans and pigs (Figures

2C and 2D). Around 25% of kinetochores were fragmented in MII eggs from pre-pubertal pigs and young women (Figures 2E, 2F, and S2E–S2H). The kinetochore inner plates here also predominantly reorganized into two lobes (Figure 2G). Consistent with our findings in aged mice, kinetochore fragmentation in human MII eggs became more apparent with advancing age, affecting 39% of meiotic kinetochores in women over 34 years (Figure 2F). Furthermore, in human kinetochores that appeared bilobular, the fragmentation similarly affected multiple layers of the kinetochore complex, as evident from the bilobular appearance of outer plates marked with Hec1 and CENP-F and the fibrous corona labeled with BubR1 (Figure S2I). Together, these data suggest that fragmentation is a prominent and widely conserved feature of the meiotic kinetochore that is already present in young women but becomes more pronounced with advancing age.

Cohesin Loss Causes Decompaction of Centromeric Chromatin and Fragmentation of Meiotic Kinetochores

We next investigated the mechanism underlying the age-related decompaction of centromeric chromatin and kinetochore fragmentation. We wondered whether the architectural changes that we observed might be linked to the loss of cohesin from chromosomes, which is well established to occur with advancing maternal age [12, 13, 30, 42]. Cohesin might be required to arrange CENP-A-containing chromatin into a compact platform that is suitable for the assembly of stable kinetochores in mammalian oocytes. This model predicts that a loss of cohesin would be sufficient to trigger CENP-A domain decompaction and kinetochore fragmentation.

To test this hypothesis, we used the Trim-Away approach to remove cohesin acutely in metaphase of meiosis II (Figure 3A). Trim-Away utilizes antibodies to target unmodified, native

(B) Immunolabeled young TRIM21 overexpressing metaphase-II mouse eggs, microinjected with either a control IgG antibody (top) or an anti-Rec8 antibody provided in excess (bottom), as in (A). Images are z projections of 63–69 sections, acquired every 0.19 μm . Microtubules (green, α -tubulin) and chromosomes (blue, Hoechst). The scale bar represents 5 μm .

(C) Representative chromosome spreads from young metaphase-II mouse eggs depleted of Smc3. Insets: a chromosome (control, left panel) or individual single chromatids (all other panels). Outer kinetochores (white, Hec1), centromeres (green, CENP-A), and chromosomes (blue, Hoechst) are shown.

(D) Normalized diameter of the CENP-A centromeric domain in control and young mouse MII eggs depleted for Smc3, as in (C). CENP-A domains were divided into three groups, based on the fragmentation status of the overlying Hec1 kinetochore. 723 centromeres from 20 MII eggs were evaluated (2 experiments).

(E) Occurrence of different kinetochore architectures based on outer kinetochore Hec1 signal in cells treated as in (C). Data are from 35 MII eggs (young mice; 2 experiments).

(F) Normalized diameter of the Hec1 kinetochore domain in control and young mouse eggs depleted for Smc3. Both the fragmentation status and the diameter measurements were based on Hec1 labeling. 755 kinetochores from 20 MII eggs were evaluated (2 experiments).

(G) The diameter of the CENP-A centromeric domain (a.u.) plotted against the Hec1 outer kinetochore diameter (a.u.) for each of the 565 MII kinetochores following a full depletion of Smc3/control MII eggs as in (C). Pearson's correlation coefficients: $r = 0.402$ (controls) and $r = 0.495$ (experimental group).

(H) Inner plates of MII kinetochores in metaphase-arrested eggs from young mice in a control chromosome (left panel; two sister kinetochores) and in single chromatids induced by a full depletion of Rec8 (other panels), achieved as in (B). Chromosomes (blue, Hoechst) and kinetochore inner plates (magenta, CREST) are shown.

(I) Occurrence of MII kinetochore configurations in young eggs following the targeting of distinct cohesin subunits (Rec8, Smc3) by Trim-Away (full depletion) and in control eggs. Data are from 79 MII eggs from young mice (3 experiments).

(J) Young metaphase-II eggs labeled with the inner kinetochore protein CENP-C. Images show a control chromosome (left panel; two sister kinetochores) and single chromatids induced by a full depletion of Rec8 (other panels), obtained as in (A). Chromosomes (blue, Hoechst) and kinetochore inner plates (yellow, CENP-C) are shown.

(K) Occurrence of different kinetochore architectures based on the inner kinetochore CENP-C signal in cells treated as in (J). Data from 36 MII eggs (young mice; 2 experiments).

Scale bars represent 2 μm in overviews, and 0.5 μm in insets in (C), (H), and (J).

p values are designated as * $p < 0.05$, ** $p < 0.01$, *** $p < 0.001$, and **** $p < 0.0001$. p values were calculated with Student's t test in (I) and Fisher's exact test in (E) and (K); in (D) and (F), mean measurements per egg were compared by one-way ANOVA followed by Tukey's test. Error bars show SEM. Box plots show median (horizontal lines), mean (small squares), 25th and 75th percentiles (boxes), and 5th and 95th percentiles (whiskers). Arrows: white point to compact kinetochores, and yellow point to lobes within a fragmented MII kinetochore.

See also Figures S3–S5 and Videos S1 and S2.

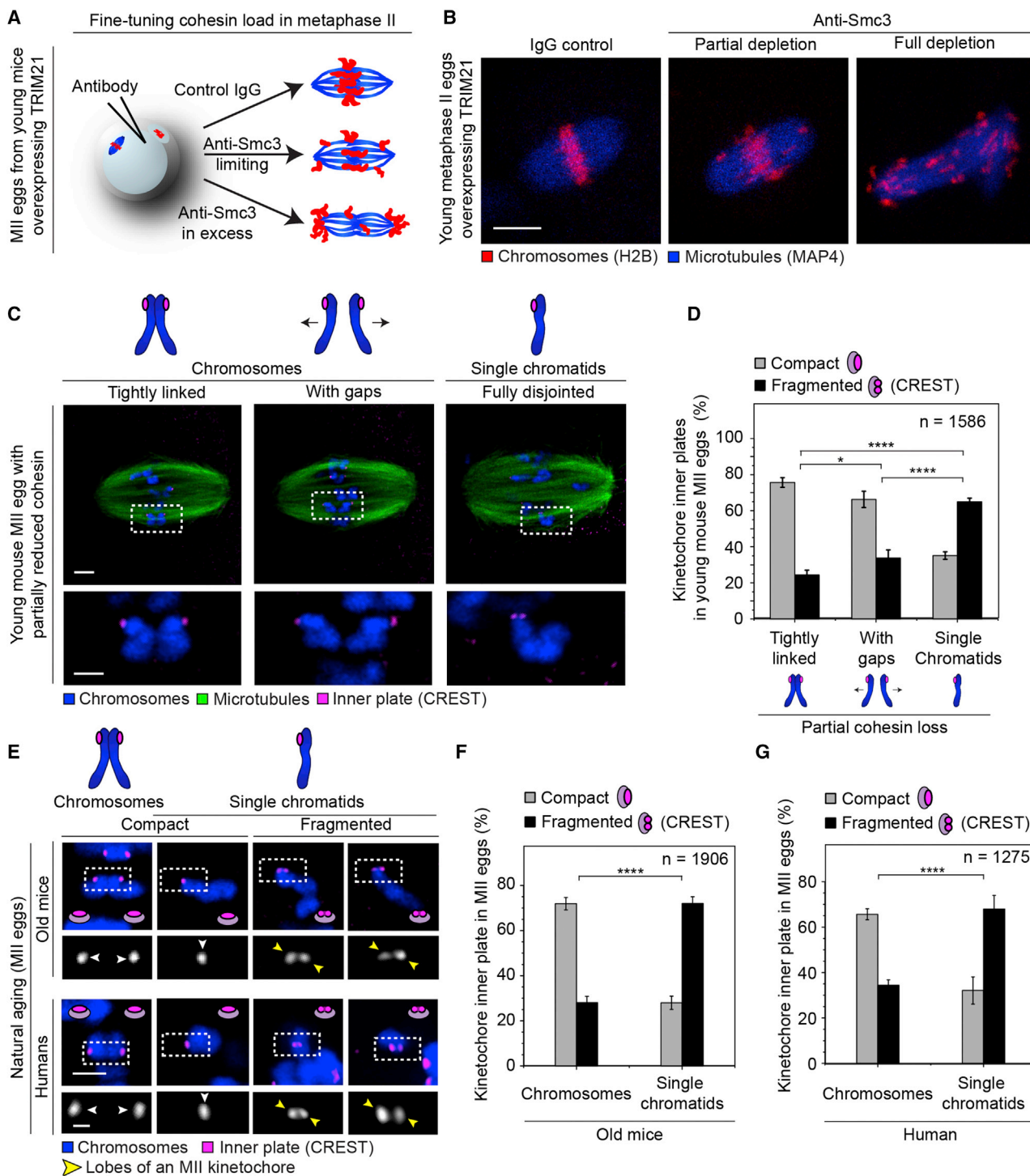


Figure 4. The Extent of Kinetochore Fragmentation Correlates with the Degree of Cohesion Loss

(A) Scheme of the partial Trim-Away method in metaphase-II eggs. The degree of cohesin loss is fine-tuned by varying the amount of microinjected antibody. (B) Representative live spindles from TRIM21-overexpressing young MII eggs microinjected with either a control IgG antibody or various concentrations of the anti-Smc3 antibody. Chromosomes (red, H2B-mRFP) and microtubules (blue, MAP4-MTBD-Snap647). The scale bar represents 10 μ m.

(C) Representative examples of the three chromosome categories aligned at the equator of the same metaphase-II spindle following partial depletion of Smc3 by Trim-Away, as in Figure S5E.

(D) Occurrence of different MII kinetochore architectures based on CREST signal in the three chromosome categories defined by Hoechst signal, as in (C), following partial depletion of Smc3 (41 young MII eggs, 4 experiments).

(legend continued on next page)

proteins for proteasome-mediated degradation via the antibody receptor/E3 ubiquitin ligase TRIM21 [43]. In particular, we used two independent approaches to target the meiotic cohesin complex in eggs, using antibodies against the cohesin subunit Smc3 [44] and the meiosis-specific α -kleisin variant Rec8 [24, 45–47]. Quantitative immunofluorescence of Rec8 (Figures S3A–S3C) and Smc3 (Figures S3D and S3E) on chromosome spreads confirmed that Trim-Away of either subunit resulted in removal of cohesin complexes from the centromeric regions of MII chromosomes. Consistent with centromeric cohesin removal, all chromosomes separated into single chromatids within minutes of Rec8 or Smc3 antibody microinjection (Figures 3B, S3F, and S3G; Video S1). Thus, Trim-Away with antibodies against either Rec8 or Smc3 is consistent, and efficiently depletes centromeric cohesins in metaphase-II-arrested eggs from young mice.

We then assessed whether acute removal of cohesin was sufficient to reproduce the changes in centromeric chromatin and kinetochore architecture that we had observed in aged mice. Indeed, degradation of Smc3 caused a prominent decompaction of centromeric chromatin (Figures 3C, 3D, and S4A) and fragmentation of the Hec1 domain into two lobes (Figures 3C, 3E, 3F, S4B, and S4C). Importantly, the increased diameter of the Hec1 domain positively correlated with the size of the underlying CENP-A centromeric domain (Figure 3G), further supporting our model that the age-related changes in centromere and kinetochore architecture are coupled. Moreover, the inner kinetochore plates (marked by CREST and CENP-C; Figures 3H–3K, S4D, and S5A; Video S2), as well as the fibrous corona (marked by BubR1; Figures S5B and S5C), also frequently fragmented into two lobes upon cohesin removal. Together, these data establish that a loss of cohesin is sufficient to trigger the decompaction of centromeric chromatin and the fragmentation of inner and outer kinetochore regions, closely resembling the changes in centromere and kinetochore architecture that we observed in aged eggs.

The Extent of Kinetochore Fragmentation Correlates with the Degree of Cohesion Loss

Chromosomes in aged MII eggs are affected by loss of cohesin to different degrees [31]. Metaphase-II chromosomes in which cohesin is depleted to a lesser degree remain intact, with both chromatids still linked, and only the distance between their sister kinetochores increases. By contrast, chromosomes with more severe cohesin depletion separate completely into single chromatids (Figure S5D). To reproduce these different chromosome architectures in eggs from young females, we modified the Trim-Away approach to enable a partial depletion of cohesin by using lower amounts of the Smc3 antibody (Figures 4A and S5E–S5G). Under these conditions, only a subset of metaphase-II chromosomes separated into single chromatids (Figure 4B, middle

panel and Figure S5E), although the proportion of disjointed chromosomes was still higher than following natural aging (Figure S5D). We then used young mouse eggs partially depleted of cohesins, as well as eggs from aged mice, to determine whether the extent of cohesion loss correlates with the extent of kinetochore fragmentation.

In young eggs with partially reduced cohesin, 67% of CREST-labeled kinetochores on single chromatids were fragmented, in comparison to only 28% on intact chromosomes (Figures 4C and 4D, left and right panels). Also within the intact chromosome class, the degree of cohesion between sister chromatids differed: some sister chromatids remained tightly associated, indicative of high cohesion levels, whereas others were still connected but separated by prominent gaps, indicative of reduced cohesion (Figure 4C, “tightly linked” and “with gaps”). Interestingly, closely associated chromatids (Figure 4D, left panel) were less likely to show kinetochore fragmentation than chromatids with gaps (Figure 4D, middle panel). This correlation between kinetochore fragmentation and the degree of cohesion loss was also apparent in naturally aged MII eggs from mice and humans (Figures 4E–4G; Video S3). Together, these data establish that the degree of cohesion loss correlates with the degree of kinetochore fragmentation.

Kinetochore Fragmentation Is Also Evident during Meiosis I

Our data established that MII kinetochores frequently fragment into multiple lobes in eggs of various mammalian species (Figure 2). However, the oocyte segregates its chromosomes twice. Because cohesion in aged oocytes is already reduced in meiosis I [8, 23], kinetochore fragmentation could in principle affect both divisions of the mammalian oocyte.

In line with this idea, fragmented kinetochores could also be detected in meiosis I in both naturally aged human and mouse oocytes (Figures S6A and S6B). To establish whether cohesin loss is also sufficient to trigger kinetochore fragmentation during meiosis I, we modified our Trim-Away approach to partially deplete cohesins at metaphase I (Figure 5A). In particular, we determined conditions that maintained homologous chromosome pairing in mouse oocytes (Figures 5B, 5C, and S6C) but caused an increase in sister kinetochore distance to a degree that we have previously reported in naturally aged human oocytes from women in their mid-thirties (Figure 5D) [17], indicative of reduced cohesion in the centromeric region.

The separation of sister kinetochores upon partial cohesin depletion (Figures 5D and 5E) was indeed coupled to changes in kinetochore architecture (Figures 5E–5G, S6D, and S6E). Despite the high proximity of sister kinetochores in meiosis I, a significant fraction of MI kinetochores became visibly

(E) Representative kinetochores in chromosomes (left panels) and single chromatids (all other panels) in MII eggs from aged mice (≥ 60 weeks) or women of all ages.

(F) Kinetochore architectures shown in (E) and their occurrence on intact chromosomes and single chromatids (50 metaphase-II eggs from aged mice, 5 experiments).

(G) Kinetochore architectures shown in (E) and their occurrence on intact chromosomes and single chromatids in 29 human MII eggs.

Scale bars, 2 μm in overview, and 0.5 μm in insets. Chromosomes (blue, Hoechst) and kinetochores (magenta, CREST) are shown in (C) and (E). In (C), microtubules are additionally labeled (green, α -tubulin).

p values are designated as * $p < 0.05$ and **** $p < 0.0001$. p values were calculated with Fisher's exact test. Error bars show SEM. Arrows: white point to compact kinetochores, and yellow point to lobes within a fragmented MII kinetochore.

See also Figure S5 and Video S3.

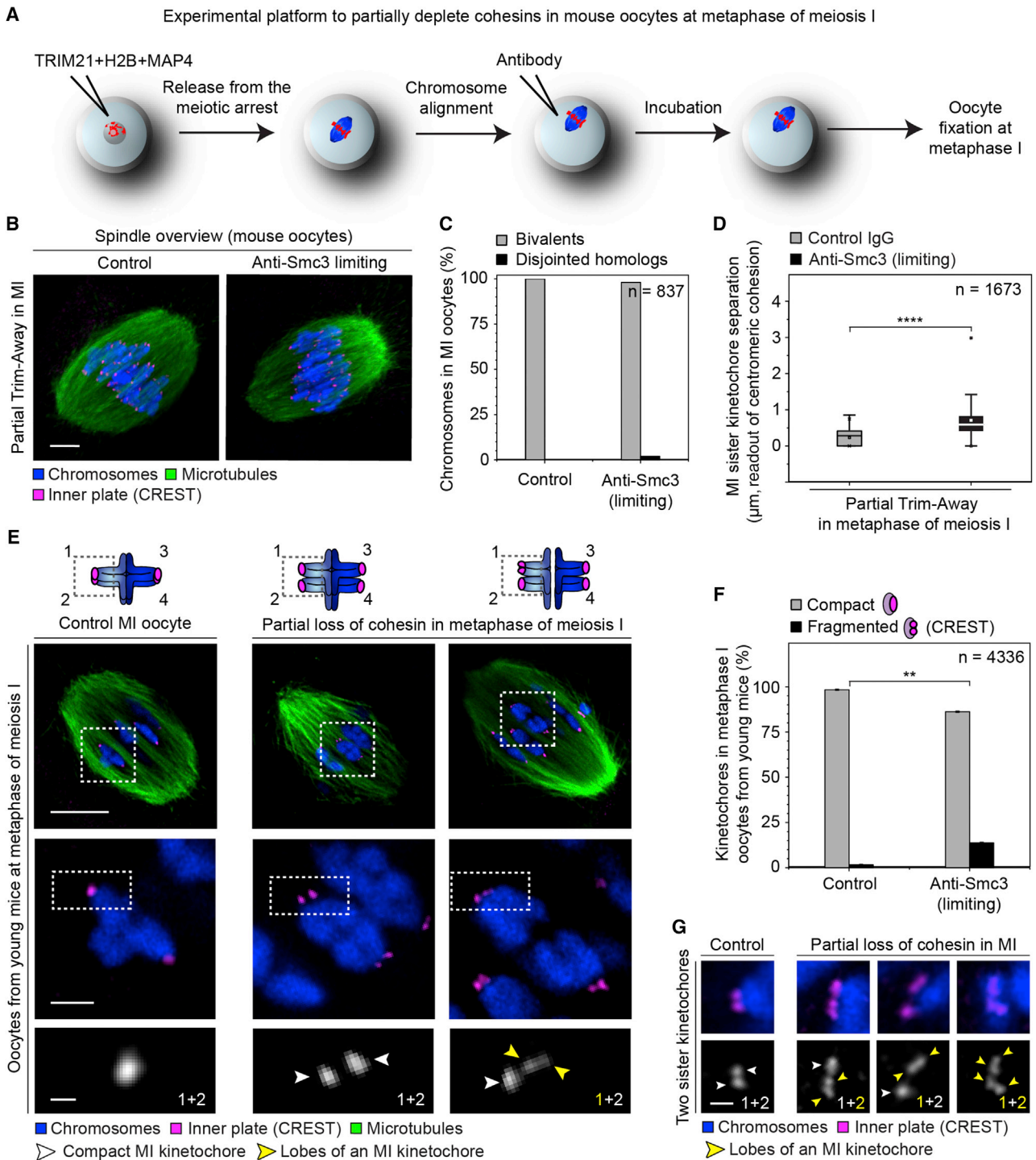


Figure 5. Kinetochore Fragmentation Is Also Evident during Meiosis I

(A) Scheme of the partial Trim-Away method in metaphase I, where cohesin levels are reduced by microinjecting an anti-Smc3 antibody at a limiting concentration.

(B) Representative Trim-Away spindles at late metaphase I, in young mouse oocytes microinjected with a control antibody (left panel) or with an anti-Smc3 antibody at a limiting concentration (right panel). Images are z projections of 82 sections acquired every 0.18 μm. The scale bar represents 5 μm.

(C) Occurrence of different chromosome architectures assessed based on the Hoechst signal in MI oocytes treated as in (B). Data are from 42 young MI oocytes (2 experiments).

(D) Distance between the two sister kinetochores of a bivalent in metaphase-I oocytes from young mice treated as in (B). Data are from 42 young MI oocytes (2 experiments). Box plots show median (horizontal white lines), mean (small white squares), 25th and 75th percentiles (boxes), and 5th and 95th percentiles (whiskers).

(legend continued on next page)

fragmented (Figures 5F, 5G, and S6E). Thus, as cohesins are lost, sister kinetochores not only uncouple but individual MI kinetochores also fragment into lobes.

Fragmented Kinetochores Are More Likely to Be Abnormally Attached to Spindle Microtubules

Next, we investigated how fragmented kinetochores interact with microtubules. We first examined whether fragmented kinetochores are still able to attach to the spindle. To achieve this, we selectively visualized kinetochore-bound microtubules (called k-fibers) by briefly exposing mouse eggs to cold [48]. This revealed that fragmented kinetochores are predominantly still functional: the number of unattached kinetochores in intact chromosomes did not differ significantly between the compact and fragmented kinetochore groups (Figure S7A). However, whereas over 90% of intact kinetochores attached as expected to one k-fiber only, 49% of fragmented kinetochores were attached to two distinct k-fiber bundles (Figure 6A).

Because kinetochores become compartmentalized into two lobes with age and each fragment frequently interacts with an independent k-fiber bundle, we wondered whether fragmented kinetochores are also more likely to be merotelically attached (Figure 6B). Chromosome segregation errors often result from merotelic attachments, where a single kinetochore is simultaneously bound to microtubules from opposite spindle poles [14, 49–51]. These merotelically attached kinetochores will lag at anaphase onset, increasing the chances of mis-segregation [49]. Our analysis revealed that over 31% of fragmented kinetochores were merotelically attached, compared to only 7% of intact kinetochores (Figure 6C). Frequently, only one fragment interacted with each spindle pole (“bilobular merotelic,” Figures 6D and 6E). This observation may also explain why single chromatids were often able to align in the center of the meiotic spindle (Figures 6D and S7B) [50], despite having a single kinetochore only. Although chromosome alignment is generally thought to rely on two distinct kinetochores that attach to spindle microtubules originating from opposite spindle poles, these data suggest that single meiotic kinetochores can also promote alignment of single chromatids, by splitting into two lobes, which both attach to k-fibers from opposite spindle poles (Figure 6D). Together, these data establish that kinetochore fragmentation correlates with abnormal kinetochore-microtubule attachments.

Microtubule Pulling Enhances and Shapes Kinetochore Fragmentation

Why are kinetochore fragmentation and merotelic attachments correlated? The age-related decompaction of centromeric chromatin and its associated kinetochore could broaden and distort

the microtubule-interacting surface, which could hinder the establishment of correct microtubule attachments. Kinetochores with lateral or end-on merotelic attachments would experience pulling from opposite directions, which could further enhance their fragmentation. Centromeric chromatin decompaction and microtubule pulling could thereby generate a positive feedback loop, which would manifest in merotelic attachments and prime eggs for chromosome segregation errors. The strain on meiotic kinetochores could be further enhanced by the dynamics of spindle assembly in meiosis: kinetochores in oocytes are exposed to prolonged pulling, because meiotic spindles in both female mice and women take multiple hours to assemble fully [52–55], in a process which in humans involves several hours of spindle reorganization [54].

To test directly whether microtubule pulling enhances kinetochore fragmentation, we decreased microtubule-dependent pulling by treating eggs with the microtubule-depolymerizing drug nocodazole. We opted for a concentration of the drug at which the pulling experienced by kinetochores is reduced but the general bipolar organization of the spindle is maintained and thus chromosomes are sufficiently individualized for kinetochore analysis. We then induced kinetochore fragmentation by Trim-Away of Smc3. We found that kinetochore fragmentation was reduced from 52% in DMSO-treated control eggs to 35% in eggs treated with low doses of nocodazole (Figure 6F). This suggests that microtubule pulling enhances fragmentation.

Our analysis also revealed that meiotic kinetochores preferentially reorganize their fragments into two distinct lobes (Figure 2G). We wondered whether the bilobular appearance of the fragmented meiotic kinetochore reflects an inherent structural feature of kinetochores in meiosis, or whether it could result from clustering of multiple kinetochore fragments into two large groups by bidirectional pulling from the two spindle poles. To discriminate between these possibilities, we treated control and partially Smc3-depleted oocytes from young mice with monastrol at the onset of meiosis I, to completely eliminate the exposure of meiotic kinetochores to bidirectional pulling (Figure S7C). Monastrol treatment leads to the formation of a microtubule ball that contains multiple microtubule-organizing centers (MTOCs) and carries the chromosomes on its surface [56, 57]. Kinetochores were still fragmented in monastrol-treated oocytes (Figures 6G and 6H, monastrol groups). However, instead of always forming two domains, some kinetochores fragmented into multiple lobes (Figures 6G and S7D). Interestingly, monastrol treatment enhanced kinetochore fragmentation even in young control mouse oocytes, without depletion of cohesin (Figure 6G, right top panel; and Figure 6H, second column). This might be due to altered pulling forces exerted on kinetochores by the

(E) Representative Trim-Away spindles treated as in (B). Insets: chromosome and kinetochore architectures in MI bivalents under these conditions. Scale bars represent 10 μm in overview, and 2 μm or 0.5 μm in insets.

(F) Kinetochore architectures shown in (E) and their occurrence in MI oocytes treated as in (B). Data are from 55 metaphase-I oocytes (2 experiments). Error bars show SEM.

(G) Representative two sister kinetochores of a bivalent in control oocytes (left panel) or anti-Smc3 microinjected Trim-Away oocytes (other panels). Scale bars represent 0.5 μm .

Chromosomes (blue, Hoechst) and kinetochores (magenta, CREST) are shown in (B), (E), and (G). In (B) and (E), microtubules are additionally labeled (green, α -tubulin). p values are designated as **p < 0.01 and ****p < 0.0001. p values were calculated with one-way ANOVA followed by Tukey's test in (D) and Student's t test in (F). Arrows: white point to compact kinetochores, and yellow point to lobes within a fragmented MI kinetochore. Numbers in insets refer to sister kinetochores shown (as in the E schematic).

See also Figure S6.

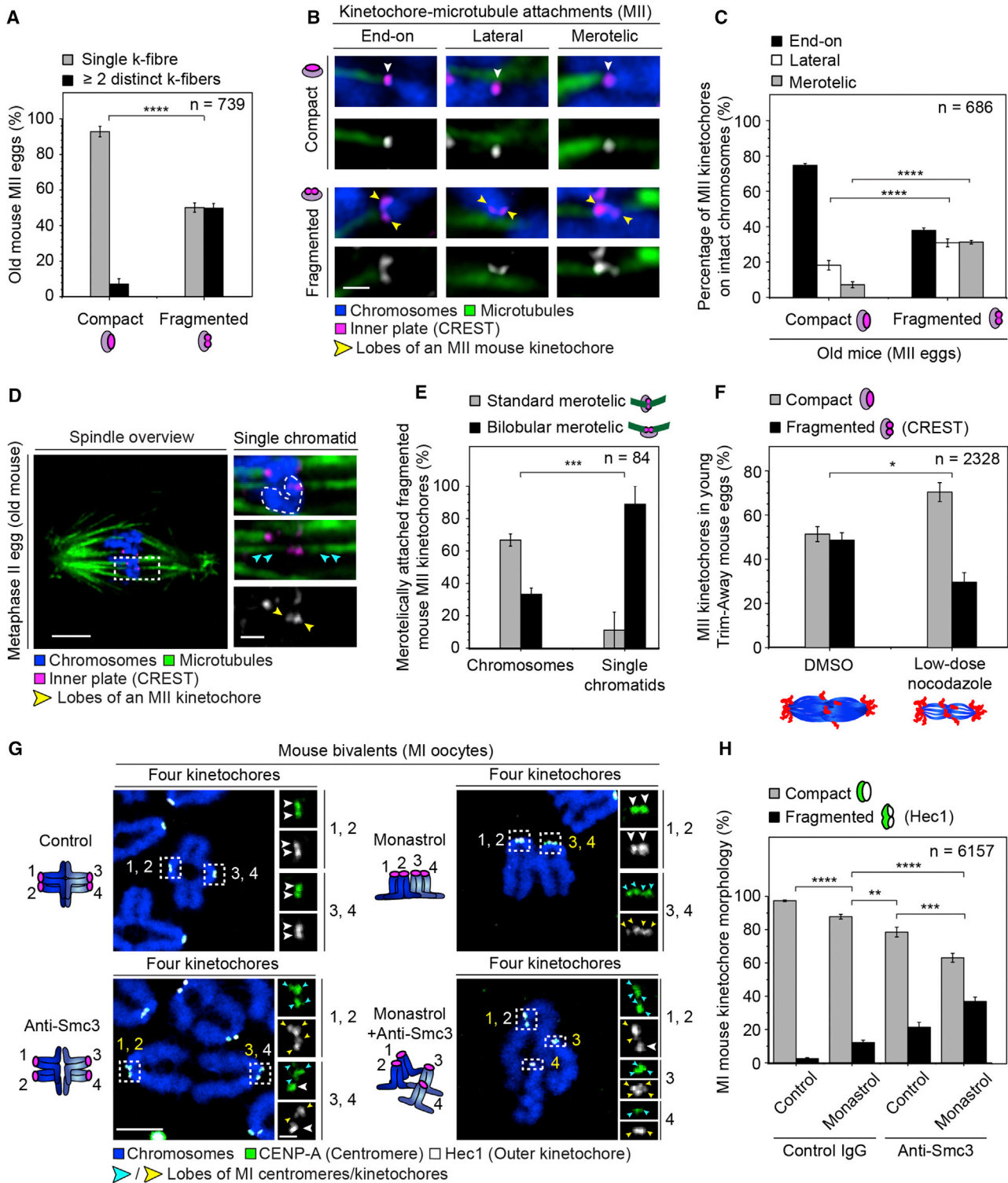


Figure 6. Fragmented Kinetochores Are More Likely to Be Abnormally Attached to Spindle Microtubules

(A) Quantification of the number of distinct k fibers attaching to compact/fragmented kinetochores at metaphase II (28 aged mouse MII eggs, 3 experiments) is shown.

(B) Representative kinetochore-microtubule attachment types, relative to the kinetochore fragmentation status. The scale bar represents 1 μ m.

(C) Quantification of the microtubule attachment types shown in (B) across the specified MII kinetochore categories on intact chromosomes (28 aged mouse MII eggs, 3 experiments).

(legend continued on next page)

MTOC aggregate. Importantly, significantly more kinetochores became fragmented under conditions of monastrol treatment in anti-Smc3-injected oocytes, as compared to control monastrol-treated cells with intact cohesin (Figure 6H, second and fourth columns), which further supports our model that cohesin loss primes kinetochores for fragmentation. Together, these findings suggest that although meiotic kinetochores may have inherent structural properties that bias them toward a bilobular appearance, the emergence of two lobes is promoted by bidirectional pulling and grouping of kinetochore fragments by spindle microtubules.

DISCUSSION

Our study reveals that the internal architecture of centromeres and kinetochores in mammalian eggs changes as females age: centromeric chromatin decompacts and kinetochores fragment, which is linked to an increase in incorrect microtubule attachments. Acute removal of cohesin from centromeric regions is sufficient to reproduce these age-related changes in centromere and kinetochore architecture (Figure 7A). We therefore favor a model whereby kinetochore distortion starts at the level of centromeric chromatin: cohesin is gradually lost from centromeric regions as females age. This loss of cohesin leads to a broadening of centromeric chromatin and an expansion of associated kinetochores (Figure 7B). The expanded kinetochores are more likely to interact with multiple microtubule bundles and, if the bundles originate from distinct spindle poles (merotelically), bidirectional pulling can have a further negative impact on kinetochore integrity. Age-related cohesin loss could thereby prime centromeres and the associated kinetochores to be attacked and altered by spindle microtubules.

Kinetochore fragmentation could contribute to the multifactorial [7–9, 23] age-related increase in aneuploidy in eggs. In support of this possibility, we detected significantly more abnormal lateral and merotelic spindle attachments in fragmented than in compact kinetochores in eggs from aged mice. Due to limited resolution in live-oocyte microscopy, we cannot currently follow how fragmented kinetochores segregate. However, merotelic attachments are well established to contribute to aneuploidy in mitosis [49]. Chromosomes with merotelically attached fragmented meiotic kinetochores could therefore mis-segregate in eggs as well. Cohesin loss may hence cause aneuploidy in

oocytes not only by leading to the premature dissociation of homologous chromosomes, sister chromatids, or sister kinetochores but also by priming kinetochores for fragmentation. We would still like to highlight that although cohesin loss was sufficient to induce changes to centromere and kinetochore morphology in eggs from young mice, multiple oocyte proteins deteriorate as females age [58] and may hence contribute to meiotic kinetochore fragmentation and the associated increase in abnormal kinetochore-microtubule attachments.

Assessing a woman's egg for kinetochore fragmentation may also help to assess the cohesin status of her oocyte pool in early stages of reproduction, because kinetochore fragmentation precedes the dissociation of chromosomes: we could already detect fragmented kinetochores in eggs from 34- to 36-week-old mice (Figure 2B), whereas dissociation of chromosomes into single chromatids only became prominent from 60 weeks onward (Figure S1A). Also in meiosis I, kinetochore fragmentation (Figure 5F) preceded the premature separation of the two homologous chromosomes within the bivalent (Figure 5C). These data therefore suggest that a loss of cohesin is first detectable at the level of the kinetochore before changes to the overall chromosome structure become evident, making kinetochore fragmentation an early readout of cohesin deterioration in aging oocytes.

Outer fibrous coronal regions of mitotic kinetochores were demonstrated to temporarily expand into a crescent before becoming stably bound by spindle microtubules [59–61]. However, these changes did not affect the centromere or inner kinetochore layers [59, 60], which is in contrast to meiotic kinetochore fragmentation that spans across multiple layers of the kinetochore complex and also affects stably bound chromosomes at the spindle equator. It will be interesting to investigate in future studies whether cohesin depletion also causes kinetochore fragmentation in mitotic cells. Following hypotonic treatment, mitotic kinetochores unravel into more than 80 distinct subunits [62], suggesting that they also have the potential to fragment. Although kinetochore stretching was previously artificially induced in maize meiocytes and mitotic cells [63–65], clear distortion is a rare event under wild-type conditions in unperturbed cells [49]. In contrast, our study demonstrates that a third of kinetochores exist in a clearly fragmented state in eggs from older females, making the bilobular appearance a prominent feature of the female meiotic kinetochore. Not only are cohesin

(D) Representative merotelically attached single chromatid and its respective kinetochore, aligned at the equator of a metaphase-II spindle in an aged mouse egg. Scale bars represent 5 μm in overview, and 1 μm in insets.

(E) Quantification of the subtypes of merotelic attachments on fragmented kinetochores, relative to the chromosome architecture and the site of microtubule attachment.

(F) Occurrence of kinetochore architectures following Trim-Away of Smc3 in mouse MII eggs subjected to either DMSO or low-dose nocodazole (62 young MII eggs, 3 experiments).

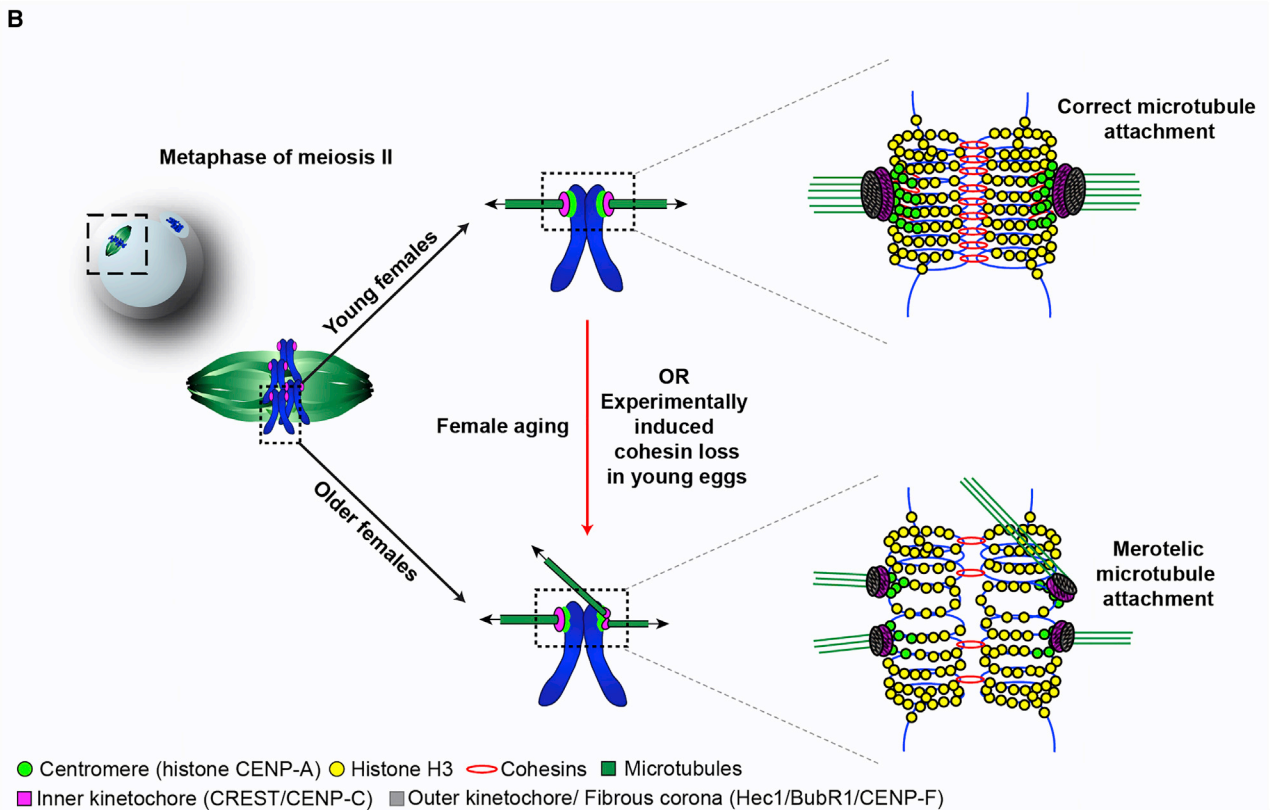
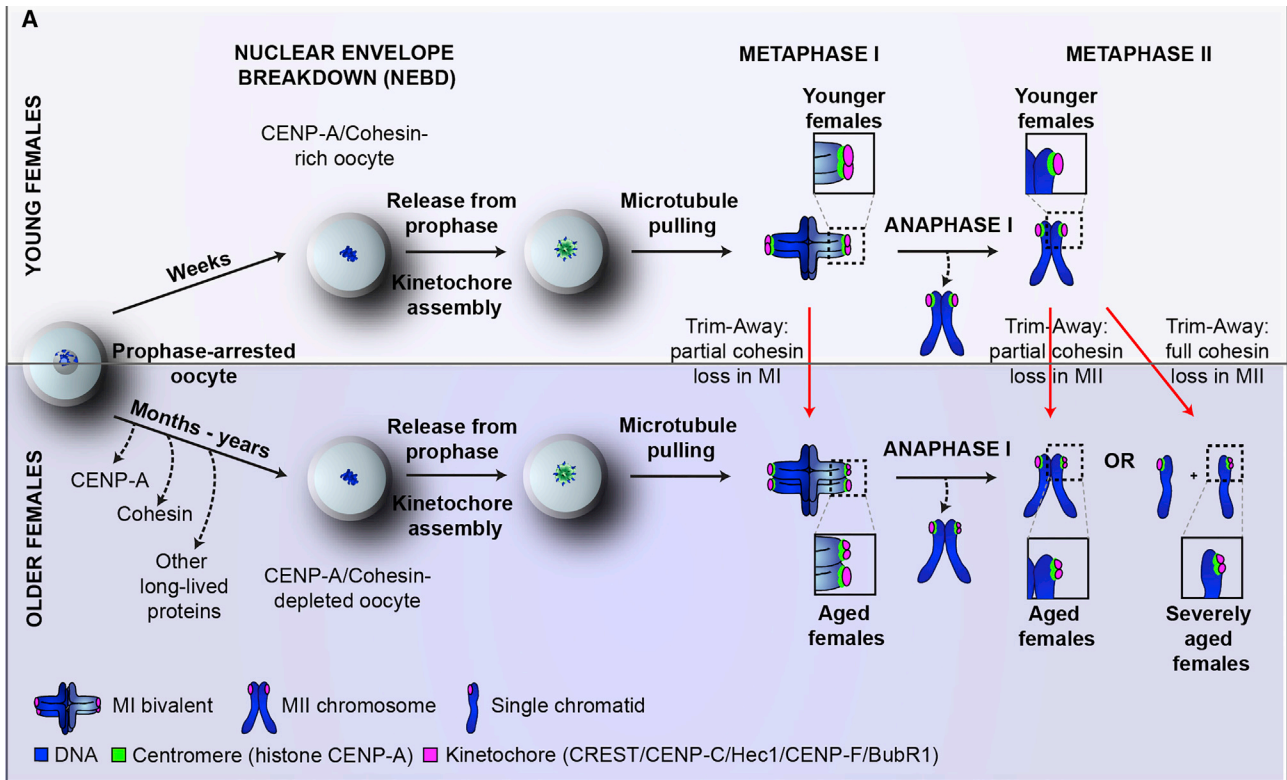
(G) Representative chromosome spreads of control and Smc3 partially depleted MI oocytes from young mice subjected to monastrol/control DMSO drug treatments. Each inset shows two sister kinetochores/centromeres only. Outer kinetochores (white, Hec1), centromeres (green, CENP-A), and chromosomes (blue, Hoechst) are shown. Scale bars represent 5 μm in overview, and 1 μm in insets.

(H) Occurrence of kinetochore architectures in MI oocytes from young mice treated as in (G). Quantifications are based on Hec1 labeling in 80 MI oocytes (2 experiments).

DNA (blue, Hoechst), microtubules (green, α -tubulin), and kinetochores (magenta, CREST) are shown in (B) and (D).

p values are designated as * $p < 0.05$, ** $p < 0.01$, *** $p < 0.001$, and **** $p < 0.0001$. p values in (F) were calculated with Student's t test and in (A), (C), and (E) with Fisher's exact test. In (H), mean measurements per oocyte were compared by one-way ANOVA followed by Tukey's test. Error bars show SEM. Arrows: white point to compact kinetochores, and yellow/blue to lobes within fragmented kinetochores/centromeres, respectively.

See also Figure S7.



(legend on next page)

levels high but also spindle assembly in mitotic cells is much more rapid than in mammalian eggs [66], which could further explain why fragmentation is a rare event in mitosis. However, microtubule pulling could also play a role here, as some kinetochores lagging at anaphase onset also appeared bilobular when merotelic attachments were artificially increased [49].

Oocyte-specific spindle dynamics could contribute to fragmentation not only through direct pulling but also by influencing chromosome cohesion. Mammalian eggs only complete anaphase II upon fertilization [8, 67]. Thus, eggs frequently remain arrested in metaphase II for over 12 h, a phenomenon termed post-ovulatory aging [68]. Mitotic cells artificially halted at the metaphase stage undergo cohesion fatigue: cohesion becomes gradually insufficient and sister chromatids prematurely separate [69, 70]. Importantly, cohesion fatigue occurs only in the presence of microtubule pulling [69, 71]. Although it is clear that the major cohesin decline in mammalian oocytes occurs during prophase arrest [23], the physiological metaphase-II arrest that is unique to female meiosis could further reduce cohesion levels and thereby contribute to kinetochore fragmentation and sister chromatid splitting. In line with this idea, chromosome cohesion in MII eggs becomes occasionally insufficient to keep all chromatids together as the metaphase-II arrest endures [21, 72].

Several experiments in this study were based on a modified Trim-Away assay, which allowed us to partially deplete cohesins in oocytes and eggs from young mice. Using this assay, we were able to cause a partial dissociation of sister chromatids in young eggs, splitting of meiosis-I sister kinetochore pairs, as well as fragmentation of meiotic kinetochores, thus closely resembling the changes in chromosome and kinetochore architecture that occur during aging and have been attributed to a gradual loss of cohesin. Western blotting confirmed protein depletion from eggs, and immunofluorescence microscopy verified that our approach indeed removes cohesin from chromosomes. Due to technical limitations, as well as limited availability of antibodies to target Smc3 and Rec8 in oocytes, we only used one antibody against each cohesin complex subunit. However, the fact that the changes induced by targeting either Smc3 or Rec8 are consistent indicates that this approach is suitable to investigate the consequences of cohesin loss in mammalian oocytes and eggs.

The partial Trim-Away assay complements the previously developed mouse models heterozygous for cohesin genes [32], which induced low cohesin levels from the time the oocytes are first formed and allowed investigations into the effects of decreased cohesin levels on the early meiotic events that precede the protracted prophase arrest. The partial Trim-Away assay allows us to deplete cohesins in oocytes that were able to progress through the early stages of meiosis with normal cohesin levels, and is therefore suitable to study the effects of a late cohesin loss, similar to that occurring in oocytes from aged females, on meiotic chromosome and kinetochore architecture.

Notably, young mice used for the Trim-Away assays have considerably larger numbers of oocytes than aged females [19]. Thus, fewer animals are required to investigate the consequences of a partial loss of cohesin for meiosis, in comparison to the natural aging mouse model. In addition, these animals only need to be maintained for short periods of time, which reduces the number of cages that have to be kept. Importantly, the partial Trim-Away approach could also be applied to other proteins that only partially deteriorate during aging, and thus further contribute to our understanding of the maternal age effect in mammals.

STAR★METHODS

Detailed methods are provided in the online version of this paper and include the following:

- **KEY RESOURCES TABLE**
- **LEAD CONTACT AND MATERIALS AVAILABILITY**
- **EXPERIMENTAL MODEL AND SUBJECT DETAILS**
 - Primary mouse oocytes
 - Primary human oocytes
 - Primary pig oocytes
 - Cell culture
- **METHOD DETAILS**
 - Expression constructs and mRNA synthesis
 - Antibody microinjection
 - Drug addition experiments
 - Chromosome spreads
 - Cold-mediated microtubule depolymerization assays
 - Oocyte immunofluorescence
 - Immunofluorescence of tissue culture cells
 - Super-resolution immunofluorescence microscopy
 - Confocal microscopy in fixed cells
 - Confocal microscopy in live cells expressing fluorescent reporters or incubated with fluorescent dyes
 - Immunoblotting
- **QUANTIFICATION AND STATISTICAL ANALYSIS**
 - Chromosome counting and assessment of kinetochore configuration
 - Assessment of the effects of Trim-Away mediated cohesin loss on chromosome architecture in the metaphase of meiosis I
 - Modes of kinetochore-microtubule attachment
 - Quantification of fluorescence intensity of the centromeric cohesin pool
 - Quantification of western blot mean band intensity
 - Statistical analysis
- **DATA AND CODE AVAILABILITY**

SUPPLEMENTAL INFORMATION

Supplemental Information can be found online at <https://doi.org/10.1016/j.cub.2019.09.006>.

Figure 7. Age-Related Cohesin Loss Alters Chromosome Architecture and Fragments Mammalian Meiotic Kinetochores into Distinct Lobes
Scheme summarizing how cohesin loss affects not only sister kinetochore pairing but also the internal kinetochore architecture in meiosis-I oocytes and meiosis-II eggs (A), and a model proposing how cohesin-dependent changes in centromeric architecture may promote the fragmentation of a meiotic kinetochore into lobes (B).

ACKNOWLEDGMENTS

We are grateful to the patients who generously donated their eggs and to the embryology teams at the Bourn Hall Clinic, Kinderwunschzentrum, Laboratory for Reproductive Biology (LRB), and INVICTA fertility clinics for their enthusiastic support of this project. The authors thank A. Webster for kindly sharing the anti-Rec8 antibody and G. Lukinavičius for the 5-TMR-Hoechst; the MPI BPC Animal Facility for technical assistance; M. Pasche for help with SIM microscopy; D. Kamin for help with STED microscopy; and M. Daniel for her dedication to harvesting pig ovaries. We thank C. Thomas, A. Faesen, L. Wartosch, and A. Webster for critical reading of the manuscript, Life Science Editors for useful comments, and the members of the Schuh lab for helpful discussions. A.P.Z., E.B., N.S., A.-S.F., and M.S. have received financial support from the Max Planck Society, European Research Council under grant agreement 337415, the Deutsche Forschungsgemeinschaft (Leibniz Prize to M.S.), and Lister Institute for Preventive Medicine. A.P.Z. is further supported by a Rosettes Trust PhD fellowship. E.R.H. and J.R.G. received support from the Novo Nordisk Foundation (16662), European Research Council (724718), and Danish National Research Foundation (DNRF115, 6110-00344B).

AUTHOR CONTRIBUTIONS

A.P.Z. and M.S. conceived the project, designed the experiments, and wrote the manuscript. A.P.Z. performed and analyzed all experiments with the following exceptions: E.B. performed the experiments and analyzed the data in [Figures S2B](#) and [S3A–S3C](#); N.S. performed the experiments and analyzed the data in [Figures S1C](#), [S3D](#), and [S3E](#); A.-S.F. analyzed the data in [Figures 1I](#), [1J](#), [S2D](#), and [3E](#) and immunolabeled/imagined the spreads from the Trim-Away experiments shown in [Figures 3C](#), [3J](#), [S4B](#), and [S5A](#). J.R.G. and E.R.H. provided the data for [Figure S6A](#). M.B., K.E., H.E., and R.M. supervised the collection of human oocytes at the IVF clinics. K.B.S. and A.P.Z. cultured and subsequently fixed the human oocytes used in this study. A.P.Z. prepared the figures and schematic diagrams for the manuscript. All authors commented on the manuscript. M.S. supervised the study.

DECLARATION OF INTERESTS

The authors declare no competing interests.

Received: February 11, 2019

Revised: July 23, 2019

Accepted: September 4, 2019

Published: October 31, 2019

REFERENCES

- Black, B.E., and Bassett, E.A. (2008). The histone variant CENP-A and centromere specification. *Curr. Opin. Cell Biol.* **20**, 91–100.
- Cheeseman, I.M. (2014). The kinetochore. *Cold Spring Harb. Perspect. Biol.* **6**, a015826.
- Pesenti, M.E., Weir, J.R., and Musacchio, A. (2016). Progress in the structural and functional characterization of kinetochores. *Curr. Opin. Struct. Biol.* **37**, 152–163.
- Pereira, A.J., and Maiato, H. (2012). Maturation of the kinetochore-microtubule interface and the meaning of metaphase. *Chromosome Res.* **20**, 563–577.
- Auckland, P., and McAinsh, A.D. (2015). Building an integrated model of chromosome congression. *J. Cell Sci.* **128**, 3363–3374.
- Amargant, F., Barragan, M., Vassena, R., and Vernos, I. (2019). Insights of the tubulin code in gametes and embryos: from basic research to potential clinical applications in humans. *Biol. Reprod.* **100**, 575–589.
- Nagaoka, S.I., Hassold, T.J., and Hunt, P.A. (2012). Human aneuploidy: mechanisms and new insights into an age-old problem. *Nat. Rev. Genet.* **13**, 493–504.
- Herbert, M., Kalleas, D., Cooney, D., Lamb, M., and Lister, L. (2015). Meiosis and maternal aging: insights from aneuploid oocytes and trisomy births. *Cold Spring Harb. Perspect. Biol.* **7**, a017970.
- Webster, A., and Schuh, M. (2017). Mechanisms of aneuploidy in human eggs. *Trends Cell Biol.* **27**, 55–68.
- Santaguida, S., and Musacchio, A. (2009). The life and miracles of kinetochores. *EMBO J.* **28**, 2511–2531.
- Hodges, C.A., Revenkova, E., Jessberger, R., Hassold, T.J., and Hunt, P.A. (2005). SMC1beta-deficient female mice provide evidence that cohesins are a missing link in age-related nondisjunction. *Nat. Genet.* **37**, 1351–1355.
- Chiang, T., Duncan, F.E., Schindler, K., Schultz, R.M., and Lampson, M.A. (2010). Evidence that weakened centromere cohesion is a leading cause of age-related aneuploidy in oocytes. *Curr. Biol.* **20**, 1522–1528.
- Lister, L.M., Kouznetsova, A., Hyslop, L.A., Kalleas, D., Pace, S.L., Barel, J.C., Nathan, A., Floros, V., Adelfalk, C., Watanabe, Y., et al. (2010). Age-related meiotic segregation errors in mammalian oocytes are preceded by depletion of cohesin and Sgo2. *Curr. Biol.* **20**, 1511–1521.
- Shomper, M., Lappa, C., and FitzHarris, G. (2014). Kinetochore microtubule establishment is defective in oocytes from aged mice. *Cell Cycle* **13**, 1171–1179.
- Danylevska, A., Kovacicova, K., Awadova, T., and Anger, M. (2014). The frequency of precocious segregation of sister chromatids in mouse female meiosis I is affected by genetic background. *Chromosome Res.* **22**, 365–373.
- Sakakibara, Y., Hashimoto, S., Nakaoka, Y., Kouznetsova, A., Höög, C., and Kitajima, T.S. (2015). Bivalent separation into univalents precedes age-related meiosis I errors in oocytes. *Nat. Commun.* **6**, 7550.
- Zielinska, A.P., Holubcova, Z., Blayney, M., Elder, K., and Schuh, M. (2015). Sister kinetochore splitting and precocious disintegration of bivalents could explain the maternal age effect. *eLife* **4**, e11389.
- Patel, J., Tan, S.L., Hartshorne, G.M., and McAinsh, A.D. (2015). Unique geometry of sister kinetochores in human oocytes during meiosis I may explain maternal age-associated increases in chromosomal abnormalities. *Biol. Open* **5**, 178–184.
- Merriman, J.A., Jennings, P.C., McLaughlin, E.A., and Jones, K.T. (2012). Effect of aging on superovulation efficiency, aneuploidy rates, and sister chromatid cohesion in mice aged up to 15 months. *Biol. Reprod.* **86**, 49.
- Duncan, F.E., Hornick, J.E., Lampson, M.A., Schultz, R.M., Shea, L.D., and Woodruff, T.K. (2012). Chromosome cohesion decreases in human eggs with advanced maternal age. *Aging Cell* **11**, 1121–1124.
- Yun, Y., Lane, S.I., and Jones, K.T. (2014). Premature dyad separation in meiosis II is the major segregation error with maternal age in mouse oocytes. *Development* **141**, 199–208.
- Lagirand-Cantaloube, J., Ciabrini, C., Charrasse, S., Ferrieres, A., Castro, A., Anahory, T., and Lorca, T. (2017). Loss of centromere cohesion in aneuploid human oocytes correlates with decreased kinetochore localization of the Sac proteins Bub1 and Bubl1. *Sci. Rep.* **7**, 44001.
- Jessberger, R. (2012). Age-related aneuploidy through cohesion exhaustion. *EMBO Rep.* **13**, 539–546.
- Parisi, S., McKay, M.J., Molnar, M., Thompson, M.A., van der Spek, P.J., van Drunen-Schoenmaker, E., Kanaar, R., Lehmann, E., Hoeijmakers, J.H., and Kohli, J. (1999). Rec8p, a meiotic recombination and sister chromatid cohesion phosphoprotein of the Rad21p family conserved from fission yeast to humans. *Mol. Cell. Biol.* **19**, 3515–3528.
- Prieto, I., Suja, J.A., Pezzi, N., Kremer, L., Martínez-A, C., Rufas, J.S., and Barbero, J.L. (2001). Mammalian STAG3 is a cohesin specific to sister chromatid arms in meiosis I. *Nat. Cell Biol.* **3**, 761–766.
- Revenkova, E., Eijpe, M., Heyting, C., Gross, B., and Jessberger, R. (2001). Novel meiosis-specific isoform of mammalian SMC1. *Mol. Cell. Biol.* **21**, 6984–6998.
- Tachibana-Konwalski, K., Godwin, J., van der Weyden, L., Champion, L., Kudo, N.R., Adams, D.J., and Nasmyth, K. (2010). Rec8-containing

- cohesin maintains bivalents without turnover during the growing phase of mouse oocytes. *Genes Dev.* **24**, 2505–2516.
28. Petronczki, M., Siomos, M.F., and Nasmyth, K. (2003). Un ménage à quatre: the molecular biology of chromosome segregation in meiosis. *Cell* **112**, 423–440.
 29. Burkhardt, S., Borsos, M., Szydłowska, A., Godwin, J., Williams, S.A., Cohen, P.E., Hirota, T., Saitou, M., and Tachibana-Konwalski, K. (2016). Chromosome cohesion established by Rec8-cohesin in fetal oocytes is maintained without detectable turnover in oocytes arrested for months in mice. *Curr. Biol.* **26**, 678–685.
 30. Liu, L., and Keefe, D.L. (2008). Defective cohesin is associated with age-dependent misaligned chromosomes in oocytes. *Reprod. Biomed. Online* **16**, 103–112.
 31. Angell, R. (1997). First-meiotic-division nondisjunction in human oocytes. *Am. J. Hum. Genet.* **61**, 23–32.
 32. Murdoch, B., Owen, N., Stevense, M., Smith, H., Nagaoka, S., Hassold, T., McKay, M., Xu, H., Fu, J., Revenkova, E., et al. (2013). Altered cohesin gene dosage affects mammalian meiotic chromosome structure and behavior. *PLoS Genet.* **9**, e1003241.
 33. Kuliev, A., Zlatopolsky, Z., Kirillova, I., Spivakova, J., and Cieslak Janzen, J. (2011). Meiosis errors in over 20,000 oocytes studied in the practice of preimplantation aneuploidy testing. *Reprod. Biomed. Online* **22**, 2–8.
 34. Fragouli, E., Alfarawati, S., Spath, K., Jaroudi, S., Sarasa, J., Enciso, M., and Wells, D. (2013). The origin and impact of embryonic aneuploidy. *Hum. Genet.* **132**, 1001–1013.
 35. Hou, Y., Fan, W., Yan, L., Li, R., Lian, Y., Huang, J., Li, J., Xu, L., Tang, F., Xie, X.S., and Qiao, J. (2013). Genome analyses of single human oocytes. *Cell* **155**, 1492–1506.
 36. Ottolini, C.S., Newnham, L., Capalbo, A., Natesan, S.A., Joshi, H.A., Cimadomo, D., Griffin, D.K., Sage, K., Summers, M.C., Thornhill, A.R., et al. (2015). Genome-wide maps of recombination and chromosome segregation in human oocytes and embryos show selection for maternal recombination rates. *Nat. Genet.* **47**, 727–735.
 37. Das, A., Smoak, E.M., Linares-Saldana, R., Lampson, M.A., and Black, B.E. (2017). Centromere inheritance through the germline. *Chromosoma* **126**, 595–604.
 38. Watanabe, Y. (2012). Geometry and force behind kinetochore orientation: lessons from meiosis. *Nat. Rev. Mol. Cell Biol.* **13**, 370–382.
 39. Smoak, E.M., Stein, P., Schultz, R.M., Lampson, M.A., and Black, B.E. (2016). Long-term retention of CENP-A nucleosomes in mammalian oocytes underpins transgenerational inheritance of centromere identity. *Curr. Biol.* **26**, 1110–1116.
 40. Hell, S.W., and Wichmann, J. (1994). Breaking the diffraction resolution limit by stimulated emission: stimulated-emission-depletion fluorescence microscopy. *Opt. Lett.* **19**, 780–782.
 41. Earnshaw, W.C., and Rothfield, N. (1985). Identification of a family of human centromere proteins using autoimmune sera from patients with scleroderma. *Chromosoma* **91**, 313–321.
 42. Tsutsumi, M., Fujiwara, R., Nishizawa, H., Ito, M., Kogo, H., Inagaki, H., Ohye, T., Kato, T., Fujii, T., and Kurahashi, H. (2014). Age-related decrease of meiotic cohesins in human oocytes. *PLoS ONE* **9**, e96710.
 43. Clift, D., McEwan, W.A., Labzin, L.I., Konieczny, V., Mogessie, B., James, L.C., and Schuh, M. (2017). A method for the acute and rapid degradation of endogenous proteins. *Cell* **171**, 1692–1706.e18.
 44. Uhlmann, F. (2004). The mechanism of sister chromatid cohesion. *Exp. Cell Res.* **296**, 80–85.
 45. Watanabe, Y., and Nurse, P. (1999). Cohesin Rec8 is required for reductional chromosome segregation at meiosis. *Nature* **400**, 461–464.
 46. Klein, F., Mahr, P., Galova, M., Buonomo, S.B., Michaelis, C., Nairz, K., and Nasmyth, K. (1999). A central role for cohesins in sister chromatid cohesion, formation of axial elements, and recombination during yeast meiosis. *Cell* **98**, 91–103.
 47. Eijpe, M., Offenberg, H., Jessberger, R., Revenkova, E., and Heyting, C. (2003). Meiotic cohesin REC8 marks the axial elements of rat synaptonemal complexes before cohesins SMC1beta and SMC3. *J. Cell Biol.* **160**, 657–670.
 48. Salmon, E.D., and Begg, D.A. (1980). Functional implications of cold-stable microtubules in kinetochore fibers of insect spermatocytes during anaphase. *J. Cell Biol.* **85**, 853–865.
 49. Cimini, D., Howell, B., Maddox, P., Khodjakov, A., Degrossi, F., and Salmon, E.D. (2001). Merotelic kinetochore orientation is a major mechanism of aneuploidy in mitotic mammalian tissue cells. *J. Cell Biol.* **153**, 517–527.
 50. Kouznetsova, A., Hernández-Hernández, A., and Höög, C. (2014). Merotelic attachments allow alignment and stabilization of chromatids in meiosis II oocytes. *Nat. Commun.* **5**, 4409.
 51. Cheng, J.M., Li, J., Tang, J.X., Hao, X.X., Wang, Z.P., Sun, T.C., Wang, X.X., Zhang, Y., Chen, S.R., and Liu, Y.X. (2017). Merotelic kinetochore attachment in oocyte meiosis II causes sister chromatids segregation errors in aged mice. *Cell Cycle* **16**, 1404–1413.
 52. Schuh, M., and Ellenberg, J. (2007). Self-organization of MTOCs replaces centrosome function during acentrosomal spindle assembly in live mouse oocytes. *Cell* **130**, 484–498.
 53. Nakagawa, S., and FitzHarris, G. (2017). Intrinsically defective microtubule dynamics contribute to age-related chromosome segregation errors in mouse oocyte meiosis-I. *Curr. Biol.* **27**, 1040–1047.
 54. Holubcová, Z., Blayney, M., Elder, K., and Schuh, M. (2015). Human oocytes. Error-prone chromosome-mediated spindle assembly favors chromosome segregation defects in human oocytes. *Science* **348**, 1143–1147.
 55. Haverfield, J., Dean, N.L., Noël, D., Rémillard-Labrosse, G., Paradis, V., Kadoch, I.J., and FitzHarris, G. (2017). Tri-directional anaphases as a novel chromosome segregation defect in human oocytes. *Hum. Reprod.* **32**, 1293–1303.
 56. Ashar, H.R., James, L., Gray, K., Carr, D., Black, S., Armstrong, L., Bishop, W.R., and Kirschmeier, P. (2000). Farnesyl transferase inhibitors block the farnesylation of CENP-E and CENP-F and alter the association of CENP-E with the microtubules. *J. Biol. Chem.* **275**, 30451–30457.
 57. Clift, D., and Schuh, M. (2015). A three-step MTOC fragmentation mechanism facilitates bipolar spindle assembly in mouse oocytes. *Nat. Commun.* **6**, 7217.
 58. Schwarzer, C., Siatkowski, M., Pfeiffer, M.J., Baeumer, N., Drexler, H.C., Wang, B., Fuellen, G., and Boiani, M. (2014). Maternal age effect on mouse oocytes: new biological insight from proteomic analysis. *Reproduction* **148**, 55–72.
 59. Hoffman, D.B., Pearson, C.G., Yen, T.J., Howell, B.J., and Salmon, E.D. (2001). Microtubule-dependent changes in assembly of microtubule motor proteins and mitotic spindle checkpoint proteins at Ptk1 kinetochores. *Mol. Biol. Cell* **12**, 1995–2009.
 60. Magidson, V., Paul, R., Yang, N., Ault, J.G., O'Connell, C.B., Tikhonenko, I., McEwen, B.F., Mogilner, A., and Khodjakov, A. (2015). Adaptive changes in the kinetochore architecture facilitate proper spindle assembly. *Nat. Cell Biol.* **17**, 1134–1144.
 61. Sacristan, C., Ahmad, M.U.D., Keller, J., Fermie, J., Groenewold, V., Tromer, E., Fish, A., Melero, R., Carazo, J.M., Klumperman, J., et al. (2018). Dynamic kinetochore size regulation promotes microtubule capture and chromosome biorientation in mitosis. *Nat. Cell Biol.* **20**, 800–810.
 62. Zinkowski, R.P., Meyne, J., and Brinkley, B.R. (1991). The centromere-kinetochore complex: a repeat subunit model. *J. Cell Biol.* **113**, 1091–1110.
 63. Khodjakov, A., Cole, R.W., McEwen, B.F., Buttle, K.F., and Rieder, C.L. (1997). Chromosome fragments possessing only one kinetochore can congress to the spindle equator. *J. Cell Biol.* **136**, 229–240.
 64. Yu, H.G., and Dawe, R.K. (2000). Functional redundancy in the maize meiotic kinetochore. *J. Cell Biol.* **151**, 131–142.
 65. Drpic, D., Pereira, A.J., Barisic, M., Maresca, T.J., and Maiato, H. (2015). Polar ejection forces promote the conversion from lateral to end-on

- kinetochore-microtubule attachments on mono-oriented chromosomes. *Cell Rep.* **13**, 460–468.
66. Ohkura, H. (2015). Meiosis: an overview of key differences from mitosis. *Cold Spring Harb. Perspect. Biol.* **7**, a015859.
 67. Clift, D., and Schuh, M. (2013). Restarting life: fertilization and the transition from meiosis to mitosis. *Nat. Rev. Mol. Cell Biol.* **14**, 549–562.
 68. Wilcox, A.J., Weinberg, C.R., and Baird, D.D. (1998). Post-ovulatory ageing of the human oocyte and embryo failure. *Hum. Reprod.* **13**, 394–397.
 69. Daum, J.R., Potapova, T.A., Sivakumar, S., Daniel, J.J., Flynn, J.N., Rankin, S., and Gorbsky, G.J. (2011). Cohesion fatigue induces chromatid separation in cells delayed at metaphase. *Curr. Biol.* **21**, 1018–1024.
 70. Stevens, D., Gassmann, R., Oegema, K., and Desai, A. (2011). Uncoordinated loss of chromatid cohesion is a common outcome of extended metaphase arrest. *PLoS ONE* **6**, e22969.
 71. Sapkota, H., Wasiak, E., Daum, J.R., and Gorbsky, G.J. (2018). Multiple determinants and consequences of cohesion fatigue in mammalian cells. *Mol. Biol. Cell* **29**, 1811–1824.
 72. Steuerwald, N.M., Steuerwald, M.D., and Mailhes, J.B. (2005). Post-ovulatory aging of mouse oocytes leads to decreased MAD2 transcripts and increased frequencies of premature centromere separation and anaphase. *Mol. Hum. Reprod.* **11**, 623–630.
 73. Bucevičius, J., Keller-Findeisen, J., Gilat, T., Hell, S.W., and Lukinavicius, G. (2018). Rhodamine-Hoechst positional isomers for highly efficient staining of heterochromatin. *Chem. Sci. (Camb.)* **10**, 1962–1970.
 74. Liman, E.R., Tytgat, J., and Hess, P. (1992). Subunit stoichiometry of a mammalian K⁺ channel determined by construction of multimeric cDNAs. *Neuron* **9**, 861–871.
 75. Mogessie, B., and Schuh, M. (2017). Actin protects mammalian eggs against chromosome segregation errors. *Science* **357**, eaal1647.
 76. Zielinska, A.P., and Schuh, M. (2018). A microscopy-based approach for studying meiosis in live and fixed human oocytes. *Methods Cell Biol.* **145**, 315–333.
 77. Jaffe, L.A., Norris, R.P., Freudzon, M., Ratzan, W.J., and Mehlmann, L.M. (2009). Microinjection of follicle-enclosed mouse oocytes. *Methods Mol. Biol.* **518**, 157–173.
 78. Silva, M.C.C., Wutz, G., Tachibana, K., and Peters, J.M. (2018). Analysis of chromosomes from mouse oocytes and mammalian cultured cells by light microscopy. *Methods Cell Biol.* **144**, 287–305.

STAR★METHODS

KEY RESOURCES TABLE

REAGENT or RESOURCE	SOURCE	IDENTIFIER
Antibodies		
Rabbit anti-Rec8	Produced in-house	Epitope based on [47]
Rat anti- α -Tubulin	Bio-Rad	MCA78G; RRID:AB_325005
CREST serum	Antibodies Incorporated	15-234-0001; RRID: AB_2687472
CREST serum	Europa Bioproducts	FZ90C- CS1058
Rabbit anti-Smc3	Abcam	ab9263; RRID:AB_307122
Rabbit anti-Smc3	Abcam	EPR7984; RRID:AB_11150430
Mouse anti-Hec1	Santa Cruz	sc-135934; RRID:AB_2149754
Mouse anti-Hec1	Abcam	ab3613; RRID:AB_303949
Rabbit anti-CENP-A	Cell Signaling	2048; RRID:AB_1147629
Rabbit anti-CENP-F	Abcam	ab5; RRID:AB_304721
Mouse anti-CENP-C	Abcam	ab50974; RRID:AB_869095
Sheep anti-BubR1	Abcam	ab28192; RRID:AB_725785
Rabbit anti-Smc3	Bethyl Laboratories	A300-060A; RRID:AB_67579
Normal Rabbit IgG	Millipore	12-370; RRID:AB_145841
Goat anti-Rabbit IgG (H+L) Highly Cross-Adsorbed Secondary Antibody, Alexa Fluor 488	ThermoFisher	A11034; RRID:AB_2576217
Goat anti-Human IgG (H+L) Cross-Adsorbed Secondary Antibody, Alexa Fluor 488	ThermoFisher	A11013; RRID:AB_2534080
Chicken anti-Rat IgG (H+L) Cross-Adsorbed Secondary Antibody, Alexa Fluor 647	ThermoFisher	A21472; RRID:AB_2535875
Goat anti-Mouse IgG (H+L) Cross-Adsorbed Secondary Antibody, Alexa Fluor 546	ThermoFisher	A11003; RRID:AB_2534071
Donkey anti-Rabbit IgG (H+L) Highly Cross-Adsorbed Secondary Antibody, Alexa Fluor 647	ThermoFisher	A31573; RRID:AB_2536183
Goat anti-Rabbit IgG (H+L) Cross-Adsorbed Secondary Antibody, HRP	ThermoFisher	31462; RRID:AB_228338
Goat anti-Rat IgG Secondary Antibody, HRP	Santa Cruz	sc-2032; RRID:AB_631755
Goat anti-Rabbit STAR RED	Abberior	2-0012-011-9; RRID: AB_2620152
Goat anti-Mouse Alexa594-conjugated	ThermoFisher	R37121; RRID:AB_2556549
Chemicals, Peptides, and Recombinant Proteins		
Hoechst 33342	ThermoFisher	H3570; RRID:AB_2651133
PicoGreen	ThermoFisher	P11496
SiR-tubulin	Spirochrome	CHF420.00
5-TMR-Hoechst	N/A	Gift from Grazyvdas Lukinavičius (see also [73])
dbcAMP (N6,2'-O-Dibutyryladenine 3',5'-cyclic monophosphate sodium salt)	Sigma	D0627
Nocodazole	Sigma	M1404
Monastrol	Sigma	M8515
Hyaluronidase	Sigma	H4272
NP-40 Alternative	Merck	492016
Critical Commercial Assays		
mMESSAGE mMACHINE T7 Transcription Kit	ThermoFisher	AM1334
SuperSignal West Femto Maximum Sensitivity Substrate	ThermoFisher	34095
SNAP-Cell Starter Kit	New England Biolabs	E9100S
Lambda Protein Phosphatase (Lambda PP)	New England Biolabs	P0753S

(Continued on next page)

Continued		
REAGENT or RESOURCE	SOURCE	IDENTIFIER
Experimental Models: Organisms/Strains		
Mouse: FVB/N	Charles River Janvier	RRID:IMSR_CRL:207
Human oocytes	IVF clinics	N/A
Pig ovaries (<i>Sus scrofa domestica</i>)	Local slaughterhouse	N/S
NIH 3T3	ATCC	CRL-1658
HEK293T	ATCC	CRL-3216
Recombinant DNA		
pGEMHE	Jan Ellenberg	[74]
pGEMHE- <i>H2B</i> -mRFP	Jan Ellenberg	[52]
pGEMHE-EGFP- <i>Map4</i>	Jan Ellenberg	[52]
pGEMHE-SNAP-MAP4-MTBD	Melina Schuh	[75]
pGEMHE-CENPB-mEmerald	This paper	N/A
pGEMHE-TRIM21	Melina Schuh	[43]
CENPB-mEmerald	Addgene	54037
Software and Algorithms		
OriginPro 2016G	OriginLab	N/A
ImageJ	N/A	N/A
Imaris	BITPLANE	N/A
AiryScan Processing Algorithm	Zeiss	N/A

LEAD CONTACT AND MATERIALS AVAILABILITY

All unique/stable reagents generated in this study are available from the Lead Contact (Melina Schuh, melina.schuh@mpibpc.mpg.de) with a completed Materials Transfer Agreement.

EXPERIMENTAL MODEL AND SUBJECT DETAILS

Primary mouse oocytes

Female FVB/N mice (6–8 weeks) were obtained directly from Janvier or from an in-house breeding colony that was generated using mice purchased from Charles River. For aging studies, 35–120 week old mice were used. All mice were maintained in a specific pathogen-free environment, according to the guidelines of the MPI-bpc animal facility. The experiments involving mice have been performed in compliance with the German Law on Animal Welfare.

Oocytes were collected from ovaries of 6–8 or 35–120 week old FVB/N mice and cultured at 37°C under mineral oil in homemade M2 medium supplemented with 250 μM dbcAMP (Sigma; D0627) to maintain the prophase arrest. To trigger resumption of meiosis, oocytes were released into dbcAMP-free medium. Oocytes from the FVB/N strain require the following amounts of time after release from prophase arrest (NEBD, nuclear envelope breakdown) to complete key meiotic events: 6 h 30 min to stably align all chromosomes at the metaphase plate of meiosis I and 8 h 30 min to undergo anaphase I (Figure S2B). Therefore, to study chromosome and kinetochore architecture in steady-state MII eggs that have reached final metaphase-II arrest, we fixed the oocytes 16 h after release into dbcAMP-free medium. In the few experiments where we investigated meiosis I chromosome and kinetochore architectures, we preserved the oocytes 7 h 15 min – 8 hours after release from prophase arrest.

Primary human oocytes

All human oocytes used in this study were sourced from women undergoing assisted reproduction treatments after having obtained fully informed consent. The use of immature unfertilized human oocytes has been approved by the UK's National Research Ethics Service under the REC reference 11/EE/0346 (IRAS Project ID 84952), the Ethics Committee of Lower Saxony (Ärztzammer Niedersachsen) under the reference 15/2016 and the Danish Capital Region's Ethics Committee (H-16044731). The unfertilized oocytes were donated by patients at Bourn Hall Clinic (Cambridge, UK) between January 2016 and March 2018, at Kinderwunschzentrum (Göttingen, Germany) between September 2016 and March 2018, at the Laboratory for Reproductive Biology, Capital Region H hospitals (Copenhagen, Denmark) and INVICTA Fertility Clinic (Gdansk, Poland) between January 2016 and April 2018. 48 meiosis II eggs from 34 donors were included in the analysis. The donors were aged between 19 and 45 years and underwent ovarian stimulation for intracytoplasmic sperm injection (ICSI). Only oocytes that were immature and hence unsuitable for the ICSI procedure were designated to the study. None of the oocytes used in this study were freeze-thawed. Oocytes were cultured as previously described [76].

In brief, following retrieval, oocytes were transported to the research lab and cultured in G-MOPS medium (Vitrolife, #10129) supplemented with 10% FBS (GIBCO, #16000044) under mineral oil (Merck, #8012-95-1) at 37°C. Only oocytes that appeared morphologically healthy and underwent NEBD within 24 hours from retrieval were included in the study. The developmental stage of the oocyte was assessed either manually by scoring for the presence of the germinal vesicle at 60 minute intervals or using a Primo Vision Evo+ timelapse camera installed inside the incubator. To analyze chromosome and kinetochore morphology at metaphase-II, the oocytes were fixed 4-9 hours after polar body extrusion.

Primary pig oocytes

Porcine ovaries were obtained from a local slaughterhouse and transported to the laboratory within 45 minutes of retrieval in a portable 37°C incubator in M2 medium supplemented with 1 mM dbcAMP. In brief, the oocytes were retrieved by aspiration of the large antral follicles with an 18-gauge needle affixed to a 1 mL disposable syringe. The fluid aspirated was then transferred to dishes containing 1 mL of M2 medium supplemented with dbcAMP and the cumulus-oocyte complexes (COC) were collected from the sediment. The COCs were then washed extensively to remove the cellular debris and transferred to droplets of M2+dbcAMP under mineral oil. Only large oocytes with homogeneous cytoplasm and surrounded by several layers of compact cumulus cells were selected for experiments. Oocytes dedicated to immunolabelling at the metaphase-II stage were released into dbcAMP-free medium and cultured for 30 hours in a 37.5°C incubator prior to fixation.

Cell culture

NIH 3T3 and HEK293T cells (ATCC) were cultured in DMEM (GIBCO; 31966021) supplemented with 10% Calf Serum (Sigma; C8056) and penicillin-streptomycin at 37°C in a 5% CO₂ humidified atmosphere and regularly checked to be mycoplasma-free.

METHOD DETAILS

Expression constructs and mRNA synthesis

Capped mRNA was synthesized with T7 RNA polymerase (mMessage mMachine Kit Ambion), precipitated with isopropanol, and dissolved in 6 µL of RNase-free water. The following constructs were used: pGEMHE-EGFP-*MAP4* and pGEMHE-SNAP-*MAP4-MTBD* (aa659-1125 of the microtubule binding domain of MAP4) to label microtubules, pGEMHE-*H2B*-mRFP to label the chromosomes, pGEMHE-*CENPB*-mEmerald to label kinetochores and pGEMHE-TRIM21 [43] to overexpress the mouse variant of the TRIM21 protein in the oocytes. To generate the kinetochore labeling construct, *CENPB*-mEmerald (Addgene, 54037) was subcloned into pGEMHE vector using the NheI and NotI restrictions sites, while other expression constructs were previously described. Quantitative microinjection was performed as outlined previously [77]. After injection of mRNAs into oocytes, the oocytes were incubated for 3 hours at 37°C to express the protein.

Antibody microinjection

The anti-Smc3 antibody used was rabbit anti-Smc3 (Abcam ab9263). The anti-Rec8 antibody was generated in-house using a previously characterized epitope [47]. The control IgG used was a normal rabbit IgG (Millipore 12-370). With the exception of anti-Smc3, all antibodies were concentrated using Amicon Ultra-0.5 100 kDa centrifugal filter devices (Millipore) to remove traces of azide and replace the buffer with PBS. Following concentrations of antibodies were used: anti-Smc3 (1 mg/ml), anti-Rec8 (2 mg/ml) and control IgG (2 mg/ml). Prior to microinjection into eggs, the antibodies were spun at 10,000 rpm (4°C) for 10 minutes and supplemented with NP-40 at a final concentration of 0.05%. Antibody microinjection into eggs was performed as described previously for mRNA microinjection [52]. For full depletion experiments in the metaphase of meiosis II, a bolus of 6 pl of anti-Smc3 or anti-Rec8 was microinjected into the eggs, whereas for partial depletion experiments 2 pl of the anti-Smc3 antibody were microinjected. For partial depletion of cohesins in meiosis I, a bolus of 4 pl of the anti-Smc3 antibody was microinjected 4.5-5.5 hours after the oocytes were released from prophase arrest. The oocytes were then fixed 7 h 15 min – 8 hours after the release.

Drug addition experiments

To assess the acute effects of drugs on chromosome and kinetochore morphologies, oocytes were matured in M2 medium until they reached meiosis II and were washed into drug containing medium immediately before imaging. To partially depolymerize microtubules, TRIM-expressing eggs were treated with 50 nM nocodazole (Sigma) before the introduction of anti-cohesin antibodies. No more than 5 eggs were microinjected with the antibody at a time, to minimize the interval between cohesin degradation and exposure to the drug-free medium. The changes in microtubule dynamics were assessed live on the microscope.

In order to prevent spindle bipolarization, TRIM21-overexpressing oocytes were released from the dbcAMP-induced arrest into M2 medium containing 150 µM of monastrol (Sigma). The oocytes were incubated in the drug-containing medium from release until the chromosome spreading procedure. 5 hours after the release, the MI oocytes were microinjected with a bolus of 4 pl of an anti-Smc3 antibody (1 mg/ml in PBS) or control IgG. Subsequently, they were placed on a microscope to assess chromosome organization. After additional 3 hours, chromosome spreading procedure was performed.

All drug experiments included appropriate DMSO control groups.

Chromosome spreads

Oocytes were transferred through droplets of acidic Tyrode's solution (pH 2.5) at 37°C to remove the zona pellucidae. After subsequent 14 min incubation in 1:1 FBS:water at 37°C, oocytes were fixed on a glass slide in a drop of 1% paraformaldehyde, supplemented with 0.15% Triton X-100 and 3 mM DTT [78]. For human oocyte spreads, as bursting of human MI oocytes is more variable, the oocytes were allowed to swell in a drop of 0.9% sodium citrate (w/v) prior to transfer to the formaldehyde solution. Glass slides were stored in a humidified chamber at room temperature overnight. In experiments where kinetochore architecture was assessed, following air-drying the oocytes were incubated the next morning with primary antibodies (mouse anti-Hec1, Santa Cruz sc-135934, 1:100; rabbit anti-CENP-A, Cell Signaling C51A7 1, 1:100; human ACA centromere CREST autoantibody, Antibodies Incorporated 15-234-0001, 1:100; mouse anti-CENP-C, ab50974, 1:20; sheep anti-BubR1, ab28192, 1:20) for 1 h at 37°C or overnight at RT. For AiryScan microscopy, appropriate Alexa488/546 conjugated secondary antibodies raised in goat (ThermoFisher, 1:200) were used for visualization. 1 µg/ml Hoechst was applied for DNA counterstaining. Samples for STED microscopy were counterstained with PicoGreen (ThermoFisher, 1:100) for 2h at room temperature to visualize the DNA, prior to incubation with the following secondary antibodies: STAR RED goat anti-rabbit (Abberior, 1:400) and Alexa594-conjugated goat anti-mouse (ThermoFisher, 1:200). In cases where anti-CENP-A antibody was used to visualize the centromeres, oocytes were treated for 30 min with Lambda Protein Phosphatase at 30°C prior to antibody incubation, as described previously [39].

In experiments where the fluorescence signal intensity of the centromeric pool of cohesin complexes was compared between control and Trim-Away eggs, slides were air-dried and subsequently incubated at 4°C with human CREST serum (1:250, Europa Bioproducts, FZ90C-CS1058) and an in-house anti-Rec8 antibody (1:100, epitope based on Eijpe et al., 2003 [47]) or an anti-Smc3 antibody (rabbit anti-Smc3, Bethyl Laboratories, A300-060A) overnight. Next morning, the slides were incubated for 1h at RT with the following secondary antibodies: donkey anti-rabbit 488 and goat anti-human 546/647 (ThermoFischer, 1:200). Additionally, the DNA was visualized with 40 µM Hoechst.

Cold-mediated microtubule depolymerization assays

To determine k-fiber stability and kinetochore-microtubule attachment modes, non-kinetochore-bound microtubules were selectively depolymerized by exposing the eggs to 4°C. The durations of the cold-treatments to obtain an optimal microtubule density were adapted as follows: 6 minutes for human eggs, 10 minutes for pig eggs and 14 minutes for mouse eggs. Following the cold-treatment, the dish was removed from ice and the cells were immediately fixed and processed for immunofluorescence microscopy. K-fiber attachments were quantified from three-dimensional volume reconstructions of spindles using Imaris (Bitplane) or maximum intensity projections of selected z sections using Fiji (SciJava).

Oocyte immunofluorescence

Before fixation, the oocyte were pre-permeabilized by a brief 10 s exposure to 0.25% Triton X-100. Oocytes were then fixed (30 min for mouse oocytes; 60 min for pig or human oocytes) at 37°C in 100 mM HEPES (pH 7; titrated with KOH), 50 mM EGTA (pH 7; titrated with KOH), 2% formaldehyde (methanol free) and 0.2% Triton X-100. Afterward, oocytes were extracted overnight at 4°C in PBS supplemented with 0.1% Triton X-100. All antibody incubations were performed in PBS, 3% BSA and 0.1% Triton X-100, either overnight at 4°C (primary antibodies) or for 3h at room temperature (secondary antibodies). Primary antibodies used were human ACA centromere CREST autoantibody (FZ90C-CS1058, Europa Bioproducts; 1:500 and 15-234-0001, Antibodies Incorporated; 1:50), rabbit anti-CENP-F (ab5, Abcam; 1:100), sheep anti-BubR1 (Abcam, ab28192; 1:50), mouse anti-Hec1 (ab3613, Abcam; 1:100) and rat anti- α -tubulin (MCA78G, Serotec; 1:1000). As secondary antibodies, Alexa Fluor488/564/647 labeled anti-mouse/anti-rabbit/anti-human/anti-sheep/anti-rat (Thermo Fisher; 1:400) were used. DNA was stained with 5 mg/ml Hoechst 33342 (Molecular Probes).

Immunofluorescence of tissue culture cells

NIH 3T3 and HEK293T cells were seeded in 35mm glass-bottom imaging dishes (MatTEK). Cells were then pre-permeabilized with 0.25% of Triton X-100 for 60 s and fixed for 10 min in 100 mM HEPES (pH 7; titrated with KOH), 50 mM EGTA (pH 7; titrated with KOH), 2% formaldehyde (methanol free) and 0.2% Triton X-100. Primary antibody was diluted in PBS, 3% BSA and 0.1% Triton X-100 and the cells were incubated for 1.5h at room temperature (ACA centromere CREST autoantibody, FZ90C-CS1058, Europa Bioproducts; 1:500). Alexa Fluor488 anti-human (Thermo Fisher; 1:500) was used as a secondary antibody and DNA was counterstained with 5 mg/ml Hoechst 33342 (Molecular Probes).

Super-resolution immunofluorescence microscopy

Super-resolution images were acquired using the AiryScan module on Zeiss LSM800 and LSM880 microscopes equipped with 40x C-Apochromat 1.2 NA water-immersion objectives and processed post-acquisition using ZEN2. Images were acquired at a spatial resolution of 0.19 µm optical sections, covering the entire spindle. In experiments used for quantitative assessment of the fragmentation status of kinetochores, the spindles were manually rotated once the imaging dish was placed on the microscope, so that the long axis of the spindle was in parallel to the plane of the imaging dish. To achieve this, a single oocyte at a time was placed in the imaging dish and prior to image acquisition the oocyte was manually rotated with a tip of an unbroken microinjection needle until the desired orientation of the spindle was achieved. Because the resolution in the z-direction is inferior to that in the xy plane in the imaging techniques that we have used, rotating the oocytes to achieve a comparable orientation of the spindle relative to the imaging plane allowed us to make reliable assessments of kinetochore morphologies across different oocytes. Images depicted in the figure

panels were recorded within the dynamic, non-saturated intensity range. The image intensities were then adjusted post-acquisition in a linear way to improve clarity of the displayed structures.

Structured illumination microscopy (SIM) of human eggs was performed on a Zeiss ELYRA S1 (SR-SIM) system equipped with a 63x C-Apochromat 1.2 NA water-immersion objective. Images were acquired at an optical slice thickness of 0.12 μm confocal sections, covering $\sim 20 \mu\text{m}$.

Stimulated emission depletion microscopy (STED) was performed on a two-color Abberior STED 775 QUAD scanning microscope (Abberior Instruments GmbH) equipped with 488 nm, 561 nm, and 640 nm pulsed excitation lasers, a pulsed 775 nm STED laser and a 100x oil immersion objective lens (N.A. 1.4). Pixel size was 20 nm for all of the images. Laser powers and dwell times were kept constant between samples.

Confocal microscopy in fixed cells

To establish the effect of Trim-Away on the centromeric cohesin pool, we imaged chromosome spreads of metaphase-II mouse eggs using confocal microscopy. Trim-Away experiments in MII eggs were performed as described above. To compare the fluorescence of the centromeric pool of cohesin complexes between Trim-Away expressing MII eggs microinjected with either a control or an anti-cohesin antibody, both groups across all experimental repetition were imaged on the same microscope (Zeiss LSM880 equipped with a Plan-Apochromat 63x/1.4 Oil immersion objective for the anti-Rec8 experiments and Zeiss LSM800 equipped with a Plan-Apochromat 63x/1.4 Oil immersion objective for the anti-Smc3 experiments) using identical imaging settings. The z-intervals used were 0.45 μm and 0.36 μm , respectively, and the same number of z sections covering the entire chromosomal signal was used for the control and the experimental groups.

Confocal microscopy in live cells expressing fluorescent reporters or incubated with fluorescent dyes

Confocal images of live oocytes were acquired using Zeiss LSM800 and LSM880 microscopes at 37.5°C. Oocytes were imaged in M2 medium under oil using a 40x C-Apochromat 1.2 NA water-immersion objective. For chromosome behavior analysis following cohesin depletion the oocytes were typically imaged at a temporal resolution of 4-10 minutes and optical slice thickness of 1.5 μm , covering the entire spindle. To assess spindle dynamics following drug treatments the oocytes were imaged for 7 hours at a temporal resolution of every 15-20 minutes and optical slice thickness of 2.5 μm . Prior to any experiment aiming to perturb kinetochore organization, the general oocyte health was assessed using fluorescently labeled chromosomes and microtubules in live oocytes.

In order to compare the timing of progression through meiosis between oocytes from old and young mice, fluorescent dyes compatible with live imaging were used to follow chromosome (SiR-tubulin, Spirochrome, 1: 10,000) and microtubule (DNA 5-TMR-Hoechst, gift from G. Lukinavičius, 1: 10,000) dynamics. In brief, isolated oocytes were transferred into M2 medium supplemented with dbcAMP and the above-mentioned dyes for 2h hours. To promote release from meiotic arrest, oocytes were washed through droplets of M2 medium lacking dbcAMP and transferred into imaging dishes containing M2 medium and the dyes only. For each experimental repetition, both old and young oocytes were imaged in the same imaging dish placed on the microscope for 22 hours (Zeiss LSM800 or LSM880). Images were acquired every 15 minutes at an optical slice thickness of 2 μm confocal sections covering 66 μm .

Immunoblotting

Oocytes were injected with mRNA coding for TRIM21 and fluorescently labeled chromosome and microtubule markers. Once the oocytes have reached the metaphase-II stage the following day, they were microinjected with anti-cohesin antibody or corresponding IgG control. After 2 hours, the chromosome morphology of each egg was scored by assessing the fluorescence signal on the microscope. Only eggs with roughly half of the chromosomes disintegrated into single chromatids at the time of assessment were selected for the “partial depletion of Smc3” group. The selected eggs were then washed in PBS, transferred in minimal volume of PBS into Eppendorf tubes and snap frozen in liquid nitrogen (20 oocytes per group). On the day of Western Blotting, the eggs were thawed and resuspended in NuPAGE LDS Sample Buffer (Thermo Fisher). The mix was then heated at 95°C for 5 mins. Samples were run at 4°C on NuPAGE 4%–12% Bis-Tris gels (Thermo Fisher) and transferred onto nitrocellulose membrane. Antibody incubations were performed in TBS with 5% skim milk powder (w/v) and 0.05% Tween-20. Primary antibodies used were rabbit anti-Smc3 (Abcam, EPR7984) and anti- α -tubulin (rat, AbD Serotec). HRP-coupled secondary anti-rabbit (Invitrogen, 31462) and anti-rat (Santa Cruz, sc-2032) antibodies were detected by enhanced chemiluminescence (SuperSignal West Femto Maximum Sensitivity Substrate, Thermo Fisher, 34095).

QUANTIFICATION AND STATISTICAL ANALYSIS

Chromosome counting and assessment of kinetochore configuration

All kinetochore fragmentation analysis in chromosome spreads and fixed eggs was performed on images that were acquired using super-resolution microscopy techniques (STED, SIM or AiryScan). Prior to analysis, the AiryScan images were processed post-acquisition using ZEN2.

First, the total chromosome count of an egg was determined by assigning a number to each DNA unit (1-23 in humans, 1-20 in mice and 1-19 in pigs). To achieve this, sister chromatids that form a chromosome were annotated and individual single chromatids were

marked in ImageJ. Subsequently, the kinetochore foci belonging to the same chromosome were identified by comparing CREST/Hec1/CENP-A and Hoechst staining in consecutive z-planes spanning the entire chromosome. The two sister kinetochores of each chromosome were then marked with “A” and “B,” corresponding to the appropriate chromosome number.

All detection of kinetochore fragments on chromosome spreads was performed using automated spot detection function based on local maxima in Imaris (Bitplane; expected foci diameter: 200–250 nm). All automated spot detections were confirmed by visual inspection with minimal manual correction. The fragmentation status of a kinetochore was then additionally scored qualitatively by comparing the appearance of each kinetochore in single z sections in ImageJ. In [Figure 1J](#), the “concordant” group includes all kinetochore/centromere pairs, where the automated spot detection function in Imaris detected multiple foci both in the CENPA signal and the Hec1 signal, or both the kinetochore and centromere were compact (single signal focus detected). All surface area, Feret’s diameter (the maximum caliper) and circularity ($\text{circularity} = 4\pi \times (\text{area}/\text{perimeter}^2)$, where circularity value of 1.0 indicates a perfect circle) measurements were performed in ImageJ on maximum intensity projections of appropriate z sections covering the entire kinetochore/centromere region. In [Figure 1G](#), the dispersal of the centromeric domain was measured by comparing the surface area of the smallest circle encompassing the CENP-A signal. In [Figure 1A](#), the fluorescence intensity of the centromere-associated CENP-A pool was quantified per centromere basis by selecting a region of interest (ROI) encompassing that centromere. Subsequently, the integrated density for that region was calculated (computed in ImageJ as Area of the ROI x Mean Grey Value) and finally the mean fluorescence of the background in that region multiplied by the area of the ROI was subtracted. The procedure was then repeated for all the centromeres in a given cell to obtain the egg’s total centromeric CENP-A fluorescence. For quantifications in fixed eggs, kinetochore configurations were scored as follows: compact – a single CREST spot visible by inspection of the brightest z-plane, with a uniform single focus in the 3D projection, and fragmented- two or more discrete CREST foci, the outlines of which could be resolved. For fragmented kinetochores, the number of domains that could be resolved with confidence was further annotated. Because in aged mice and in the Trim-Away experiments targeting cohesins in young mice the CENP-A centromeric domain was observed to fragment into numerous foci of a diameter too small for a reliable evaluation of the exact number of foci by automated spot detection, we did not count the number of CENP-A foci and instead measured CENP-A fragmentation by evaluating Feret’s diameter, surface area of the domain or its circularity.

Assessment of the effects of Trim-Away mediated cohesin loss on chromosome architecture in the metaphase of meiosis I

The separation between sister kinetochores within the same pair (also known as iKT, intrakinetochore distance) and the distance between the two sister kinetochore pairs (bivalent’s long axis or interkinetochore distance) was determined by an assessment of 3D reconstructions of meiosis I spindles fixed at the metaphase stage (Imaris, Bitplane). iKT depends on the amount of centromeric cohesion, while bivalent’s long axis is a readout of the physical linkage between the homologous chromosomes of a bivalent and depends on arm cohesion. CREST and Hoechst signals were used to identify the four kinetochores of any given bivalent. The center of each kinetochore was detected with subpixel accuracy using the automated spot detection function based on local maxima in Imaris (Bitplane). The iKT and bivalent long axis length were then computed in Microsoft Excel using the Pythagorean Theorem on xyz coordinates of kinetochore centers defined by the automated spot detection function. In instances where the two sister kinetochores were too tightly linked to be resolved as two independent spots by AiryScan microscopy, the iKT was set to 0 μm .

Modes of kinetochore-microtubule attachment

All eggs that were included in the analysis were recorded using super-resolution microscopy techniques and single eggs were rotated on the microscope prior to image acquisition, as described in detail in the microscopy section above. Microtubule-kinetochore attachments were determined by 3D analysis of appropriate z sections. For quantification of k-fibers involved in an interaction, first the number of discrete k-fibers attaching to a kinetochore was determined. Then, the fragmentation status of the kinetochore was linked to its attachment mode, based on number assigned to the chromosome/chromatid (as described above). For k-fiber attachment modes, only kinetochores with end-on attachments originating from opposite spindle poles were included in the merotelic group, whereas k-fibers which were in a direct contact with a kinetochore, but were extending beyond the kinetochore, were scored as lateral.

Quantification of fluorescence intensity of the centromeric cohesin pool

The quantification of the efficiency of Trim-Away mediated depletion of the centromeric Rec8 and Smc3 cohesin pools was performed on MII chromosome spreads imaged with Zeiss confocal microscopes, as described above. All repetitions for each of the two experiments were performed on the same microscope using identical imaging conditions. The number of z sections recorded was the same for the control and the experimental group. Subsequently, a Sum Intensity Projection of all z sections was performed and the signal intensities were compared in ImageJ. In brief, first the centromeric region in each chromosome was identified in the control group using the CREST channel and an ROI (Region of Interest) was marked using a free drawing tool. Thus, the ROI included the two sister kinetochores of a chromosome and the centromeric regions located medially to the kinetochores. The ROI was then copied to the Rec8/Smc3 channel by using the ctrl+shift+E command and the Mean Intensity of the Rec8 signal in that region was computed. This procedure was performed for all remaining chromosomes in any given cell, with the area of ROI being kept constant. In our experimental group, the Trim-Away targeting of Smc3 or Rec8 resulted in the complete separation of chromosomes into sister chromatids, which was in line with our prediction. Analogous to the control cells, a ROI encompassing a kinetochore and its

centromere was selected for each chromatid. The area ROI was kept constant for all measurements and as predicted from the separation of all chromosomes into single chromatids in our assays, the area occupied by the kinetochore and its centromere in the Trim-Away experimental group was roughly half of that in control cells, in which the two sister chromatids were still linked. To determine the value for background in our images, we calculated in each control/experimental cell the mean background intensity across five randomly selected regions on distal chromosome arms, which in meiosis II are cohesin-free. Subsequently, we computed the Final Fluorescence Intensity as Mean Fluorescence Intensity of ROI – Mean Background Intensity. In the few instances where the Mean Background Intensity was higher than the measured Mean Fluorescence Intensity in the centromeric region (0.78% for the control measurements, $n = 510$ and 9.75% for the Trim-Away experimental group, $n = 800$), likely indicative of centromeric cohesin depletion to a level that is lower than non-specific background signal, the negative values were assigned as zero. The values in each experiment were subsequently normalized to the mean Final Fluorescence Intensity of the control group, and all Final Fluorescence Intensity measurements were plotted in the form of boxplots.

Quantification of western blot mean band intensity

To assess the specificity and efficiency of protein depletion using the Trim-Away approach, the mean band intensities of the Smc3 signal were normalized to the intensity of the loading control standard (α -tubulin signal). Gel analysis plugin in ImageJ was used to quantify the band intensity and mean across three experimental replicates was calculated. All control and experimental groups for each experiment were blotted on the same membrane and exposed uniformly to the ECL solutions.

Statistical analysis

Average (mean), standard error of the mean and standard deviation were calculated in Microsoft Excel or OriginPro (OriginLab). Unless specified otherwise, significance analyses were based on Student's *t* test (always two-tailed) and were calculated using OriginPro. For comparison of absolute values, significance analysis was performed with the Fisher's Exact test using the XLSTAT add-on to Excel. In instances where the absolute values were coming from multiple experimental repetitions, an extension to Fisher's Exact test was applied (Cochran-Mantel-Haenszel test, CMH). Three to six independent experimental replicates were performed for each experiment, with the following exceptions, where two experimental replicates were quantified: Hec1/CENP-C morphology assessment in MII eggs after full Trim-Away, CREST morphology evaluation in partial depletion of Smc3 in meiosis I and upon DMSO/Monastrol treatments, and Smc3 immunofluorescence intensity following Trim-Away. The data describing these experiments is presented in a form of boxplots, with the exception of [Figures 3E, 3K, 5F, and 6H](#), where the average fragmentation rate across all samples is plotted. For quantitative analysis of these experiments, the average value of all measurements per oocyte (80 kinetochores in meiosis I and 40 kinetochores in meiosis II, in at least 20 oocytes microinjected twice) was compared by one-way ANOVA followed by Turkey's test to compare the experimental groups. In [Figure 1A](#), the Integrated Density of 42 eggs coming from three independent experimental replicates was normalized and compared as above, with the total centromeric CENP-A intensity per egg compared across the two groups. The STED measurements in [Figure 1G](#) were performed on 1776 kinetochores from young/aged mice and 46 independent images were acquired. *P* values are designated as * $p < 0.05$, ** $p < 0.01$, *** $p < 0.001$ and **** $p < 0.0001$. Non-significant values are indicated as "N.S." All diagrams were generated using Origin 8 Pro. All box plots show median (horizontal lines), mean (small squares), 25th and 75th percentiles (boxes), and 5th and 95th percentiles (whiskers).

DATA AND CODE AVAILABILITY

This study did not generate any unique datasets or code.

Current Biology, Volume 29

Supplemental Information

**Meiotic Kinetochores Fragment into Multiple Lobes
upon Cohesin Loss in Aging Eggs**

Agata P. Zielinska, Eirini Bellou, Ninadini Sharma, Ann-Sophie Frombach, K. Bianka Seres, Jennifer R. Gruhn, Martyn Blayney, Heike Eckel, Rüdiger Moltrecht, Kay Elder, Eva R. Hoffmann, and Melina Schuh

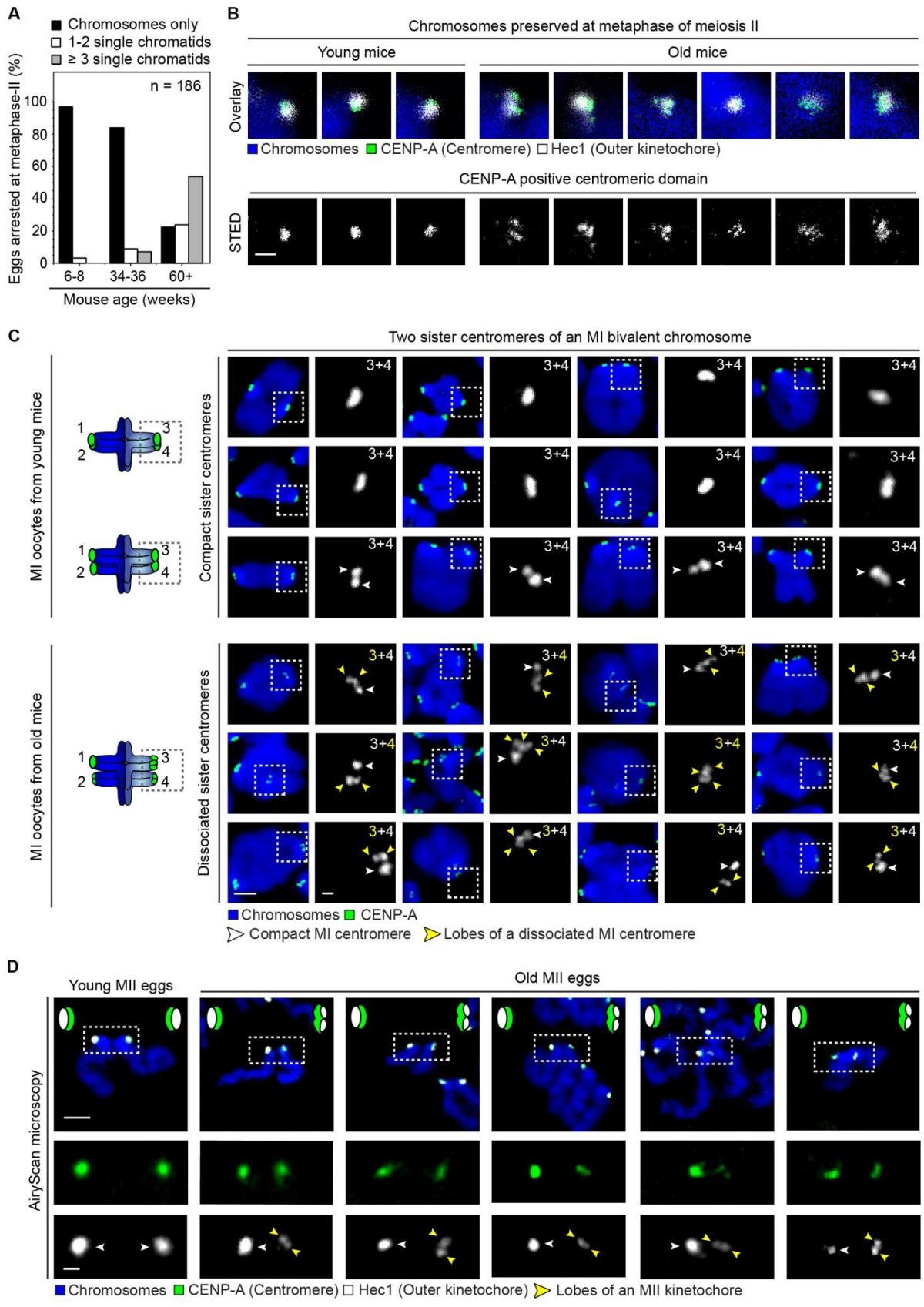


Figure S1| The centromeric CENP-A domain decompacts in aged MI oocytes and MII eggs, related to Figure 1

(A) Fraction of metaphase-II eggs from mice of different ages that contained single chromatids, indicative of pronounced weakening of centromeric cohesion. Data from 186 MII eggs (8 experiments).

(B) Representative images of CENP-A positive centromeric domains in metaphase-II eggs from mice aged either 8 weeks (young) or 60-64 weeks (old). Top panel shows an overlay of DNA signal (blue, Picogreen, confocal mode), outer kinetochore region (white, Hec1, confocal mode) and the centromeric signal (green, CENP-A, STED mode). Below each panel, the corresponding centromeric CENP-A signal is additionally shown in greyscale (STED mode). Scale bar: 0.5 μm .

(C) Representative images of the centromeric CENP-A domain in young (8 week old females) and old (65-67 week old females) oocytes preserved at metaphase of meiosis I and visualized with AiryScan microscopy. Numbers in insets refer to sister kinetochores shown (as in the schematic on the left).

(D) Representative metaphase-II chromosome spreads in eggs from aged mice (>60 weeks old) visualized with AiryScan microscopy. Centromeres are labelled in green (top, CENP-A), outer kinetochores in white (bottom, Hec1) and chromosomes in blue (Hoechst).

(C and D) Scale bars represent 2 μm in overviews and 0.5 μm in insets. White arrows point to compact kinetochores/centromeres and yellow arrows point to lobes within fragmented kinetochores/centromeres.

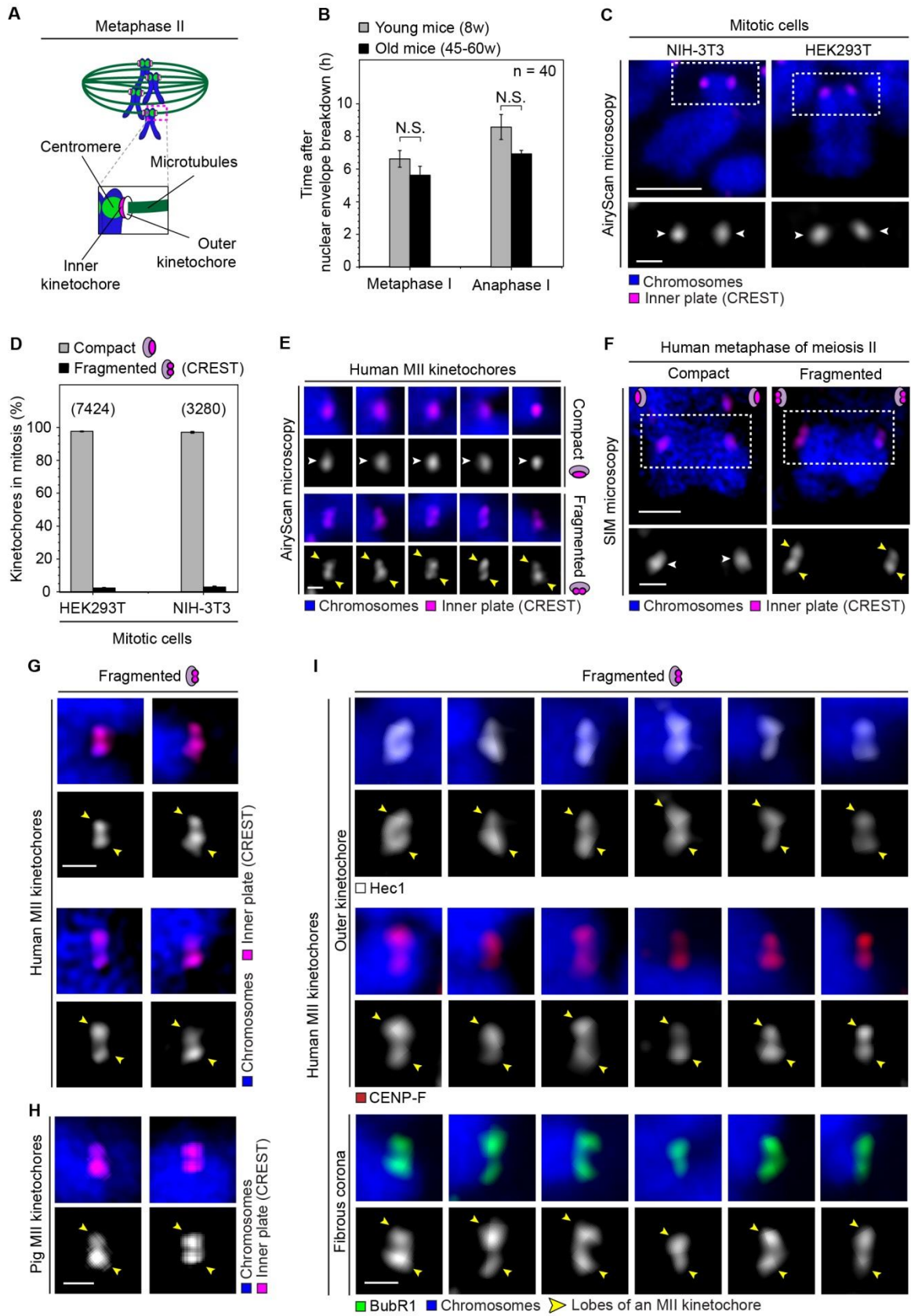


Figure S2| Meiosis II kinetochores in humans, pigs and mice frequently reorganize into two distinct lobes, related to Figure 2

(A) Schematic diagram showing the spatial arrangement of the centromere (green), the inner kinetochore (magenta) and the microtubule-interacting outer kinetochore (white) in a metaphase-II chromosome.

(B) Time required for oocytes from young mice (8 weeks) and old mice (45-62 weeks, 15 females) to complete the key meiotic events. Metaphase-I timepoint refers to full chromosome alignment on the MI spindle. Chromosome (DNA 5-TMR-Hoechst) and spindle (SiR-tubulin) dynamics were followed live using fluorescent dyes (4 experimental repetitions). Timings were compared using Student's t-test ($p = 0.085$, N.S.). Error bars show SEM.

(C) Representative immunofluorescence images of kinetochores in mouse and human mitotic cells imaged with AiryScan microscopy.

(D) Quantifications of kinetochore configurations in mitotic cells as in **(C)**. Data from 67 NIH-3T3 and 68 HEK293T cells (3 experiments each). Error bars show SEM.

(E) Representative images of compact (top panel) and fragmented (bottom panel) kinetochores in human MII eggs imaged with AiryScan microscopy.

(F) Representative SIM microscopy images of human MII chromosomes with both kinetochores compact (left) or both fragmented (right). Both chromosomes were captured on the same metaphase-II spindle. Scale bars: 1 μm in overviews and 0.5 μm in insets.

(G) Representative SIM microscopy examples of fragmented MII kinetochores in human eggs.

(H) Representative images of fragmented MII kinetochores in pigs, imaged with AiryScan.

(I) Representative images of fragmented human MII kinetochores labelled with outer kinetochore markers (Hec1, white and CENP-F, red), and stained for the fibrous corona component BubR1 (green). DNA is labelled with Hoechst (blue).

(C, E-H) Kinetochores are labelled with CREST (magenta) and the DNA is labelled with Hoechst (blue).

(C, F) Scale bars: 2 μm in overviews and 0.5 μm in insets.

(E, G, H and I) Scale bars: 0.5 μm .

White arrows point to compact kinetochores and yellow arrows point to lobes within a fragmented MII kinetochore.

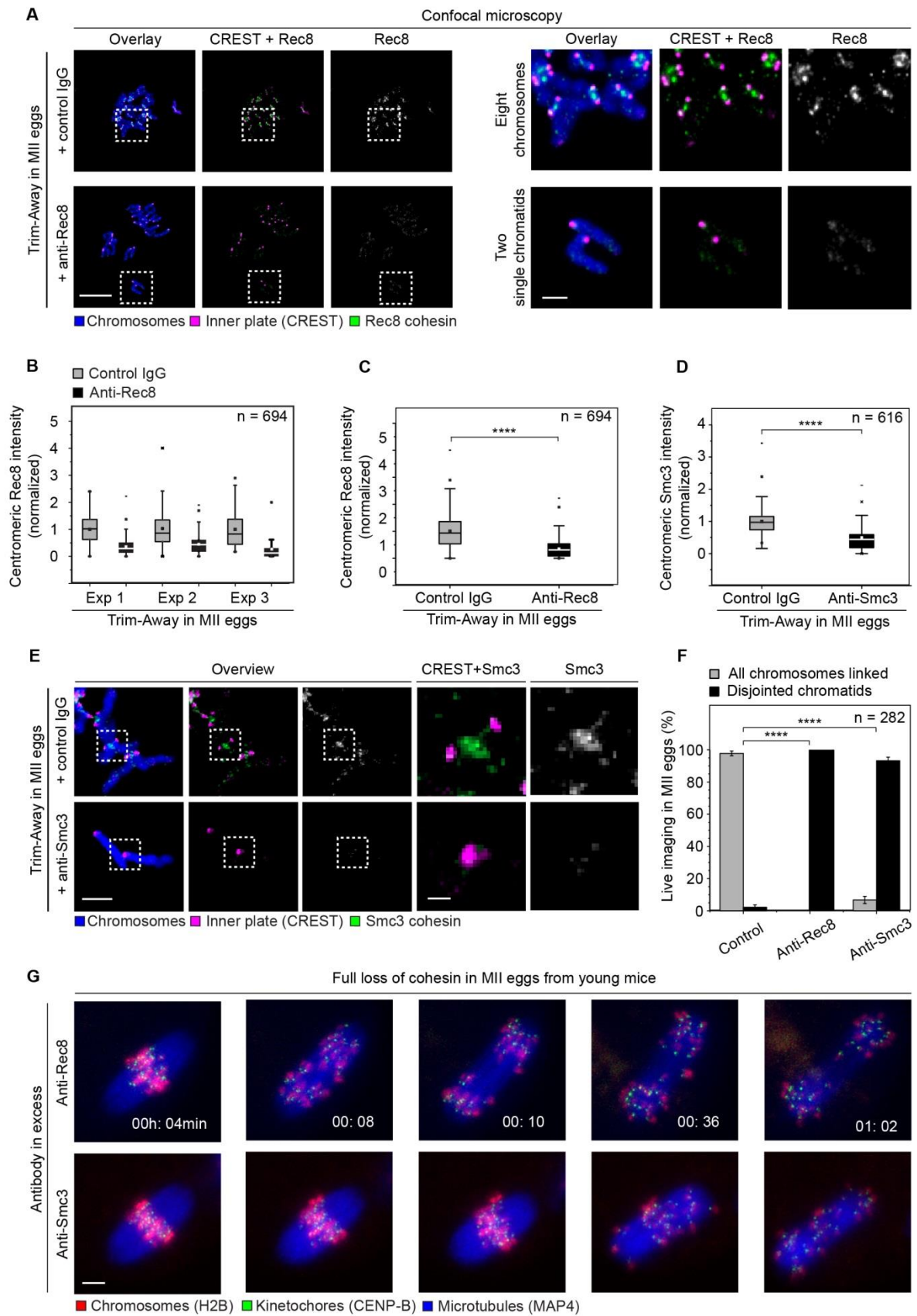


Figure S3| Trim-away efficiently depletes the centromeric cohesin pool in young eggs arrested at metaphase II, related to Figure 3

(A) Representative confocal images of metaphase-II chromosome spreads from young mice following the full Trim-Away assay as in **Figure 3A**, where TRIM21 overexpressing MII eggs were microinjected with either a control IgG antibody (top) or an anti-Rec8 antibody provided in excess (bottom). Images are maximum intensity z-projections of 19 z-sections acquired every 0.45 μm . The anti-Rec8 signal in both the control and the experimental groups is shown using identical brightness and contrast settings. Scale bars: 10 μm in overview and 2 μm in insets.

(B) Quantification of the centromeric Rec8 signal in MII eggs treated as in **(A)**. Measurements obtained for each experimental repetition are shown and these were normalized to the mean intensity of the young group. 29 MII eggs from 3 independent experimental repetitions were analyzed.

(C) Summary of all measurements obtained as in **(B)**

(D) Quantification of the centromeric Smc3 signal in MII eggs treated as in **(E)**. The measurements were normalized to the mean intensity of the young group. 22 MII eggs from 2 independent experimental repetitions were analysed.

(E) Representative confocal images of metaphase-II chromosome spreads from young mice following the full Trim-Away assay (as in **Figure 3A**), where TRIM21 overexpressing MII eggs were microinjected with either a control IgG antibody (top) or an anti-Smc3 antibody provided in excess (bottom). Images are maximum intensity z-projections of 12 z-sections acquired every 0.36 μm . The anti-Smc3 signal in both the control and the experimental groups is shown using identical brightness and contrast settings. Scale bars: 5 μm in overview and 1 μm in insets.

(F) Evaluation of the efficiency of the Trim-Away approach to induce loss of chromosome integrity, as in **(G)**. Data from 282 live MII eggs (young mice) from 19 experiments.

(G) Frames from time-lapse movies of live TRIM21 overexpressing MII eggs from young mice, microinjected with either an excess of anti-Rec8 or anti-Smc3. Chromosomes are labelled in red (H2B-mRFP), kinetochores in green (CENP-B-mEmerald) and microtubules in blue (MAP4-MTBD-Snap647). Time shows minutes (min) from antibody microinjection. Scale bar: 5 μ m.

(A and E) Kinetochores are labelled with CREST (magenta), DNA is labelled with Hoechst (blue) and cohesins (green) are labelled in **(A)** with anti-Rec8 and in **(E)** with anti-Smc3.

P values are designated as **p* < 0.05, ***p* < 0.01, ****p* < 0.001 and *****p* < 0.0001. *P* values in **(F)** were calculated with Student's t-test and in **(B-D)** the two groups were compared by one-way ANOVA followed by Turkey's test. Error bars show SEM. Box plots show median (horizontal lines), mean (small squares), 25th and 75th percentiles (boxes) and 5th and 95th percentiles (whiskers).

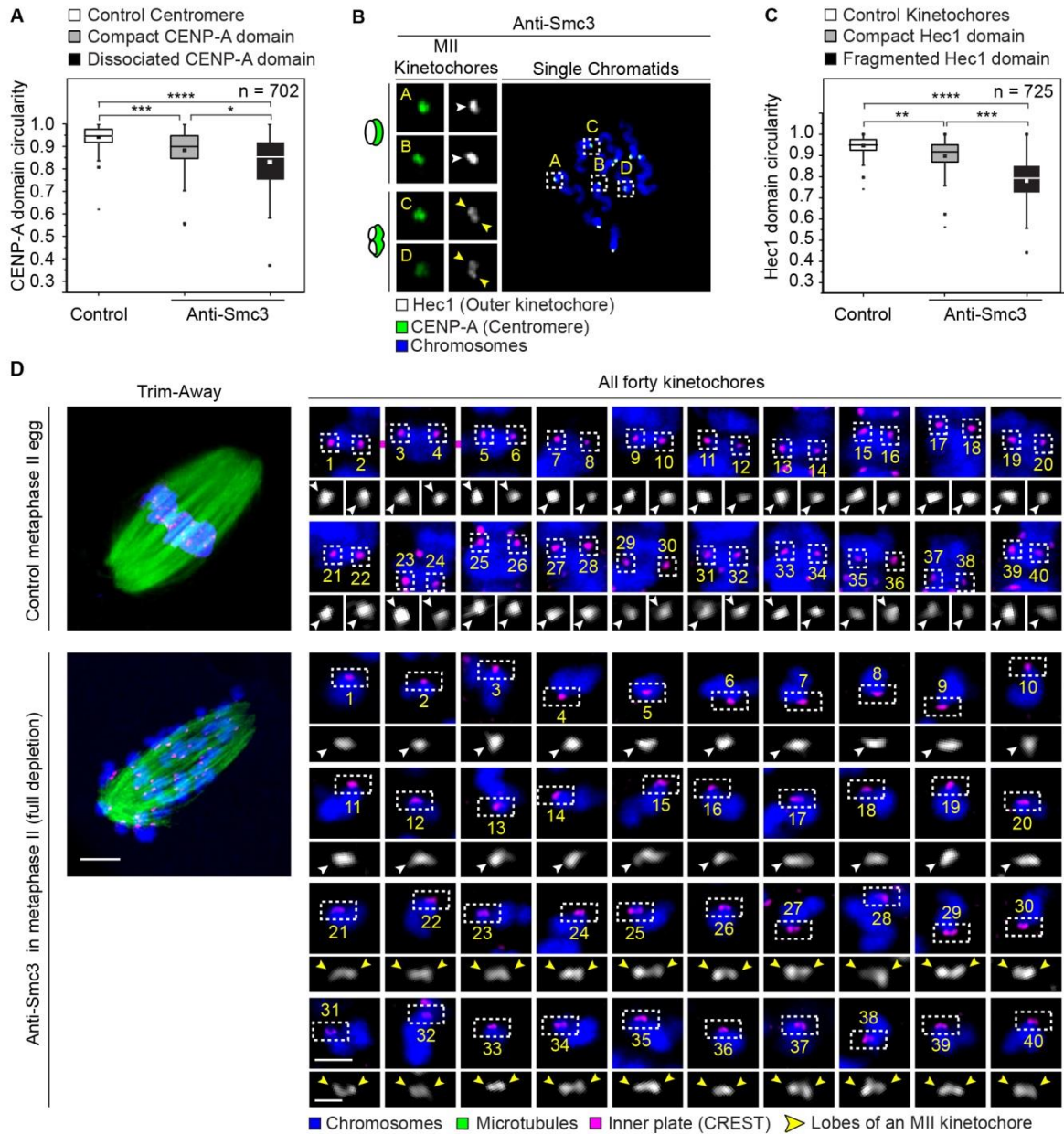


Figure S4| Centromeres decompact and inner/outer kinetochore plates fragment upon cohesin loss, related to Figure 3

(A) Assessment of the circularity (circularity of a perfect circle = 1.0) of the CENP-A domain in control eggs and young MII eggs depleted for Smc3. Centromere circularity and fragmentation status were assessed based on the CENP-A signal. 702 kinetochores from 20 MII eggs were evaluated (2 experiments).

(B) Representative chromosome spread images of single chromatids in Smc3-depleted MII eggs from young mice. Outer kinetochores are labelled in white (Hec1), centromeres in green (CENP-A) and chromosomes in blue (Hoechst). Scale bars: 2 μm in overviews and 1 μm in insets.

(C) Assessment of the circularity (circularity of a perfect circle = 1.0) of the Hec1 domain in control eggs and young MII eggs depleted for Smc3. Both the fragmentation status of a kinetochore and the circularity measurements were based on Hec1 labelling. 725 kinetochores from 20 MII eggs were evaluated (2 experiments).

(D) Representative examples of all 40 kinetochores of 20 chromosomes from a control MII egg (top) and all 40 kinetochores of 40 single chromatids following Trim-Away of Smc3 (bottom). Scale bars: 5 μm for spindle overviews, 2 μm for chromosome overviews and 0.5 μm for kinetochore insets. A projection through z-sections of the same Trim-Away MII egg microinjected with anti-Smc3 is shown in **Video S2**.

P values are designated as * $p < 0.05$, ** $p < 0.01$, *** $p < 0.001$ and **** $p < 0.0001$. *P* values were compared by one-way ANOVA followed by Turkey's test. Box plots show median (horizontal lines), mean (small squares), 25th and 75th percentiles (boxes) and 5th and 95th percentiles (whiskers). White arrows point to compact kinetochores and yellow arrows point to lobes within a fragmented MII kinetochore.

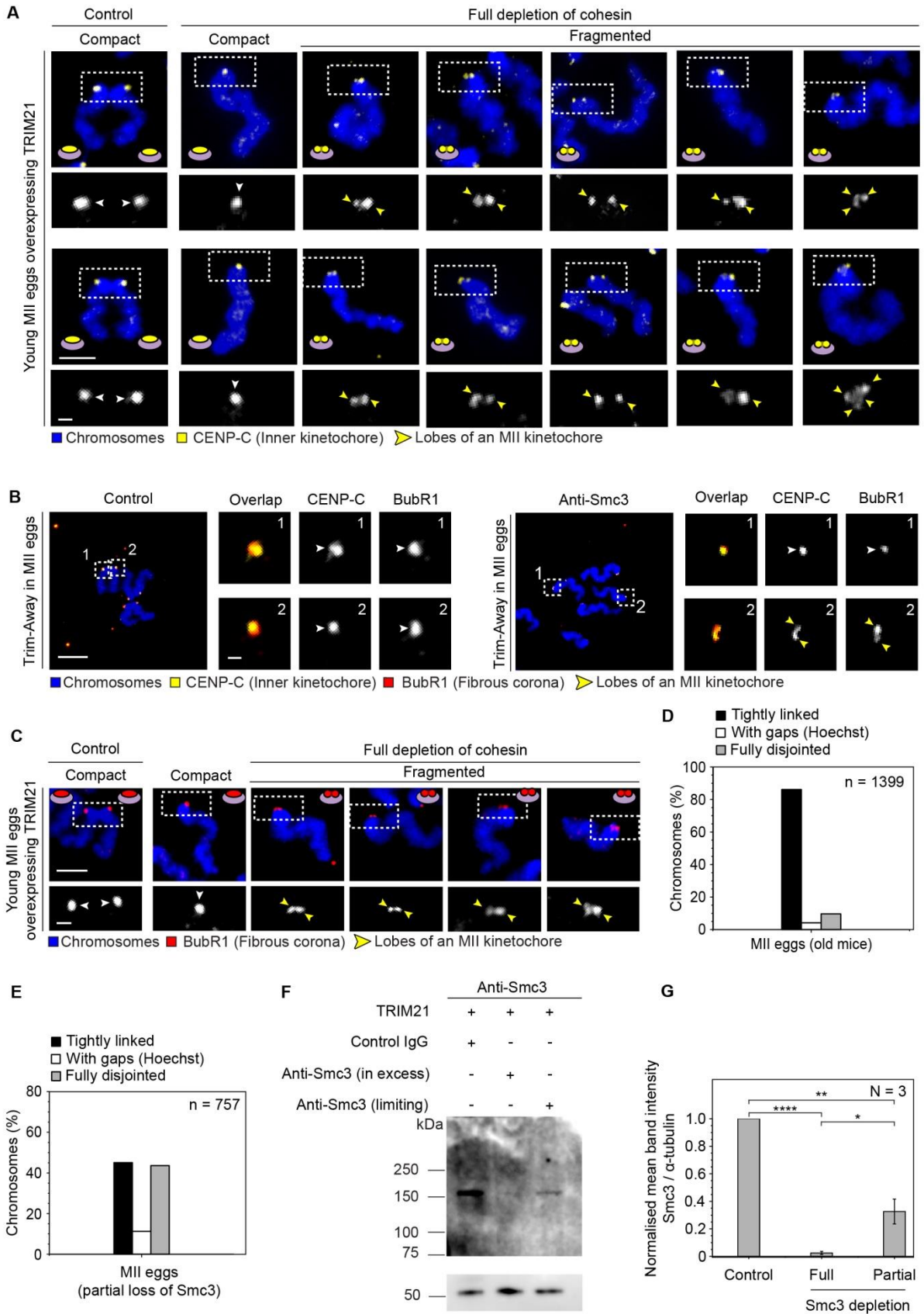


Figure S5| Fragmentation affects all key layers of the kinetochore complex and is linked to chromosome architecture, related to Figure 4

(A) MII kinetochores labelled with inner plate protein CENP-C in metaphase-II arrested eggs from young mice. Images show control chromosomes (left panels; two sister kinetochores) and single chromatids (other panels) induced by a full depletion of Rec8. Chromosomes are labelled in blue (Hoechst) and kinetochore inner plates in yellow (CENP-C). Scale bars: 2 μm in overviews and 0.5 μm in insets.

(B) MII kinetochores in young eggs treated as in **(A)** and co-labelled with anti-CENP-C (yellow) and anti-BubR-1 (red). Scale bars: 5 μm in overviews and 0.5 μm in insets.

(C) MII kinetochores in young eggs treated as in **(A)** and labelled with anti-BubR-1 (red). Scale bars: 2 μm in overviews and 0.5 μm in insets.

(D) Chromosome configurations as in **Figure 4C** and their occurrence in MII eggs from naturally aged mice. Kinetochores were labelled with CREST and the DNA was labelled with Hoechst. "With gaps" refers to no detectable Hoechst signal between sister chromatids that are still linked. *n* refers to the number of chromosomes analyzed. Data from 67 MII eggs.

(E) Chromosome configurations as in **Figure 4C** and their occurrence in MII eggs from young mice with reduced cohesin following partial Trim-Away. Kinetochores were labelled with CREST and the DNA was labelled with Hoechst. "With gaps" refers to no detectable Hoechst signal between sister chromatids that are still linked. Data from 41 MII eggs (4 experiments). *n* refers to the total number of chromosomes analyzed.

(F) Representative anti-Smc3 immunoblot of whole MII egg lysates following microinjection of either a control IgG or an anti-Smc3 antibody (provided in excess or at a rate-limiting concentration) to TRIM21 overexpressing MII eggs from young mice.

(G) Quantification of the relative Smc3 protein levels in **(F)** across 3 experimental repetitions following Smc3 depletion. *P* values are designated as **p* < 0.05, ***p* < 0.01, ****p* < 0.001 and *****p* < 0.0001 and were calculated with Student's t-test. Error bars show SEM.

White arrows point to compact kinetochores and yellow arrows point to lobes within a fragmented MII kinetochore. DNA is labelled in all panels with Hoechst (blue).

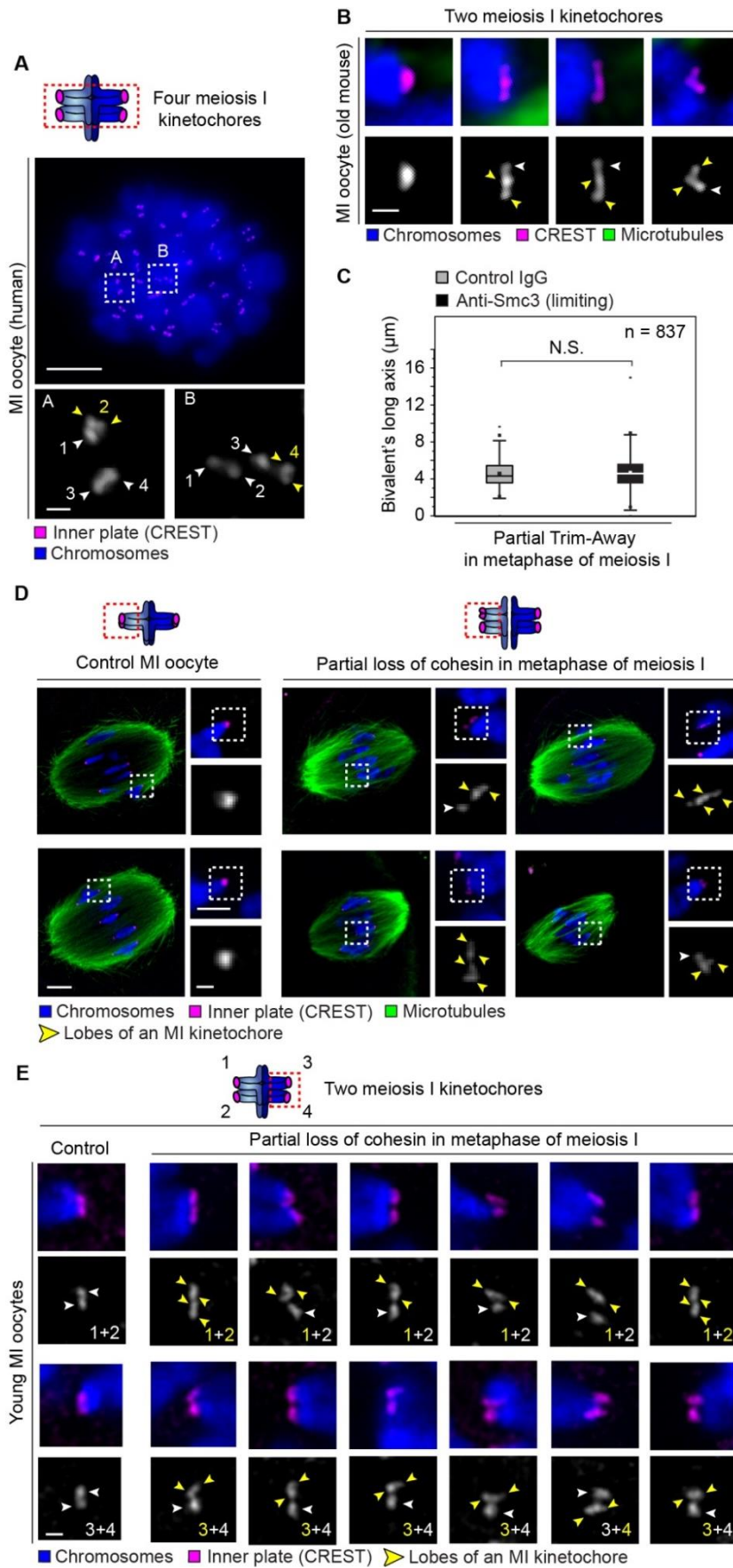


Figure S6| Cohesin loss results in sister kinetochore splitting and fragmentation of MI kinetochores into lobes, related to Figure 5

(A) Representative image of a human metaphase-I chromosome spread from a 25 year old donor. The four kinetochores of two representative bivalents are shown in insets. Scale bars: 10 μm in overview and 1 μm in insets.

(B) Representative images of inner plates of fragmented MI kinetochores in meiosis I oocytes from old mice. Scale bar: 0.5 μm .

(C) Distance between the two sister kinetochore pairs of a meiosis I bivalent in metaphase I (bivalent's long axis). Oocytes have been treated as in **Figure 5B**. Data from 42 MI oocytes from young mice (2 experiments). Box plots show median (horizontal lines), mean (small squares), 25th and 75th percentiles (boxes) and 5th and 95th percentiles (whiskers). *P* values are designated as **p* < 0.05, ***p* < 0.01, ****p* < 0.001 and *****p* < 0.0001. *P* value was calculated with one-way ANOVA followed by Turkey's test (N.S.).

(D) Representative images of Trim-Away meiotic spindles treated as in **Figure 5B**. Insets demonstrate chromosome and kinetochore architectures in MI bivalents under these conditions. Scale bars: 5 μm in overview, and 2 μm or 0.5 μm in insets.

(E) Representative immunofluorescence images of two sister kinetochores of a bivalent in control oocytes (left panels) or anti-Smc3 microinjected oocytes in Trim-Away experiments (other panels). Scale bar: 0.5 μm

(A, B, D, E) Chromosomes are labelled in blue (Hoechst) and kinetochores in magenta (CREST). In **(B and D)**, microtubules are additionally labelled in green (α -tubulin). White arrows point to compact kinetochores and yellow arrows point to lobes within a fragmented MI kinetochore. Numbers in insets refer to sister kinetochores shown (as in the schematic in **(E)**).

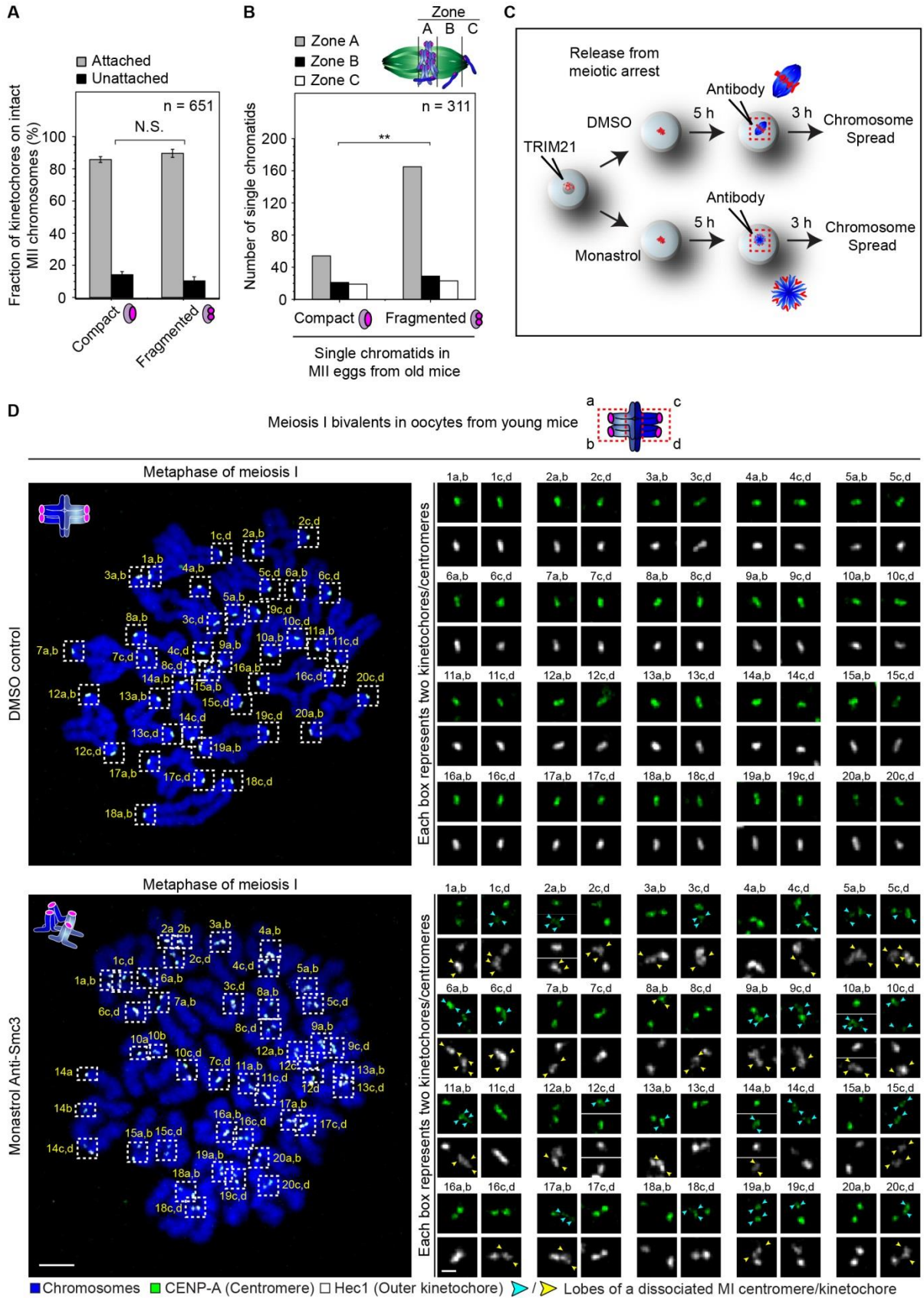


Figure S7| Microtubule pulling shapes kinetochore fragmentation, related to

Figure 6

(A) Occurrence of unattached kinetochores, in relationship to their fragmentation status in MII cold-treated eggs from aged mice.

(B) Distribution of single chromatids on the metaphase-II spindle of aged mice. Zone definitions as in the scheme. The location of 311 single chromatids relative to spindle poles was evaluated.

(C) Schematic diagram of Trim-Away experiments to degrade cohesins during meiosis I in control DMSO or monastrol-treated oocytes. Monastrol prevents spindle bipolarization.

(D) Representative examples of chromosome spreads showing all 20 bivalents from a control MI oocyte (top) and a monastrol treated oocyte with cohesion weakened by partial Trim-Away with anti-Smc3 (bottom). Each inset shows a sister kinetochore pair (a, b: one pair and c, d: the other kinetochore pair of the same bivalent). Outer kinetochores are labelled in white (Hec1), centromeres are labelled in green (CENP-A) and chromosomes are labelled in blue (Hoechst). Scale bars: 5 μm in overview and 1 μm in insets. Yellow/blue arrows point to lobes within fragmented MI kinetochores/centromeres, respectively.

(A and B) Data from 28 aged MII eggs (3 experiments).

P values are designated as **p* < 0.05, ***p* < 0.01, ****p* < 0.001 and *****p* < 0.0001. *P* values were calculated with Fisher's exact test. Error bars show SEM.

5. Discussion

5.1 New factors contributing to human oocyte aneuploidy

The work performed in this PhD thesis identifies a new factor that increases the aneuploidy probability for certain chromosomes in mammalian oocytes. I identified that the morphology of acrocentric bivalents in meiosis I correlates with an increased missegregation frequency of those chromosomes. More specifically, the group of acrocentric chromosomes is less likely to form end-on microtubule attachments in meiosis I and more likely to interact with microtubules in a lateral/merotelic way. The small achiasmatic arm of the acrocentric chromosomes appears to sterically hinder the formation of correct attachments. This is the first time that the bivalent morphology is linked to chromosome segregation errors in meiosis I.

In the second manuscript, my colleague Agata Zielinska demonstrated that aging affects the architecture of the centromeres and the kinetochores in mammalian eggs. Cohesin loss causes centromeres to decompact and kinetochores to fragment into multiple lobes. This allows kinetochores to interact simultaneously with more than one microtubules, with interactions often arising from opposite spindle poles. This increase in merotelic kinetochore-microtubule attachments is one of the factors that accounts for higher aneuploidy rates upon aging.

5.2 Porcine oocytes are a suitable model for studying human meiosis

Research in human oocytes is limited by sample availability. As a consequence, it is important to find alternative models for human oocyte meiosis. Previously, the mouse has been extensively used as a model to study meiosis. However, mouse has a karyotype with only telocentric chromosomes, in which the kinetochores are located at the very end of the chromosomes. This makes it different from the human karyotype which has both, acrocentric and metacentric chromosomes. Together the above data shows that mouse chromosome and kinetochore morphology differ from human and are

suboptimal for comparing different chromosome classes in one system. Further differences in the spindle assembly between mouse and human indicate that an alternative model might be more suitable for understanding the meiotic process in human (Holubcova et al., 2015; Schuh & Ellenberg, 2007; So et al., 2022).

In addition to a recent study that showed how the morphology of the porcine meiotic spindle is more similar to that in humans (So et al., 2022), my work shows that porcine oocytes better mimic the chromosome and kinetochore morphology of human oocytes. Furthermore, porcine oocytes are available in large numbers from local slaughterhouses and at low cost.

One more reason that made porcine oocytes the ideal model for this study is the conserved pericentromeric region for each chromosome group (Rogel-Gaillard et al., 1997). This was key for labeling each chromosome class and allowed us to study different groups without the need of labelling individual chromosomes.

5.3 Bivalent morphology is associated with missegregation

Studies performed in other model systems help us to better understand meiosis and its error-prone nature. However, still little is known about the mechanisms that play a role in human oocytes. Spindle instability (Holubcova et al., 2015) and kinetochore splitting (Zielinska et al., 2015) are two factors that have been shown to contribute to the error-prone nature of human oocytes even in younger women. Other factors that have been confirmed to play a role in oocytes of other mammalian species, like the less efficient SAC activity, should also be verified in the future and it needs to be investigated if at all or to what extent they play a role in human oocytes.

Bivalent morphology is a new factor that explains why some chromosomes are more vulnerable to missegregation than others. Aneuploidy in human oocytes ranges from 25% to 50% in a U-shaped curve (Gruhn et al., 2019). A baseline aneuploidy of 25% is present in all women independently of their

age and an increment of aneuploidy is shown in very young and also in older women (Gruhn et al., 2019). The error-prone bivalent morphology of acrocentric chromosomes is a potential risk factor for all women independent of their age.

One of the most common viable trisomies is trisomy 21, which causes Down syndrome (Nagaoka et al., 2012). Chromosome 21 is a small acrocentric chromosome. This is an example that depicts the importance of understanding why and how the acrocentric chromosomes missegregate so often. Understanding the reason for missegregation may give us insights that might allow us to potentially reduce aneuploidy in the future.

For deeper understanding of chromosome-specific aneuploidy in humans, the next step will be to combine live-cell imaging of human meiosis with cytogenetic studies. For that, it is important to use oocytes of women of different ages, image them live, and subsequently perform a biopsy of the two polar bodies and the corresponding activated oocyte. This will help us to delve deeper inside the chromosome groups and look into missegregation of individual chromosomes. The cytogenetic studies will help to identify the identity and the parental origin of the missegregated chromosomes, while the live imaging can indicate the mechanism that caused chromosomes to missegregate.

5.4 Chromosome labelling with TALEs

TALEs are a very robust system for labelling chromosomes (Miyazari et al., 2013). However, finding the correct target-sequence for the TALEs has been reported to be difficult. Existing literature and online tools provide recommendations for efficient design of the target (Cermak et al., 2011). However, they do not always make correct predictions and it is often unclear why TALEs bind one target but not the other.

In this study, acrocentric chromosomes in humans were identified by the presence of the telomere in the proximity of the kinetochore. An alternative way to identify the acrocentric chromosomes would

be to use TALEs and label the group of acrocentric or metacentric chromosomes as done in porcine oocytes. In the scope of this study, endeavours to create a TALE labelling for human chromosome groups have been performed. Previously published TALE plasmid (Ren et al., 2017) and also new targets that were identified bioinformatically were tested but unfortunately did not achieve successful labelling.

5.5 Two different configurations of the small arm of acrocentric chromosomes

In this thesis, I identified for the first time that the small arm of acrocentric chromosomes can have two different configurations: on top or at the side of kinetochores. The small arm of acrocentric bivalents in human and porcine oocytes is very small and condensed, making it challenging to be visualized by DNA labelling. Thus, I used telomeres as a proxy to indicate the relative position of the small arm respective to the kinetochores.

From the experiments, I found that kinetochores with telomeres on top fail to form end-on attachments, while kinetochores with the configuration at the side do not. Also, I observed a decrease in the percentage of the configuration on top in spindles from early to late metaphase I. However, it is not clear how the mechanism functions. There are two different possibilities: 1) the microtubules first establish an end-on attachment and this causes the small arm to change from the configuration on-top to the configuration at the side or 2) the small arm randomly switches from one to the other configuration, and once it is at the side, allows the microtubules to establish end-on attachments. Live-cell imaging with high spatio-temporal resolution will be required to distinguish these two scenarios in the future.

The length of the small arm can potentially determine the level of interference of the end-on attachment creation. The size of the small arm in human cell is known (Nurk et al., 2021). However, sequencing of the porcine genome is limited so far. Thus, we do not exactly know the length of the

small arm in porcine cells. Once the full genome is sequenced in other species, it will be interesting to investigate how the length of the small arm is correlated with the level of interference in different species.

5.6 Kinetochores of acrocentric chromosomes

Acrocentric kinetochores are often aligned in the spindle parallel to the spindle axis. Together with the fact that the kinetochores of acrocentric chromosomes struggle to create end-on attachments, this suggests that the parallel angle might not favour end-on attachment creation. It would be interesting to distinguish how the angle is changing during meiotic progression and end-on attachment creation. More specifically, it would be interesting to know if the attachment creation turns the kinetochore in a vertical position or the kinetochore changes the angle before the establishment of a correct attachment. Combination of live-cell imaging with highspatio-temporal resolution would allow us to delve deeper into this question in the future.

In this study, the kinetochores were labelled with human CREST serum, which is a mix of antibodies against proteins of the inner kinetochore layer (Ford et al., 1998). Observation of the small arm together with outer kinetochore layers might give us more insight into its relative position. The ideal candidate for labelling the outer kinetochore layer would be the Ndc80 complex, which is the key player in the end-on attachment creation (Ciferri et al., 2008). However, after extensive tests of different antibodies I was not able to identify one that gave a good signal for porcine kinetochores.

5.7 Spermatocytes and aneuploidy

Key contributors that have been identified to play a role in the error-prone mouse female meiosis are the protracted dictyate arrest (Burkhardt et al., 2016; Tachibana-Konwalski et al., 2010) and the large volume of the oocyte cytoplasm that affects the efficient communication of the SAC pathway (Kyogoku

& Kitajima, 2017; Lane & Jones, 2017). However, these factors are not expected to play a role in male meiosis. Spermatocytes are produced throughout the male life span. Male meiosis is completed within 50-70 days and produces 4 equal gametes with a very small cytoplasm (Neto et al., 2016). As expected spermatocytes have in total a lower aneuploidy rate (Hassold & Hunt, 2001) and are not affected by age-related aneuploidy in the same way as oocytes. However, also in spermatocyte meiosis, homologous chromosomes pair with each other and create bivalents with the same morphology as in oocytes. Thus, bivalent geometry is expected to play a similar role as in female meiosis. Studies have shown that despite the lower aneuploidy rates in spermatocytes compared to oocytes, acrocentric chromosomes are still the ones that missegregate the most (Bell et al., 2020; Soares et al., 2001). This indicates that acrocentric chromosomes are missegregating even in the absence of other known aneuploidy factors. Thus, these data further support our hypothesis that the bivalent morphology affects the interactions with the microtubules and that it contributes to missegregation in an age-independent manner.

5.8 Differences between meiosis and mitosis in missegregation

In mitosis, sister chromatids are segregated to the daughter cells, and the sister kinetochores orient towards different spindle poles. The chromosome arms are all vertically oriented to the spindle axis and the kinetochores are also vertically exposed to face the spindle poles. Thus, it is easy to envision that chromosome arms do not block the kinetochore surface. Thus, differences in the size of arms should not have an impact on chromosome segregation.

Studies on chromosome-specific aneuploidy in mitotic cells suggest that larger chromosomes are mainly affected by aneuploidy (Dumont et al., 2020; Tovini & McClelland, 2019; Worrall et al., 2018) and acrocentric chromosomes do not missegregate in the same way as shown here for meiosis. Thus, factors other than chromosome morphology seem to have a more important role in mitosis.

5.9 Other factors that have been suggested to affect chromosome aneuploidy

As discussed above chromosome morphology does not seem to play a role in chromosome missegregation in mitosis. However other factors have been reported to prime specific chromosomes to aneuploidy in mitosis. Kinetochore size has been suggested to play a role in the types of attachments created in *Indian muntjac*. More specifically, large kinetochores are more prone to create merotelic attachments (Drpic et al., 2018). In human chromosomes, kinetochore sizes differ by 2-fold (Drpic et al., 2018). It can be envisioned that kinetochore size plays a role in attachment creation in both human meiotic and mitotic cells. We do not exclude the possibility that this plays a role and affects individual chromosome segregation in meiosis. It can potentially contribute in a lower degree compared to other factors because I did not measure any differences in the kinetochore size of acrocentric chromosomes in the porcine system.

A further factor that has been proposed to affect the segregation outcome in meiosis is the position of chiasmata (Nagaoka et al., 2012). Chiasmata formed close to the telomere or the centromere are more prone to affect cohesion, which holds the chromosomes together and create errors either in meiosis I or in meiosis II (Lamb et al., 1996). Thus, suboptimal positioning of chiasmata on the chromosome arms can increase the likelihood of specific chromosomes to missegregate. A study has shown that aneuploid cells in general tend to have lower recombination rates and reports that recombination rates differ among people and among individual chromosomes (Ottolini et al., 2015). Smaller chromosomes, including the small acrocentric chromosome 21 and 22 have a maximum of one crossover (Ottolini et al., 2015). Thus, the position and the amount of crossovers is another factor that affects chromosome specific anuploidy.

5.10 Aging and aneuploidy

Cohesin loss is among the main causes of age-related aneuploidy in oocytes (Chiang et al., 2010; Lister et al., 2010; Tsutsumi et al., 2014). Studies in human oocytes show that acrocentric chromosomes missegregate at higher frequencies upon aging (Gruhn et al., 2019). In this study, I examined the levels of cohesin in each chromosome group in porcine oocytes and found that in general acrocentric chromosomes have less cohesin than metacentric chromosomes. Thus, it is tempting to speculate that age-related cohesin loss has a larger impact on chromosomes that initially possess a lower amount of cohesin.

When I trimmed-away REC8 in porcine oocytes, I noticed that acrocentric chromosomes always separate first. However, not all acrocentric chromosomes separate before the metacentric ones. This indicates that even though on average acrocentric chromosomes have less cohesin than metacentric chromosomes, there are also differences in the cohesin level among individual chromosomes of the same group in porcine oocytes.

Human acrocentric chromosomes have been shown to be particularly prone to age-related aneuploidy (Gruhn et al., 2019). Thus, it is tempting to envision that human acrocentric chromosomes might on average have less cohesin than metacentric chromosomes. However, whether this is true still remains unclear. In the scope of this study, endeavours to label the cohesin with different antibodies in intact human metaphase I oocytes have been performed. However, the antibody specificity did not allow us to perform any measurements. Developing an antibody that will allow us to measure cohesion on individual chromosomes or in chromosome spreads, will be useful for examining cohesin levels on individual chromosomes in human oocytes in the future.

5.11 Conclusion

Accurate chromosome segregation is crucial for the creation of a healthy embryo. In this PhD thesis, I identified a new factor that influences aneuploidy levels of certain chromosomes during female meiosis. I demonstrate that acrocentric chromosomes fail to establish end-on attachments and are more prone to interact with spindle microtubules in an erroneous way. This leads to lagging chromosomes and missegregations during anaphase. I identified for the first time that the small arm of acrocentric chromosomes has two different configurations, and that the configuration “on top” is correlated with the establishment of incorrect attachments to spindle microtubules. These data provide an explanation for the high missegregation frequency of acrocentric chromosomes in meiosis as observed in biopsies of human polar bodies, and sheds light on why this chromosome group is so likely to be affected by aneuploidy during both female and male meiosis.

6. References

- Bajar, B. T., Wang, E. S., Lam, A. J., Kim, B. B., Jacobs, C. L., Howe, E. S., Davidson, M. W., Lin, M. Z., & Chu, J. (2016). Improving brightness and photostability of green and red fluorescent proteins for live cell imaging and FRET reporting. *Sci Rep*, *6*, 20889. <https://doi.org/10.1038/srep20889>
- Bell, A. D., Mello, C. J., Nemes, J., Brumbaugh, S. A., Wysoker, A., & McCarroll, S. A. (2020). Insights into variation in meiosis from 31,228 human sperm genomes. *Nature*, *583*(7815), 259-264. <https://doi.org/10.1038/s41586-020-2347-0>
- Bindels, D. S., Haarbosch, L., van Weeren, L., Postma, M., Wiese, K. E., Mastop, M., Aumonier, S., Gotthard, G., Royant, A., Hink, M. A., & Gadella, T. W., Jr. (2017). mScarlet: a bright monomeric red fluorescent protein for cellular imaging. *Nat Methods*, *14*(1), 53-56. <https://doi.org/10.1038/nmeth.4074>
- Bochtler, T., Kartal-Kaess, M., Granzow, M., Hielscher, T., Cosenza, M. R., Herold-Mende, C., Jauch, A., & Kramer, A. (2019). Micronucleus formation in human cancer cells is biased by chromosome size. *Genes Chromosomes Cancer*, *58*(6), 392-395. <https://doi.org/10.1002/gcc.22707>
- Bucevicius, J., Kostiuk, G., Gerasimaite, R., Gilat, T., & Lukinavicius, G. (2020). Enhancing the biocompatibility of rhodamine fluorescent probes by a neighbouring group effect. *Chem Sci*, *11*(28), 7313-7323. <https://doi.org/10.1039/d0sc02154g>
- Bullejos, M., & Koopman, P. (2004). Germ cells enter meiosis in a rostro-caudal wave during development of the mouse ovary. *Mol Reprod Dev*, *68*(4), 422-428. <https://doi.org/10.1002/mrd.20105>
- Burkhardt, S., Borsos, M., Szydlowska, A., Godwin, J., Williams, S. A., Cohen, P. E., Hirota, T., Saitou, M., & Tachibana-Konwalski, K. (2016). Chromosome Cohesion Established by Rec8-Cohesin in Fetal Oocytes Is Maintained without Detectable Turnover in Oocytes Arrested for Months in Mice. *Curr Biol*, *26*(5), 678-685. <https://doi.org/10.1016/j.cub.2015.12.073>
- Cavazza, T., Takeda, Y., Politi, A. Z., Aushev, M., Aldag, P., Baker, C., Choudhary, M., Bucevicius, J., Lukinavicius, G., Elder, K., Blayney, M., Lucas-Hahn, A., Niemann, H., Herbert, M., & Schuh, M. (2021). Parental genome unification is highly error-prone in mammalian embryos. *Cell*, *184*(11), 2860-2877 e2822. <https://doi.org/10.1016/j.cell.2021.04.013>
- Cermak, T., Doyle, E. L., Christian, M., Wang, L., Zhang, Y., Schmidt, C., Baller, J. A., Somia, N. V., Bogdanove, A. J., & Voytas, D. F. (2011). Efficient design and assembly of custom TALEN and other TAL effector-based constructs for DNA targeting. *Nucleic Acids Res*, *39*(12), e82. <https://doi.org/10.1093/nar/gkr218>

- Cermak, T., Starker, C. G., & Voytas, D. F. (2015). Efficient design and assembly of custom TALENs using the Golden Gate platform. *Methods Mol Biol*, *1239*, 133-159. https://doi.org/10.1007/978-1-4939-1862-1_7
- Cheeseman, I. M. (2014). The kinetochore. *Cold Spring Harb Perspect Biol*, *6*(7), a015826. <https://doi.org/10.1101/cshperspect.a015826>
- Cheeseman, I. M., & Desai, A. (2008). Molecular architecture of the kinetochore-microtubule interface. *Nat Rev Mol Cell Biol*, *9*(1), 33-46. <https://doi.org/10.1038/nrm2310>
- Chiang, T., Duncan, F. E., Schindler, K., Schultz, R. M., & Lampson, M. A. (2010). Evidence that weakened centromere cohesion is a leading cause of age-related aneuploidy in oocytes. *Curr Biol*, *20*(17), 1522-1528. <https://doi.org/10.1016/j.cub.2010.06.069>
- Ciferri, C., Pasqualato, S., Screpanti, E., Varetti, G., Santaguida, S., Dos Reis, G., Maiolica, A., Polka, J., De Luca, J. G., De Wulf, P., Salek, M., Rappsilber, J., Moores, C. A., Salmon, E. D., & Musacchio, A. (2008). Implications for kinetochore-microtubule attachment from the structure of an engineered Ndc80 complex. *Cell*, *133*(3), 427-439. <https://doi.org/10.1016/j.cell.2008.03.020>
- Cimini, D., Cameron, L. A., & Salmon, E. D. (2004). Anaphase spindle mechanics prevent mis-segregation of merotelically oriented chromosomes. *Curr Biol*, *14*(23), 2149-2155. <https://doi.org/10.1016/j.cub.2004.11.029>
- Clift, D., McEwan, W. A., Labzin, L. I., Konieczny, V., Mogessie, B., James, L. C., & Schuh, M. (2017). A Method for the Acute and Rapid Degradation of Endogenous Proteins. *Cell*, *171*(7), 1692-1706 e1618. <https://doi.org/10.1016/j.cell.2017.10.033>
- Clift, D., & Schuh, M. (2013). Restarting life: fertilization and the transition from meiosis to mitosis. *Nat Rev Mol Cell Biol*, *14*(9), 549-562. <https://doi.org/10.1038/nrm3643>
- Craske, B., & Welburn, J. P. I. (2020). Leaving no-one behind: how CENP-E facilitates chromosome alignment. *Essays Biochem*, *64*(2), 313-324. <https://doi.org/10.1042/EBC20190073>
- Drpic, D., Almeida, A. C., Aguiar, P., Renda, F., Damas, J., Lewin, H. A., Larkin, D. M., Khodjakov, A., & Maiato, H. (2018). Chromosome Segregation Is Biased by Kinetochore Size. *Curr Biol*, *28*(9), 1344-1356 e1345. <https://doi.org/10.1016/j.cub.2018.03.023>
- Duijff, P. H., Schultz, N., & Benezra, R. (2013). Cancer cells preferentially lose small chromosomes. *Int J Cancer*, *132*(10), 2316-2326. <https://doi.org/10.1002/ijc.27924>
- Dumont, M., Gamba, R., Gestraud, P., Klaasen, S., Worrall, J. T., De Vries, S. G., Boudreau, V., Salinas-Luypaert, C., Maddox, P. S., Lens, S. M., Kops, G. J., McClelland, S. E., Miga, K. H., & Fachinetti, D. (2020). Human chromosome-specific aneuploidy is influenced by DNA-dependent centromeric features. *EMBO J*, *39*(2), e102924. <https://doi.org/10.15252/emj.2019102924>

- Eijpe, M., Offenberg, H., Jessberger, R., Revenkova, E., & Heyting, C. (2003). Meiotic cohesin REC8 marks the axial elements of rat synaptonemal complexes before cohesins SMC1beta and SMC3. *J Cell Biol*, *160*(5), 657-670. <https://doi.org/10.1083/jcb.200212080>
- Fauth, E., Scherthan, H., & Zankl, H. (1998). Frequencies of occurrence of all human chromosomes in micronuclei from normal and 5-azacytidine-treated lymphocytes as revealed by chromosome painting. *Mutagenesis*, *13*(3), 235-241. <https://doi.org/10.1093/mutage/13.3.235>
- Ford, A. L., Kurien, B. T., Harley, J. B., & Scofield, R. H. (1998). Anti-centromere autoantibody in a patient evolving from a lupus/Sjogren's overlap to the CREST variant of scleroderma. *J Rheumatol*, *25*(7), 1419-1424. <https://www.ncbi.nlm.nih.gov/pubmed/9676778>
- Fragouli, E., Alfarawati, S., Goodall, N. N., Sanchez-Garcia, J. F., Colls, P., & Wells, D. (2011). The cytogenetics of polar bodies: insights into female meiosis and the diagnosis of aneuploidy. *Mol Hum Reprod*, *17*(5), 286-295. <https://doi.org/10.1093/molehr/gar024>
- Fragouli, E., Katz-Jaffe, M., Alfarawati, S., Stevens, J., Colls, P., Goodall, N. N., Tormasi, S., Gutierrez-Mateo, C., Prates, R., Schoolcraft, W. B., Munne, S., & Wells, D. (2010). Comprehensive chromosome screening of polar bodies and blastocysts from couples experiencing repeated implantation failure. *Fertil Steril*, *94*(3), 875-887. <https://doi.org/10.1016/j.fertnstert.2009.04.053>
- Franasiak, J. M., Forman, E. J., Hong, K. H., Werner, M. D., Upham, K. M., Treff, N. R., & Scott, R. T. (2014). Aneuploidy across individual chromosomes at the embryonic level in trophectoderm biopsies: changes with patient age and chromosome structure. *J Assist Reprod Genet*, *31*(11), 1501-1509. <https://doi.org/10.1007/s10815-014-0333-x>
- Gabriel, A. S., Thornhill, A. R., Ottolini, C. S., Gordon, A., Brown, A. P., Taylor, J., Bennett, K., Handyside, A., & Griffin, D. K. (2011). Array comparative genomic hybridisation on first polar bodies suggests that non-disjunction is not the predominant mechanism leading to aneuploidy in humans. *J Med Genet*, *48*(7), 433-437. <https://doi.org/10.1136/jmg.2010.088070>
- Gershon, E., & Dekel, N. (2020). Newly Identified Regulators of Ovarian Folliculogenesis and Ovulation. *Int J Mol Sci*, *21*(12). <https://doi.org/10.3390/ijms21124565>
- Gomez, R., Valdeolillos, A., Parra, M. T., Viera, A., Carreiro, C., Roncal, F., Rufas, J. S., Barbero, J. L., & Suja, J. A. (2007). Mammalian SGO2 appears at the inner centromere domain and redistributes depending on tension across centromeres during meiosis II and mitosis. *EMBO Rep*, *8*(2), 173-180. <https://doi.org/10.1038/sj.embor.7400877>
- Gruhn, J. R., Zielinska, A. P., Shukla, V., Blanshard, R., Capalbo, A., Cimadomo, D., Nikiforov, D., Chan, A. C., Newnham, L. J., Vogel, I., Scarica, C., Krapchev, M., Taylor, D., Kristensen, S. G., Cheng, J., Ernst, E., Bjorn, A. B., Colmorn, L. B., Blayney, M., . . . Hoffmann, E. R. (2019). Chromosome

- errors in human eggs shape natural fertility over reproductive life span. *Science*, 365(6460), 1466-1469. <https://doi.org/10.1126/science.aav7321>
- Handyside, A. H., Montag, M., Magli, M. C., Repping, S., Harper, J., Schmutzler, A., Vesela, K., Gianaroli, L., & Geraedts, J. (2012). Multiple meiotic errors caused by predivision of chromatids in women of advanced maternal age undergoing in vitro fertilisation. *Eur J Hum Genet*, 20(7), 742-747. <https://doi.org/10.1038/ejhg.2011.272>
- Hansen, K. (1977). Identification of the chromosomes of the domestic pig (*Sus scrofa domestica*). An identification key and a landmark system. *Ann Genet Sel Anim*, 9(4), 517-526. <https://doi.org/10.1186/1297-9686-9-4-517>
- Hassold, T., Abruzzo, M., Adkins, K., Griffin, D., Merrill, M., Millie, E., Saker, D., Shen, J., & Zaragoza, M. (1996). Human aneuploidy: incidence, origin, and etiology. *Environ Mol Mutagen*, 28(3), 167-175. [https://doi.org/10.1002/\(SICI\)1098-2280\(1996\)28:3<167::AID-EM2>3.0.CO;2-B](https://doi.org/10.1002/(SICI)1098-2280(1996)28:3<167::AID-EM2>3.0.CO;2-B)
- Hassold, T., & Hunt, P. (2001). To err (meiotically) is human: the genesis of human aneuploidy. *Nat Rev Genet*, 2(4), 280-291. <https://doi.org/10.1038/35066065>
- Herbert, M., Kalleas, D., Cooney, D., Lamb, M., & Lister, L. (2015). Meiosis and maternal aging: insights from aneuploid oocytes and trisomy births. *Cold Spring Harb Perspect Biol*, 7(4), a017970. <https://doi.org/10.1101/cshperspect.a017970>
- Hodges, C. A., Revenkova, E., Jessberger, R., Hassold, T. J., & Hunt, P. A. (2005). SMC1beta-deficient female mice provide evidence that cohesins are a missing link in age-related nondisjunction. *Nat Genet*, 37(12), 1351-1355. <https://doi.org/10.1038/ng1672>
- Holubcova, Z., Blayney, M., Elder, K., & Schuh, M. (2015). Human oocytes. Error-prone chromosome-mediated spindle assembly favors chromosome segregation defects in human oocytes. *Science*, 348(6239), 1143-1147. <https://doi.org/10.1126/science.aaa9529>
- Ishiguro, K. I. (2019). The cohesin complex in mammalian meiosis. *Genes Cells*, 24(1), 6-30. <https://doi.org/10.1111/gtc.12652>
- Itoh, G., Ikeda, M., Iemura, K., Amin, M. A., Kuriyama, S., Tanaka, M., Mizuno, N., Osakada, H., Haraguchi, T., & Tanaka, K. (2018). Author Correction: Lateral attachment of kinetochores to microtubules is enriched in prometaphase rosette and facilitates chromosome alignment and bi-orientation establishment. *Sci Rep*, 8(1), 7003. <https://doi.org/10.1038/s41598-018-25175-4>
- Jaffe, L. A., & Terasaki, M. (2004). Quantitative microinjection of oocytes, eggs, and embryos. *Methods Cell Biol*, 74, 219-242. [https://doi.org/10.1016/s0091-679x\(04\)74010-8](https://doi.org/10.1016/s0091-679x(04)74010-8)
- Jaqaman, K., Loerke, D., Mettlen, M., Kuwata, H., Grinstein, S., Schmid, S. L., & Danuser, G. (2008). Robust single-particle tracking in live-cell time-lapse sequences. *Nat Methods*, 5(8), 695-702. <https://doi.org/10.1038/nmeth.1237>

- Kapoor, T. M., Lampson, M. A., Hergert, P., Cameron, L., Cimini, D., Salmon, E. D., McEwen, B. F., & Khodjakov, A. (2006). Chromosomes can congress to the metaphase plate before biorientation. *Science*, *311*(5759), 388-391. <https://doi.org/10.1126/science.1122142>
- Kitajima, T. S., Kawashima, S. A., & Watanabe, Y. (2004). The conserved kinetochore protein shugoshin protects centromeric cohesion during meiosis. *Nature*, *427*(6974), 510-517. <https://doi.org/10.1038/nature02312>
- Kitajima, T. S., Ohsugi, M., & Ellenberg, J. (2011). Complete kinetochore tracking reveals error-prone homologous chromosome biorientation in mammalian oocytes. *Cell*, *146*(4), 568-581. <https://doi.org/10.1016/j.cell.2011.07.031>
- Kouznetsova, A., Lister, L., Nordenskjold, M., Herbert, M., & Hoog, C. (2007). Bi-orientation of achiasmatic chromosomes in meiosis I oocytes contributes to aneuploidy in mice. *Nat Genet*, *39*(8), 966-968. <https://doi.org/10.1038/ng2065>
- Kudo, N. R., Wassmann, K., Anger, M., Schuh, M., Wirth, K. G., Xu, H., Helmhart, W., Kudo, H., McKay, M., Maro, B., Ellenberg, J., de Boer, P., & Nasmyth, K. (2006). Resolution of chiasmata in oocytes requires separase-mediated proteolysis. *Cell*, *126*(1), 135-146. <https://doi.org/10.1016/j.cell.2006.05.033>
- Kyogoku, H., & Kitajima, T. S. (2017). Large Cytoplasm Is Linked to the Error-Prone Nature of Oocytes. *Dev Cell*, *41*(3), 287-298 e284. <https://doi.org/10.1016/j.devcel.2017.04.009>
- Lamb, N. E., Freeman, S. B., Savage-Austin, A., Pettay, D., Taft, L., Hersey, J., Gu, Y., Shen, J., Saker, D., May, K. M., Avramopoulos, D., Petersen, M. B., Hallberg, A., Mikkelsen, M., Hassold, T. J., & Sherman, S. L. (1996). Susceptible chiasmate configurations of chromosome 21 predispose to non-disjunction in both maternal meiosis I and meiosis II. *Nat Genet*, *14*(4), 400-405. <https://doi.org/10.1038/ng1296-400>
- Lampson, M. A., & Cheeseman, I. M. (2011). Sensing centromere tension: Aurora B and the regulation of kinetochore function. *Trends Cell Biol*, *21*(3), 133-140. <https://doi.org/10.1016/j.tcb.2010.10.007>
- Lane, S. I. R., & Jones, K. T. (2017). Chromosome biorientation and APC activity remain uncoupled in oocytes with reduced volume. *J Cell Biol*, *216*(12), 3949-3957. <https://doi.org/10.1083/jcb.201606134>
- Legland, D., Arganda-Carreras, I., & Andrey, P. (2016). MorphoLibJ: integrated library and plugins for mathematical morphology with ImageJ. *Bioinformatics*, *32*(22), 3532-3534. <https://doi.org/10.1093/bioinformatics/btw413>
- Lister, L. M., Kouznetsova, A., Hyslop, L. A., Kalleas, D., Pace, S. L., Barel, J. C., Nathan, A., Floros, V., Adelfalk, C., Watanabe, Y., Jessberger, R., Kirkwood, T. B., Hoog, C., & Herbert, M. (2010).

- Age-related meiotic segregation errors in mammalian oocytes are preceded by depletion of cohesin and Sgo2. *Curr Biol*, 20(17), 1511-1521. <https://doi.org/10.1016/j.cub.2010.08.023>
- Liu, S. T., Rattner, J. B., Jablonski, S. A., & Yen, T. J. (2006). Mapping the assembly pathways that specify formation of the trilaminar kinetochore plates in human cells. *J Cell Biol*, 175(1), 41-53. <https://doi.org/10.1083/jcb.200606020>
- Llano, E., Gomez, R., Gutierrez-Caballero, C., Herran, Y., Sanchez-Martin, M., Vazquez-Quinones, L., Hernandez, T., de Alava, E., Cuadrado, A., Barbero, J. L., Suja, J. A., & Pendas, A. M. (2008). Shugoshin-2 is essential for the completion of meiosis but not for mitotic cell division in mice. *Genes Dev*, 22(17), 2400-2413. <https://doi.org/10.1101/gad.475308>
- MacLennan, M., Crichton, J. H., Playfoot, C. J., & Adams, I. R. (2015). Oocyte development, meiosis and aneuploidy. *Semin Cell Dev Biol*, 45, 68-76. <https://doi.org/10.1016/j.semcd.2015.10.005>
- Magli, M. C., Grugnetti, C., Castelletti, E., Paviglianiti, B., Ferraretti, A. P., Geraedts, J., & Gianaroli, L. (2012). Five chromosome segregation in polar bodies and the corresponding oocyte. *Reprod Biomed Online*, 24(3), 331-338. <https://doi.org/10.1016/j.rbmo.2011.11.019>
- Maiato, H., DeLuca, J., Salmon, E. D., & Earnshaw, W. C. (2004). The dynamic kinetochore-microtubule interface. *J Cell Sci*, 117(Pt 23), 5461-5477. <https://doi.org/10.1242/jcs.01536>
- McCoy, R. C., Demko, Z. P., Ryan, A., Banjevic, M., Hill, M., Sigurjonsson, S., Rabinowitz, M., & Petrov, D. A. (2015). Evidence of Selection against Complex Mitotic-Origin Aneuploidy during Preimplantation Development. *PLoS Genet*, 11(10), e1005601. <https://doi.org/10.1371/journal.pgen.1005601>
- Mihajlovic, A. I., Haverfield, J., & FitzHarris, G. (2021). Distinct classes of lagging chromosome underpin age-related oocyte aneuploidy in mouse. *Dev Cell*, 56(16), 2273-2283 e2273. <https://doi.org/10.1016/j.devcel.2021.07.022>
- Miyanari, Y., Ziegler-Birling, C., & Torres-Padilla, M. E. (2013). Live visualization of chromatin dynamics with fluorescent TALEs. *Nat Struct Mol Biol*, 20(11), 1321-1324. <https://doi.org/10.1038/nsmb.2680>
- Musacchio, A., & Salmon, E. D. (2007). The spindle-assembly checkpoint in space and time. *Nat Rev Mol Cell Biol*, 8(5), 379-393. <https://doi.org/10.1038/nrm2163>
- Nagaoka, S. I., Hassold, T. J., & Hunt, P. A. (2012). Human aneuploidy: mechanisms and new insights into an age-old problem. *Nat Rev Genet*, 13(7), 493-504. <https://doi.org/10.1038/nrg3245>
- Nagpal, H., & Fukagawa, T. (2016). Kinetochore assembly and function through the cell cycle. *Chromosoma*, 125(4), 645-659. <https://doi.org/10.1007/s00412-016-0608-3>
- Nakhuda, G., Jing, C., Butler, R., Guimond, C., Hitkari, J., Taylor, E., Tallon, N., & Yuzpe, A. (2018). Frequencies of chromosome-specific mosaicisms in trophoectoderm biopsies detected by

- next-generation sequencing. *Fertil Steril*, 109(5), 857-865.
<https://doi.org/10.1016/j.fertnstert.2018.01.011>
- Neto, F. T., Bach, P. V., Najari, B. B., Li, P. S., & Goldstein, M. (2016). Spermatogenesis in humans and its affecting factors. *Semin Cell Dev Biol*, 59, 10-26.
<https://doi.org/10.1016/j.semcdb.2016.04.009>
- Nurk, S., Koren, S., Rhie, A., Rautiainen, M., Bzikadze, A. V., Mikheenko, A., Vollger, M. R., Altemose, N., Uralsky, L., Gershman, A., Aganezov, S., Hoyt, S. J., Diekhans, M., Logsdon, G. A., Alonge, M., Antonarakis, S. E., Borchers, M., Bouffard, G. G., Brooks, S. Y., . . . Phillippy, A. M. (2021). The complete sequence of a human genome. *bioRxiv*, 2021.2005.2026.445798.
<https://doi.org/10.1101/2021.05.26.445798>
- Orisaka, M., Tajima, K., Tsang, B. K., & Kotsuji, F. (2009). Oocyte-granulosa-theca cell interactions during preantral follicular development. *J Ovarian Res*, 2(1), 9. <https://doi.org/10.1186/1757-2215-2-9>
- Ottolini, C. S., Newnham, L., Capalbo, A., Natesan, S. A., Joshi, H. A., Cimadomo, D., Griffin, D. K., Sage, K., Summers, M. C., Thornhill, A. R., Housworth, E., Herbert, A. D., Rienzi, L., Ubaldi, F. M., Handyside, A. H., & Hoffmann, E. R. (2015). Genome-wide maps of recombination and chromosome segregation in human oocytes and embryos show selection for maternal recombination rates. *Nat Genet*, 47(7), 727-735. <https://doi.org/10.1038/ng.3306>
- Palmer, D. K., O'Day, K., Wener, M. H., Andrews, B. S., & Margolis, R. L. (1987). A 17-kD centromere protein (CENP-A) copurifies with nucleosome core particles and with histones. *J Cell Biol*, 104(4), 805-815. <https://doi.org/10.1083/jcb.104.4.805>
- Parslow, A., Cardona, A., & Bryson-Richardson, R. J. (2014). Sample drift correction following 4D confocal time-lapse imaging. *J Vis Exp*(86). <https://doi.org/10.3791/51086>
- Patel, J., Tan, S. L., Hartshorne, G. M., & McAinsh, A. D. (2015). Unique geometry of sister kinetochores in human oocytes during meiosis I may explain maternal age-associated increases in chromosomal abnormalities. *Biol Open*, 5(2), 178-184.
<https://doi.org/10.1242/bio.016394>
- Pepling, M. E., & Spradling, A. C. (1998). Female mouse germ cells form synchronously dividing cysts. *Development*, 125(17), 3323-3328. <https://www.ncbi.nlm.nih.gov/pubmed/9693136>
- Petronczki, M., Siomos, M. F., & Nasmyth, K. (2003). Un menage a quatre: the molecular biology of chromosome segregation in meiosis. *Cell*, 112(4), 423-440. [https://doi.org/10.1016/s0092-8674\(03\)00083-7](https://doi.org/10.1016/s0092-8674(03)00083-7)
- Politi, A. Z., Cai, Y., Walther, N., Hossain, M. J., Koch, B., Wachsmuth, M., & Ellenberg, J. (2018). Quantitative mapping of fluorescently tagged cellular proteins using FCS-calibrated four-dimensional imaging. *Nat Protoc*, 13(6), 1445-1464. <https://doi.org/10.1038/nprot.2018.040>

- A proposed standard system of nomenclature of human mitotic chromosomes (Denver, Colorado). (1960). *Ann Hum Genet*, 24, 319-325. <https://doi.org/10.1111/j.1469-1809.1960.tb01744.x>
- Ren, R., Deng, L., Xue, Y., Suzuki, K., Zhang, W., Yu, Y., Wu, J., Sun, L., Gong, X., Luan, H., Yang, F., Ju, Z., Ren, X., Wang, S., Tang, H., Geng, L., Zhang, W., Li, J., Qiao, J., . . . Liu, G. H. (2017). Visualization of aging-associated chromatin alterations with an engineered TALE system. *Cell Res*, 27(4), 483-504. <https://doi.org/10.1038/cr.2017.18>
- Rimon-Dahari, N., Yerushalmi-Heinemann, L., Alyagor, L., & Dekel, N. (2016). Ovarian Folliculogenesis. *Results Probl Cell Differ*, 58, 167-190. https://doi.org/10.1007/978-3-319-31973-5_7
- Rogel-Gaillard, C., Hayes, H., Coullin, P., Chardon, P., & Vaiman, M. (1997). Swine centromeric DNA repeats revealed by primed in situ (PRINS) labeling. *Cytogenet Cell Genet*, 79(1-2), 79-84. <https://doi.org/10.1159/000134687>
- Rojas, J., Chavez-Castillo, M., Olivar, L. C., Calvo, M., Mejias, J., Rojas, M., Morillo, J., & Bermudez, V. (2015). Physiologic Course of Female Reproductive Function: A Molecular Look into the Prologue of Life. *J Pregnancy*, 2015, 715735. <https://doi.org/10.1155/2015/715735>
- Sakakibara, Y., Hashimoto, S., Nakaoka, Y., Kouznetsova, A., Hoog, C., & Kitajima, T. S. (2015). Bivalent separation into univalents precedes age-related meiosis I errors in oocytes. *Nat Commun*, 6, 7550. <https://doi.org/10.1038/ncomms8550>
- Sanchez, F., & Smitz, J. (2012). Molecular control of oogenesis. *Biochim Biophys Acta*, 1822(12), 1896-1912. <https://doi.org/10.1016/j.bbadis.2012.05.013>
- Schindelin, J., Arganda-Carreras, I., Frise, E., Kaynig, V., Longair, M., Pietzsch, T., Preibisch, S., Rueden, C., Saalfeld, S., Schmid, B., Tinevez, J. Y., White, D. J., Hartenstein, V., Eliceiri, K., Tomancak, P., & Cardona, A. (2012). Fiji: an open-source platform for biological-image analysis. *Nat Methods*, 9(7), 676-682. <https://doi.org/10.1038/nmeth.2019>
- Schuh, M., & Ellenberg, J. (2007). Self-organization of MTOCs replaces centrosome function during acentrosomal spindle assembly in live mouse oocytes. *Cell*, 130(3), 484-498. <https://doi.org/10.1016/j.cell.2007.06.025>
- Schuh, M., & Ellenberg, J. (2008). A new model for asymmetric spindle positioning in mouse oocytes. *Curr Biol*, 18(24), 1986-1992. <https://doi.org/10.1016/j.cub.2008.11.022>
- Shahbazi, M. N., Wang, T., Tao, X., Weatherbee, B. A. T., Sun, L., Zhan, Y., Keller, L., Smith, G. D., Pellicer, A., Scott, R. T., Jr., Seli, E., & Zernicka-Goetz, M. (2020). Developmental potential of aneuploid human embryos cultured beyond implantation. *Nat Commun*, 11(1), 3987. <https://doi.org/10.1038/s41467-020-17764-7>

- Silkworth, W. T., Nardi, I. K., Scholl, L. M., & Cimini, D. (2009). Multipolar spindle pole coalescence is a major source of kinetochore mis-attachment and chromosome mis-segregation in cancer cells. *PLoS One*, 4(8), e6564. <https://doi.org/10.1371/journal.pone.0006564>
- So, C., Menelaou, K., Uraji, J., Harasimov, K., Steyer, A. M., Seres, K. B., Bucevicius, J., Lukinavicius, G., Mobius, W., Sibold, C., Tandler-Schneider, A., Eckel, H., Moltrecht, R., Blayney, M., Elder, K., & Schuh, M. (2022). Mechanism of spindle pole organization and instability in human oocytes. *Science*, 375(6581), eabj3944. <https://doi.org/10.1126/science.abj3944>
- So, C., Seres, K. B., Steyer, A. M., Monnich, E., Clift, D., Pejkovska, A., Mobius, W., & Schuh, M. (2019). A liquid-like spindle domain promotes acentrosomal spindle assembly in mammalian oocytes. *Science*, 364(6447). <https://doi.org/10.1126/science.aat9557>
- Soares, S. R., Vidal, F., Bosch, M., Martinez-Pasarell, O., Nogues, C., Egozcue, J., & Templado, C. (2001). Acrocentric chromosome disomy is increased in spermatozoa from fathers of Turner syndrome patients. *Hum Genet*, 108(6), 499-503. <https://doi.org/10.1007/s004390100521>
- Tachibana-Konwalski, K., Godwin, J., van der Weyden, L., Champion, L., Kudo, N. R., Adams, D. J., & Nasmyth, K. (2010). Rec8-containing cohesin maintains bivalents without turnover during the growing phase of mouse oocytes. *Genes Dev*, 24(22), 2505-2516. <https://doi.org/10.1101/gad.605910>
- Thomas, C., Cavazza, T., & Schuh, M. (2021). Aneuploidy in human eggs: contributions of the meiotic spindle. *Biochem Soc Trans*, 49(1), 107-118. <https://doi.org/10.1042/BST20200043>
- Thompson, S. L., & Compton, D. A. (2011). Chromosome missegregation in human cells arises through specific types of kinetochore-microtubule attachment errors. *Proc Natl Acad Sci U S A*, 108(44), 17974-17978. <https://doi.org/10.1073/pnas.1109720108>
- Touati, S. A., & Wassmann, K. (2016). How oocytes try to get it right: spindle checkpoint control in meiosis. *Chromosoma*, 125(2), 321-335. <https://doi.org/10.1007/s00412-015-0536-7>
- Tovini, L., & McClelland, S. E. (2019). Impaired CENP-E Function Renders Large Chromosomes More Vulnerable to Congression Failure. *Biomolecules*, 9(2). <https://doi.org/10.3390/biom9020044>
- Tsuiko, O., Vanneste, M., Melotte, C., Ding, J., Debrock, S., Masset, H., Peters, M., Salumets, A., De Leener, A., Pirard, C., Kluyskens, C., Hostens, K., van de Vijver, A., Peeraer, K., Denayer, E., Vermeesch, J. R., & Dimitriadou, E. (2021). Haplotyping-based preimplantation genetic testing reveals parent-of-origin specific mechanisms of aneuploidy formation. *NPJ Genom Med*, 6(1), 81. <https://doi.org/10.1038/s41525-021-00246-0>
- Tsutsumi, M., Fujiwara, R., Nishizawa, H., Ito, M., Kogo, H., Inagaki, H., Ohye, T., Kato, T., Fujii, T., & Kurahashi, H. (2014). Age-related decrease of meiotic cohesins in human oocytes. *PLoS One*, 9(5), e96710. <https://doi.org/10.1371/journal.pone.0096710>

- Wang, X., & Pepling, M. E. (2021). Regulation of Meiotic Prophase One in Mammalian Oocytes. *Front Cell Dev Biol*, 9, 667306. <https://doi.org/10.3389/fcell.2021.667306>
- Wartosch, L., Schindler, K., Schuh, M., Gruhn, J. R., Hoffmann, E. R., McCoy, R. C., & Xing, J. (2021). Origins and mechanisms leading to aneuploidy in human eggs. *Prenat Diagn*, 41(5), 620-630. <https://doi.org/10.1002/pd.5927>
- Webster, A., & Schuh, M. (2017). Mechanisms of Aneuploidy in Human Eggs. *Trends Cell Biol*, 27(1), 55-68. <https://doi.org/10.1016/j.tcb.2016.09.002>
- Worrall, J. T., Tamura, N., Mazzagatti, A., Shaikh, N., van Lingen, T., Bakker, B., Spierings, D. C. J., Vladimirov, E., Fojer, F., & McClelland, S. E. (2018). Non-random Mis-segregation of Human Chromosomes. *Cell Rep*, 23(11), 3366-3380. <https://doi.org/10.1016/j.celrep.2018.05.047>
- Zielinska, A. P., Bellou, E., Sharma, N., Frombach, A. S., Seres, K. B., Gruhn, J. R., Blayney, M., Eckel, H., Moltrecht, R., Elder, K., Hoffmann, E. R., & Schuh, M. (2019). Meiotic Kinetochores Fragment into Multiple Lobes upon Cohesin Loss in Aging Eggs. *Curr Biol*, 29(22), 3749-3765 e3747. <https://doi.org/10.1016/j.cub.2019.09.006>
- Zielinska, A. P., Holubcova, Z., Blayney, M., Elder, K., & Schuh, M. (2015). Sister kinetochore splitting and precocious disintegration of bivalents could explain the maternal age effect. *Elife*, 4, e11389. <https://doi.org/10.7554/eLife.11389>